Aus dem
Max-Planck-Institut für Herz- und Lungenforschung, Bad Nauheim
Am Fachbereich 08 – Biologie und Chemie
der Justus-Liebig-Universität Gießen

Long non-coding RNA ADPGK-AS1 regulates mitochondrial and metabolic remodeling in macrophages and influences tumor progression

Inauguraldissertation
zur Erlangung des Doktorgrades
der Naturwissenschaften (Dr. rer. nat.)

Vorgelegt von
Annika Michaela Magdalena Karger

Gießen 2022

1. Gutachter: Prof. Dr. Reinhard Dammann
2. Gutachter: Prof. Dr. Rajkumar Savai

Table of content

Abbreviations

ΔC_T	Threshold-cycle difference (HPRT-GOI)
αKG	Alpha-Ketoglutarate
ATP	Adenosintriphosphate
bp	Basepairs
BSA	Bovine serum albumine
cDNA	Complementary DNA
ddH_2O	Double distilled water
DMEM	Dulbecco's modified eagle medium
DMSO	Dimethyl-Sulfoxid
DNA	Deoxyribonucleic acid
E. coli	*Escherichia coli*
ELISA	Enzyme linked immunosorbent assay
et al.	*et alterae* („and others")
FCS	Fetal calf serum
G6PD	Glucose-6-phosphate dehydrogenase
GOI	Gene of interest
h	Hour
IFNɣ	Interferon gamma
IL	Interleukin
kDa	Kilo Dalton
LDH	Lactate dehydrogenase
LPS	Lipopolysaccharide
MDH	Malate dehydrogenase
min	Minute
Mt	Mitochondrial
NSCLC	Non-small cell lung cancer
NSG	NOD.Cg-Prkdcscid Il2rgtm1Wj1 / SzJ
nt	Nucleotides
PCLS	Precision cut lung slices
PCNA	Proliferating cell nuclear antigen
RNA	Ribonucleic acid
rpm	Rounds per minute
RT	Room temperature
SDH	Succinate dehydrogenase
SEM	Standard error of mean
TAM	Tumor-associated macrophages
TCA	Tricarboxylic acid
TGFβ	Transforming growth factor beta
TNFα	Tumor necrosis factor alpha
U	Units
UTR	Untranslated region
v/v	Volume per volume
WT	Wildtype
w/v	Weight per volume

1 Introduction

1.1 Lung Cancer

The human lungs are sponge-like organs in the chest that are divided into three (right lung) or two (left lung) lobes (Drake, Vogl, and Mitchell 2014). The trachea connects the throat with the lungs, further dividing into smaller bronchi, bronchioles and finally alveoli, which are crucial in the process of gas exchange. To accomplish successful respiration, the lung is composed of approximately 40 different resident cell types (Franks et al. 2008), such as several airway epithelial cells (e.g. goblet cells, clara cells, ciliated cells, basal cells), alveolar cells (type I and type II), salivary gland cells, interstitial connective tissue (e.g. smooth muscle cells, fibroblasts and myofibroblasts, neural cells), blood vessels, and hematopoietic cells (e.g. alveolar macrophages, neutrophils, lymphocytes). Uncontrollable division of one of the cell types in the lung can lead to tumor formation and ultimately, lung cancer (Sarode, Mansouri, et al. 2020).

1.1.1 Statistics

Cancer is a major health problem worldwide and, shortly behind heart diseases, the second leading cause of death in the United States (Siegel et al. 2021). Lung cancer is one of the most commonly diagnosed cancer types in both men and women. In 2021, estimated new cases of lung cancer were around 12 % in men and 13 % in women, taking the second place behind prostate cancer (26 %) and breast cancer (30 %). Nevertheless, lung cancer is still the most fatal cancer type, having the lead in cancer related deaths among both men (22 %) and women (22 %) in the United States and Europe with a devastating 5-year survival rate of ≤15 %. Worldwide, it is responsible for most cancer deaths among men, while for women lung cancer is on second place shortly after breast cancer (Brambilla and Gazdar 2009; Siegel, Miller, and Jemal 2020; Torre, Siegel, and Jemal 2016). Around 82 % of lung cancer cases are directly caused by cigarette smoking (Islami et al. 2018), which is why smoking continues to be the leading preventable cause of deaths. Notably, quitting smoking by the age of 40 reduces the risk of death by smoking-related disease by around 90 % compared to continued smokers. The lung cancer overall incidence and mortality however is generally decreasing (Siegel et al. 2021), resulting from reductions in smoking, improvements in early detection and improved treatments (Howlader et al. 2020). This is reflected by increase of the 2-year survival rate from 30 % in 2009 to 36 % in 2016.

1.1.2 Classifications and Pathogenesis

Lung cancer is a highly complex, very heterogeneous disease. Histologically, lung cancer is divided into two main groups; non-small cell lung carcinoma (NSCLC), which makes up approximately 85 % of the cases, and small cell lung carcinoma (SCLC), that are around 15 % of the cases. NSCLC can be classified further into adenocarcinoma (55 %), squamous cell carcinoma (34 %), large cell carcinoma (10 %) and others (1 %) (Travis et al. 2015; Travis, Brambilla, and Riely 2013). Depending on the size and if or how far the cancer has spread, it is classified into four (I–IV) stages, in which stage IV describes the most advanced and malignant stage (ACS 2019). Lung cancer is usually diagnosed at very late stages, although recent technology such as spiral computed tomography slightly improved early detection rates. At the late stage, when the lung cancer already became a systemic disease, the current standard therapies rarely lead to successful cure of the patient (Brambilla and Gazdar 2009). Around 85 % of NSCLC and 98 % of SCLC cases are caused by tobacco smoke that leads to accumulation of genetic and epigenetic mutations. Tobacco smoke contains several carcinogens associated with lung cancer. The best described ones are polycyclic aromatic hydrocarbons and nicotine-derived nitrosoaminoketone (NKK), that lead to DNA adduct formation and therefore genetic mutations (Hecht 1999). However, around 20–25 % of lung cancer patients worldwide are non- or never-smokers.

There are several signaling pathways known that, when the involved molecules are mutated, are linked with lung cancer development. The epidermal growth factor receptor (EGFR) is a transmembrane protein with cytoplasmic kinase activity and part of a large group of receptor tyrosine kinases (RTKs) that mediate cell signaling via extracellular growth factors (da Cunha Santos, Shepherd, and Tsao 2011). EGFR has been frequently found to be highly expressed in NSCLC and an overexpression is often associated with poor prognosis (Hirsch et al. 2003; Nicholson, Gee, and Harper 2001). EGFR signaling is associated with RAS/RAF/mitogen-activated protein kinase (MAPK) and PI3K/PTEN/AKT pathways as major signaling networks, linking EGFR activation to cell proliferation, enhanced survival and reduced apoptosis (Sharma et al. 2007; da Cunha Santos, Shepherd, and Tsao 2011). Numerous members of the EGFR signaling pathway have been found to be mutated in NSCLC, such as KRAS, HER2, HER4, BRAF or PIK3CA (Brambilla and Gazdar 2009). KRAS is one of the best documented oncogenes of this signaling pathway. Around 20 % of NSCLC patients have changes in the KRAS gene and around 13 % of NSCLC patients inherit the specific KRAS G12C mutation. Along with KRAS, somatic mutation in the PIK3CA gene coding for a regulatory subunit in the PI3K/AKT pathway is one of the most commonly mutated oncogenes and occur in many epithelial cancers.

In around 7 % of NSCLC cases, gene fusion of echinoderm microtubule-associated protein-like 4 (EML 4) and the anaplastic lymphoma kinase (ALK) gene can be observed

(Inamura et al. 2008; Soda et al. 2007). Fusion of these genes results in activation of a potent ALK fusion protein that contributes to lung cancer pathogenesis and is usually seen in non-smokers. Interestingly, this type of mutation is negatively associated with the presence of KRAS or EGFR mutations. However, detailed knowledge of the underlying signaling pathway is limited.

The thyroid transcription factor 1 (TTF1, also known as NKX2-1) is crucial in development of the peripheral airways (Maeda, Dave, and Whitsett 2007). It is frequently overexpressed and sometimes amplified in tumors developing from the peripheral respiratory unit. Inhibition of this transcription factor showed decrease of proliferation and enhanced apoptosis in adenocarcinoma cell lines expressing TTF1. High expression of TTF1 in lung cancer is often observed together with high EGFR expression.

Another important signaling pathway involves the MYC gene family consisting of the nuclear phospho-proteins C-MYC, N-MYC and L-MYC. This gene family strongly controls cellular growth and apoptosis and is found to be amplified in 15–30 % of SCLC (Gazzeri et al. 1994; Gazzeri et al. 1990).

The p53 protein is one of the most prominent tumor suppressor genes, sometimes referred to as a “cellular gatekeeper” against genetic abnormalities. The p53 pathway includes several genes of large up- and downstream sub-pathways and functions as a sensor of stress signals, including DNA damage response, oncogene activation or hypoxia. Downstream targets of this transcription factor are involved in cell cycle arrest, DNA repair or apoptosis. P53 is the most frequently mutated gene in lung cancer (Olivier et al. 2009) and inactivation by mutation of its binding domain can be found in 90 % of SCLC and large cell neuroendocrine carcinoma as well as 50 % of NSCLC. P53 alteration and stabilization is linked with both tobacco smoker and non-smoker lung cancer patients.

1.2 Lung Cancer Treatment

Today, there are different treatment options available for lung cancer. Which treatment is used depends mainly on the stage of the cancer, but other factors, such as overall health and lung function of the patient, are also important. Classical treatment options comprise surgery, radio- and chemotherapy. More novel approaches include targeted therapy or immunotherapy. In the following sections each approach will be discussed separately, however, it is common practice that patients receive a combination of different treatment options.

1.2.1 Surgery

Surgery is one of the oldest methods to treat cancer (NCI 2019a). The goal of surgery is to completely remove the lung tumor and the nearby lymph nodes to the chest. To successfully remove the whole tumor tissue, it is crucial to also remove part of the surrounding healthy lung tissue. Depending on the size and localization of the tumor within the lung, either the tumor alone, the whole lung lobe, or the whole lung of the patient is removed. Surgery is the treatment of choice for patients with stage I lung cancer.

1.2.2 Radiation

Radiation therapy uses high energy x-rays or other particles to destroy cancer cells by induction of DNA damage (NCI 2019b). Either external beam radiation therapy, where an external machine aims to radiate the cancer, or internal therapy (brachytherapy), in which a source of radiation is put inside the body near the tumor tissue via bronchoscopy or surgery, is used. For lung cancer treatment, radiation therapy is mainly used in SCLC, since it is more sensitive to this type of therapy compared to NSCLC.

1.2.3 Chemotherapy

Chemotherapeutic agents aim to target the rapid proliferation rate of cancer cells compared to most other cell types. Typically, chemotherapy is designed to target molecular drivers of tumorigenesis by e.g. interfering with cell division (Malhotra and Perry 2003).

The era of chemotherapy began in 1942, when Louis Goodman and Alfred Gilman performed a first clinical trial with nitrogen mustard on non-Hodgkin's lymphoma (Gilman 1963), leading to regression of the lymphatic masses of the patient. At the same time, Sydney Farber found that antifolates were able to suppress acute lymphoblastic leukemia (ALL) in children by decreasing proliferation of malignant cells (Farber et al. 1948). Today, a variety of chemotherapeutics are in use and applied before or after surgery to shrink the tumor mass, or to slow down progression and reduce symptoms in later stages. Types of chemotherapy include alkylating agents, antimetabolites, plant alkaloids and antitumor antibiotics (NCI 2019a). Lung cancer is often treated with a combination of chemotherapy drugs, including either cisplatin or carboplatin. Other chemotherapeutics include vinorelbine, gemcitabine, paclitaxel (taxol), docetaxel (taxotere) or etoposide (VP-16), which are injected into the bloodstream.

1.2.4 Targeted therapy

Targeted therapy is based on targeting specific mutations in cancer cells and was the first step into personalized medicine. Tumors in different organs and even in different locations

within the lung differ in their mutational burden. Hence, before starting targeted therapy it is crucial to characterize the tumor regarding feasible targets in commonly mutated signaling pathways (see 1.1.2). Small molecule inhibitors are usually named ending with “-ib” and are ≤500 kDa in size, allowing translocation through the membrane, while monoclonal antibodies (mAbs) used for therapy are usually named ending with “-mab” (Seebacher et al. 2019).

Frequent deregulation of EGFR signaling pathway in NSCLC led to selection of EGFR as one of the first molecules for targeted therapy. Today, there are several drugs available blocking EGFR signaling, including Osimertinib for early-stage lung cancer after surgery, and Erlotinib or Gefitinib for advanced stage lung cancer. However, patients with a KRAS mutation are often resistant to EGFR inhibitors and need to be treated with Sotorasib, a specific KRAS inhibitor (Hong et al. 2020).

About 7 % of NSCLC have mutations in the ALK gene, which is often seen in younger patients and non-smokers. ALK inhibitors targeting the mutated protein include Alectinib, Ceritinib or Lorlatinib and are used instead of chemotherapy or in advanced stages, when chemotherapy has stopped working.

Other, less frequent mutations used in targeted therapy for lung cancer include changes in the *ROS1* gene (Crizotinib, Ceritinib, Lorlatenib), mutations in the *BRAF* (Dabrafenib, Tramatinib), *RET* (Selpercatinib, Pralsetinib), *MET* (Capmatinib, Tepotinib), or *NTRK* gene (Larotrectinib).

Some targets, such as angiogenesis inhibitors that block the formation of new blood vessels, are not specific to only lung cancer. Here, e.g. Avastin and Ramucirumab are used in NSCLC, both based on monoclonal antibody therapy targeting VEGF. Angiogenesis blockers are often used in combination with chemotherapy.

1.2.5 Immunotherapy

One of the hallmarks of cancer is the ability to escape the immune anti-tumor response (Hanahan and Weinberg 2011). Immunotherapy has emerged as a promising alternative in the arsenal against cancer by harnessing the power of the immune system to specifically target malignant tissues. The connection between the immune system and cancer has been described as early as the 18th century, when the two physicians Busch and Fehleisen independently noticed tumor regression after *Streptococcus pyogenes* infection (Oiseth and Aziz 2017). In 1891 William Coley, later often referred to as the “Father of immunotherapy”, followed up on these observations and started injecting patients with extracts of heat-inactivated bacteria (“Coleys toxins”) to treat inoperable cancer types (Decker and Safdar 2009). He reported a significant number of favorable responses, especially in patients with sarcoma, but lack of deeper scientific understanding, reproducibility, and development of chemo- and radiotherapy led to gradual disappearance of his toxins. The concept of

immunotherapy however resurfaced several times, e.g. with development of more advanced technologies, such as knock out mouse models, which were necessary to prove the link between immunodeficiency and tumor development (Chow, Moller, and Smyth 2012). Today, cancer immunotherapy has revolutionized the field of oncology by significantly increasing the survival of patients with fatal cancers.

T lymphocytes with their capacity for antigen-directed cytotoxicity are one of the central cell types in the focus of immunotherapy (Waldman, Fritz, and Lenardo 2020). For instance, immune checkpoint inhibitors such as cytotoxic T lymphocyte associated protein (CTLA-4) and programmed death 1 (PD1) have been developed to enhance cytotoxic T cell function and are used to treat various cancer types including NSCLC (Buchbinder and Desai 2016). In 2015, pembrolizumab was approved to treat PDL1-expressing NSCLC and provided a 4.3-month increase in progression-free survival compared to classical platinum-based chemotherapeutics and was more effective than chemotherapeutic paclitaxel (Herbst et al. 2016; Reck et al. 2016). Other approaches in immunotherapy include tumor vaccines, monoclonal antibodies, small molecule inhibitors or adoptive cell therapy.

In the last years, the role of macrophages in cancer progression has also been clearly demonstrated and macrophage functions are slowly becoming more interesting targets for immunotherapy. Macrophages have been shown to regulate several key functions of malignant tumors, such as metastasis, angiogenesis or therapeutic resistance (Duan and Luo 2021). For instance, CC-chemokine receptor 2 (CCR2) is predominantly expressed in monocytes and macrophages with pro-inflammatory functions and targeting the CCL2/CCR2 axis has been shown to directly contribute to survival, growth and metastasis of several tumor types (Fei et al. 2021). Additionally, agents targeting colony-stimulating factor 1 receptor (CSF-1R) expressed by macrophages are being investigated in various cancer clinical trials (Cannarile et al. 2017).

1.2.6 Limitation of available therapies

Cancer is a very heterogeneous disease highly varying from patient to patient. Due to this, current available therapies still have their limitations. Surgery for instance, is only an option in early stages of cancer. Additionally, microscopic or metastatic cancer sites might be missed. Radiation therapy causes indirect damage to the surrounding tissue, leading to wound complications and poor healing (Baskar et al. 2012; Haubner et al. 2012). Chemotherapy, still the standard therapeutic option, is a systemic drug interfering with cell division. Thus, not only cancer cells are targeted, but non-specifically all rapidly dividing cells, such as hair cells or bone marrow cells, resulting in systemic toxicities, development of drug resistance and the commonly known side effects such as hair loss (Malhotra and Perry 2003). In addition, e.g. platinum-based chemotherapy offers only symptomatic relief and mostly survival

improvements with a median of 7–10 months (Kelly et al. 2001; Scagliotti et al. 2002; Schiller et al. 2002).

Targeted therapies only target specific mutations in the tumor, limiting their success to patients inheriting these mutations. To date, the best characterized molecular targets in NSCLC are the EGFR and ALK. Despite steady advances in targeted therapies within these molecular subsets, however, acquired resistance to therapy is near universal. Further these inhibitors may not work in KRAS mutated patients since this molecule is further downstream in the signaling cascade.

For immunotherapy, similar problems have emerged. In general, the heterogeneity of the immunosuppressive tumor microenvironment (TME) makes it difficult to predict which patient will respond to the therapy. Only around 15–20 % of patients achieve durable results with immunotherapy (inHealth 2021). In addition, it was shown that CTLA-4 therapy for example, led to benefits in various cancer types, but less immunogenic cancer types such as mammary carcinoma did not respond favorably. Also, greater tumor burden correlates with reduced anti-tumor response, since larger tumors have a more robust anti-inflammatory TME (Waldman, Fritz, and Lenardo 2020). Furthermore, immune checkpoint therapy carries a risk of severe autoimmune complications or development of toxicities i.e. effects on the gastrointestinal tract, hypothyroidism, or pneumonitis. Still, it has been shown that checkpoint blockage leads to better tolerated toxicities compared to traditional chemotherapeutics.

In summary, the current non-specific treatments result in modest increase of survival at the cost of high toxicity to the patients. On the other hand, efficacy of novel treatment agents has usually been usually quite low. Despite many advances, there are still significant limitations regarding treatment options for NSCLC patients, especially with advanced disease. There is a need of identification of novel agents to provide improved clinical benefits with better safety and tolerability.

1.3 The Tumor Microenvironment

Knowledge of the tumor microenvironment (TME) is the foundation of successful cancer immunotherapy. The TME surrounds the tumor and is a complex and heterogeneous network of accumulated non-neoplastic host cells (Figure 1-1). This includes stromal fibroblasts, endothelial cells and immune cells such as macrophages, neutrophils, dendritic cells and lymphocytes (T cells and B cells) and the non-cellular components of extracellular matrix including but not limited to collagen, fibronectin, hyaluronate and laminin among others (Labani-Motlagh, Ashja-Mahdavi, and Loskog 2020; El-Nikhely et al. 2012). Next to the cellular composition, the complexity of the tumor structure is extended depending on nutrient availability. Due to the density of tumor and stromal cells, low amounts of oxygen (hypoxia) are found within the tumor center. The hypoxic conditions lead to a high production of lactate,

which further acidifies the surrounding area. Therefore, the conditions in the tumor center, also referred to as the “hypoxic core”, often lead to tumor cell necrosis (Luo and Wang 2019; Ancel et al. 2021; Damaghi, Wojtkowiak, and Gillies 2013; Zheng, Mansouri, et al. 2020).

In the following chapters macrophages will be described in more detail since they are one of the most abundant cell types in the TME and the main cell type analyzed in the present study.

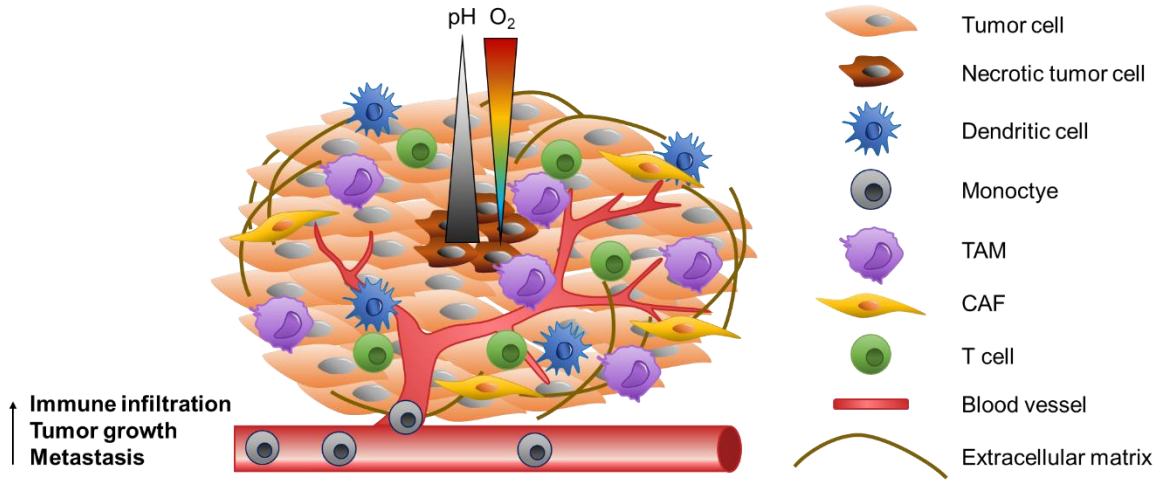

Figure 1-1 Schematic representation of the tumor microenvironment. The TME consists of tumor cells, extracellular matrix, blood vessels and infiltrating immune cells such as dendritic cells, tumor associated macrophages (TAMs), cancer associated fibroblasts (CAFs) and leukocytes, such as T cells. Dependent on the tumor area, many factors can differ, such as availability of O_2 or the pH. The tumor center, also referred to as “hypoxic core”, has a low amount of oxygen, therefore high amounts of lactate are produced, leading to acidification and necrotic areas.

1.3.1 Macrophages

Macrophages play crucial roles in both innate and adaptive immunity and are known for their remarkable phenotypic heterogeneity and their functional diversity (Pan et al. 2020). Macrophages in the TME, also referred as tumor associated macrophages (TAMs), have critical functions in tumor progression and high TAM density has been shown to correlated with poor overall survival rate in patients with different cancer types (Jung et al. 2015; Zheng, Weigert, et al. 2020).

1.3.1.1 Macrophage origin

Macrophages are phagocytic cells and, together with monocytes and dendritic cells, part of a body-wide mononuclear phagocyte system (van Furth and Cohn 1968; Auffray, Sieweke, and Geissmann 2009). This system is involved in the innate immune response,

supports the adaptive immune response and helps to maintain tissue homeostasis. Bone marrow (BM)-derived monocytes can infiltrate tissues and differentiate to macrophages. For a long time, these circulating BM-derived monocytes in the blood stream were considered to be the only origin for tissue macrophages. However, macrophages in many tissues such as the liver, spleen or brain, are now known to be established prenatally during embryonic development from progenitor cells derived from the yolk sac or fetal liver (Hettinger et al. 2013; Hoeffel and Ginhoux 2015). These macrophages are maintained differently and independently from monocyte-derived macrophages. Interestingly, monocyte-derived macrophages were shown to support the prenatally established tissue resident macrophages, especially under stress conditions such as inflammation (Schulz et al. 2012; Yona et al. 2013). In the TME, the majority of TAMs are recruited from the peripheral monocytic precursors. However, some studies show evidence of embryonic-derived resident macrophages infiltrating the TME in certain tumors (Zhu et al. 2017), although their impact on tumor development and progression still needs to be further investigated.

1.3.1.2 Macrophage activation and regulation within the TME

Macrophages are very plastic and can be activated into two distinct activation states depending on the tissue environment: M1 phenotype or M2 phenotype, which differ in their immune response, cytokine expression as well as metabolic profile (Galvan-Pena and O'Neill 2014; Zheng et al. 2017). M1 macrophages are generally known as pro-inflammatory cells, acting in host-defense against bacteria by activating cells of the adaptive immune system. They are activated by stimulation with bacterial products such as LPS and IFNɣ and express high levels of pro-inflammatory genes such as Interleukin (IL)-8, IL-12 or TNFα. On a metabolic level, M1 macrophages are known to rely on energy production through aerobic glycolysis together with high production of reactive oxygen species (ROS) (Tannahill et al. 2013; Mills et al. 2016). M2 macrophages on the other hand are described as the anti-inflammatory phenotype, highly expressing genes such as IL-10, CD206 or CSF-1R. They are involved in wound healing and tissue remodeling and have increased fatty acid oxidization and mitochondrial metabolic activity, producing energy predominantly through the tricarboxylic acid (TCA) cycle and the electron transport chain (Figure 1-2). Although the classification of macrophages into M1 and M2 phenotype is largely accepted, it is worth noting that in some cases this concept appears to be oversimplified and several other subtypes have been described (Pan et al. 2020). M2 macrophages for instance can be further divided into M2a, M2b, M2c or M2d phenotype, all slightly differing in their function and being induced by different molecules (Duan and Luo 2021; Shapouri-Moghaddam et al. 2018). Additionally, macrophages are able to respond to different environmental cues, leading to a change in their activation

state and a phenotypic switch. For these reasons, the following sections refer to the M1 and M2 macrophage activation states as “M1-like” and “M2-like”.

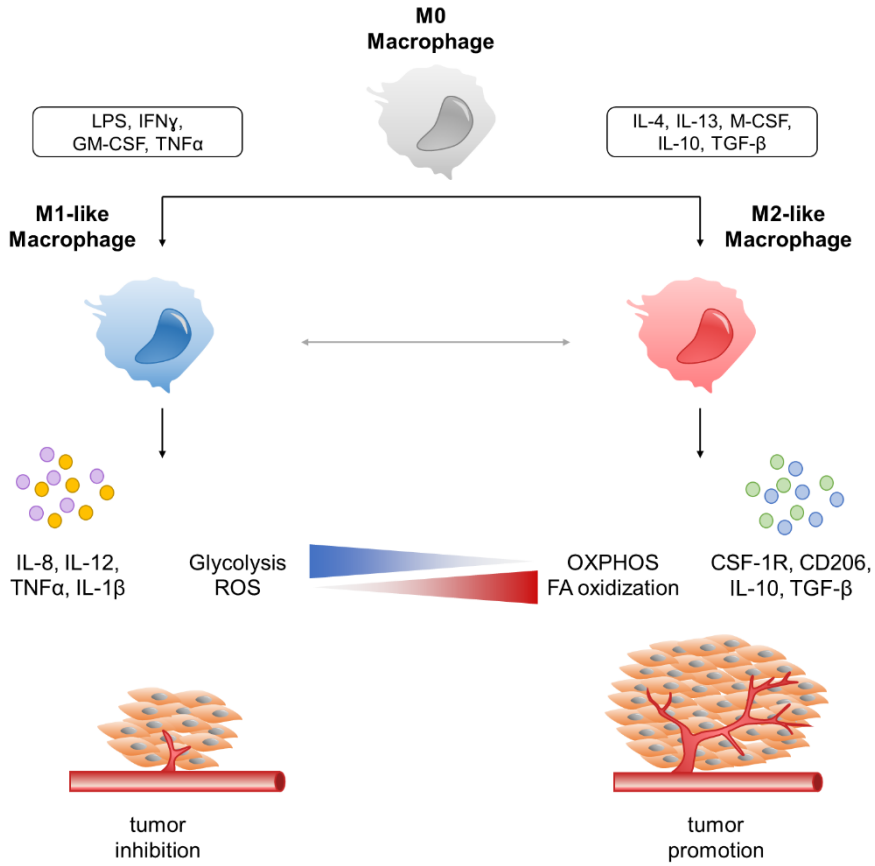

Figure 1-2 Schematic representation of macrophage activation states. Unstimulated M0 macrophages can be activated with LPS/IFNɣ/GM-CSF/TNFα to the M1-like phenotype or with IL-4/IL-12/M-CSF/IL-10/TGF-β to M2-like phenotype. M1-like macrophages secrete pro-inflammatory cytokines such as IL-8, IL-12, TNFα or IL-1β, have enhanced aerobic glycolysis and ROS production, ultimately leading to inhibition of tumor formation and growth. M2-like macrophages express anti-inflammatory molecules such as CSF-1R, CD206, IL-10 or TGF-β, have enhanced mitochondrial oxidative phosphorylation (OXPHOS) and fatty acid (FA) oxidization, therefore promoting tumor progression.

In the context of tumors, M1-like macrophages lead to enhanced tumor-cell apoptosis, while M2-like macrophages promote tumor progression by increasing tumor-cell proliferation and migration. In the TME, macrophages do not inherit only one specific phenotype, but TAMs are known to be a combination of different subpopulations due to the dynamics in the TME in which TAMs must adopt their expression and metabolic based on the availability of oxygens and nutrients (Netea-Maier, Smit, and Netea 2018; Chavez-Galan et al. 2015). However, TAMs are often considered to be predominantly activated towards a tumor promoting M2-like phenotype. Particularly, a high ratio of M2-like to M1-like macrophages together with close proximity of the M2-like TAMs to tumor cells has been shown to be correlated with poor patient

survival, which was shown e.g. in lung cancer, breast cancer and ovarian cancer (Zheng, Weigert, et al. 2020; Laoui et al. 2011; Mantovani et al. 2002; Zhang, He, et al. 2014). Through secretion of various factors such as VEGF or TGF-β, TAMs stimulate other immune cells and lead to chronic inflammation, but also initiate and promote development of cancer or stimulate angiogenesis and therapeutic resistance (Duan and Luo 2021). In addition, TAM-derived metabolites, such as lactate, fatty acids, or glutamine are able to enhance tumor immunosuppression as well as enhance angiogenesis or CCL2 production, further leading to macrophage recruitment (Zheng, Mansouri, et al. 2020; Schmall et al. 2015).

1.3.1.3 Macrophage therapeutic options

As stated before, macrophages play crucial roles in the immune system as well as maintenance of tissue homeostasis. Thus, it is not surprising that deregulation or dysfunction of macrophages and their activation happen in several diseases' context such as sepsis, infection, chronic inflammatory diseases like rheumatoid arthritis, asthma, chronic obstructive pulmonary disease (COPD), diabetes, and cancer (Ardura et al. 2019; Zhang, Yang, and Ericsson 2021; Schultze, Schmieder, and Goerdt 2015). Therefore, macrophages have become of interest as potential therapeutic targets. Due to their ability to acquire different phenotypes in response to different stimuli, several approaches have been developed to target this regulation in disease context.

For instance, macrophage depletion via antibodies can be done by e.g. using clodronate liposomes, CD206 and CSF-1R antibodies packed in liposomes that are taken up by macrophages (Schmall et al. 2015; Azad, Rajaram, and Schlesinger 2014; Hume and MacDonald 2012). One of the first diseases in which liposomal clodronate was applied is the chronic inflammatory disease rheumatoid arthritis (van Lent et al. 1993; Van Lent et al. 1998), leading to effective macrophage depletion and reduction of cartilage destruction. Macrophage depletion was also used in a COPD mouse model, resulting in reduced smoke-induced epithelial thickening and emphysema development (Beckett et al. 2013). In addition, it was shown that systemic macrophage depletion also led to reduced primary and metastatic lung tumor growth (Schmall et al. 2015). Furthermore, macrophages and the associated antiviral immune response have been investigated as targets in coronavirus infections (Gracia-Hernandez, Sotomayor, and Villagra 2020).

In cancer immunotherapy, macrophage "re-education", aiming a phenotypic switch from pro-tumoral M2-like macrophages to anti-tumoral M1-like macrophages, is one of the most prominent strategies. For example, the WNT/β-catenin signaling pathway has been recently identified as a driver for a molecular switch, regulating TAM phenotype in the lung TME (Sarode, Zheng, et al. 2020). Inhibition of β-catenin transcriptional activation led to reprogramming M2-like TAMs to M1-like TAMs, resulting in suppression of primary and

metastatic lung tumor growth. In addition, bioconjugated manganese dioxide nanoparticles were used to prime TAMs to an M1-like phenotype, resulting in higher sensitivity and better response to chemotherapy (Song et al. 2016). Furthermore, nanoparticles encapsulating small interfering RNAs (siRNAs) against IκBα were able to selectively target CD206-expressing TAMs and restore NF-κB signaling (Ortega et al. 2016). However, most of the present studies are limited to *in vitro* studies or mouse models and have not yet been translated into clinical studies. Nevertheless, current immune checkpoint therapeutic anti-PD-1/anti-PD-L1, initially aiming to enhance cytotoxic T cell function, has been shown to also affect macrophages, inducing M1-like macrophage polarization (Sun et al. 2019; Gubin et al. 2018). Thus, understanding the regulation and activation process of TAMs within the TME is extremely important to understand cancer biology and harness TAMs for novel anticancer strategies.

1.4 Non-coding RNAs

The ability of sequencing whole genomes and transcriptomes identified all kinds of transcripts and showed that approximately 90 % of the human genome is actively transcribed. However, only about 2 % of those transcripts are translated into proteins, with the rest remaining as non-coding (nc) RNAs (Djebali et al. 2012; Santosh, Varshney, and Yadava 2015). The most prominent ncRNAs are microRNAs (miRNAs) and long non-coding RNAs (lncRNAs), but also include transfer RNAs (tRNAs), small nucleolar RNAs (snoRNAs) or ribosomal RNAs (rRNAs).

1.4.1 MicroRNAs

MiRNAs are short single stranded RNA sequences of 21–24 nucleotides and mainly function via binding mRNAs, leading to their degradation and therefore translational inhibition. The majority of miRNAs are transcribed from the genome into primary miRNAs (pri-miRNAs), which are further processed into precursor miRNAs (pre-miRNAs) and lastly mature miRNAs (Ha and Kim 2014). Mature miRNAs usually bind the 3'-UTR of their target mRNAs, but some miRNAs have been described to bind on other regions, such as the 5'-UTR or even promotor regions (Broughton et al. 2016). MiRNA-mRNA-interaction usually leads to translational repression and degradation of the mRNA via recruitment of the miRNA-induced silencing complex (miRISC). The miRISC complex consists of the miRNA-guide sequence and an AGO2 protein with endonuclease activity leading to mRNA cleavage at the specific recruitment site (Jo et al. 2015; Kawamata and Tomari 2010). To date, numerous miRNAs have been described as critical modulators of various biological processes such as normal development and to be deregulated in many human diseases (Fu et al. 2013; Tufekci et al. 2014; Paul et al. 2018).

1.4.2 Long non-coding RNAs

LncRNAs include all ncRNAs larger than 200 nucleotides. Due to lack of a clear unitary sub-classification, the group of lncRNAs is very large, heterogeneous, and functionally diverse. LncRNAs have been described to be localized in all kinds of cellular compartments and to be able to interact with proteins, DNA, or other RNAs. Additionally, they can fold into complex secondary or tertiary structures. LncRNAs emerged from being considered as “transcriptional noise” to crucial regulators of diverse cellular mechanisms. LncRNAs have been observed in all kinds of species, including animals, plants, yeast, bacteria and even viruses (Ma, Bajic, and Zhang 2013). However, lncRNAs seem to be very poorly evolutionary conserved between species and often show tissue and even cell type specific expression pattern (Statello et al. 2021).

1.4.2.1 Classification, functions, and mechanisms of lncRNAs

Although lncRNAs lack a clear classification, there are different approaches to divide lncRNAs into different groups, e.g. according to the following two aspects: the location of their gene within the genome or their molecular mechanism.

Classification of lncRNAs by location within the genome describes how the lncRNA-genes are encoded in the genome with respect to neighboring protein coding genes. This results in categories of long intergenic RNAs (lincRNAs) with genes encoded between protein-coding genes, overlapping lncRNAs (sense and antisense) with genes encoded in an area that is overlapping a protein-coding gene either on the same or the opposite strand, and intronic lncRNAs (sense and antisense) with genes encoded within an intron of a protein coding gene (Ma, Bajic, and Zhang 2013).

Dividing lncRNAs into groups based on their molecular mechanisms describes lncRNAs that function as guides, scaffolds or decoys for proteins (Wang and Chang 2011). Guide lncRNAs can recruit e.g. chromatin modifying enzymes to their target genes and scaffold lncRNAs bind multiple proteins, leading to formation of a complex, such as the ribonucleoprotein complex. Decoy lncRNAs on the other hand can bind proteins, preventing them from their usual targets and thereby inhibiting the signaling.

However, these classifications are not sufficient to describe all mechanisms and signaling pathways in which lncRNAs have been described to date. LncRNAs are present in all kinds of compartments of the cell and regulate on the transcriptional level, by alternative splicing, on post-transcriptional level by regulating translation, or by direct interaction with proteins to influence their modification and activation (Figure 1-3) (Karger et al. 2021).

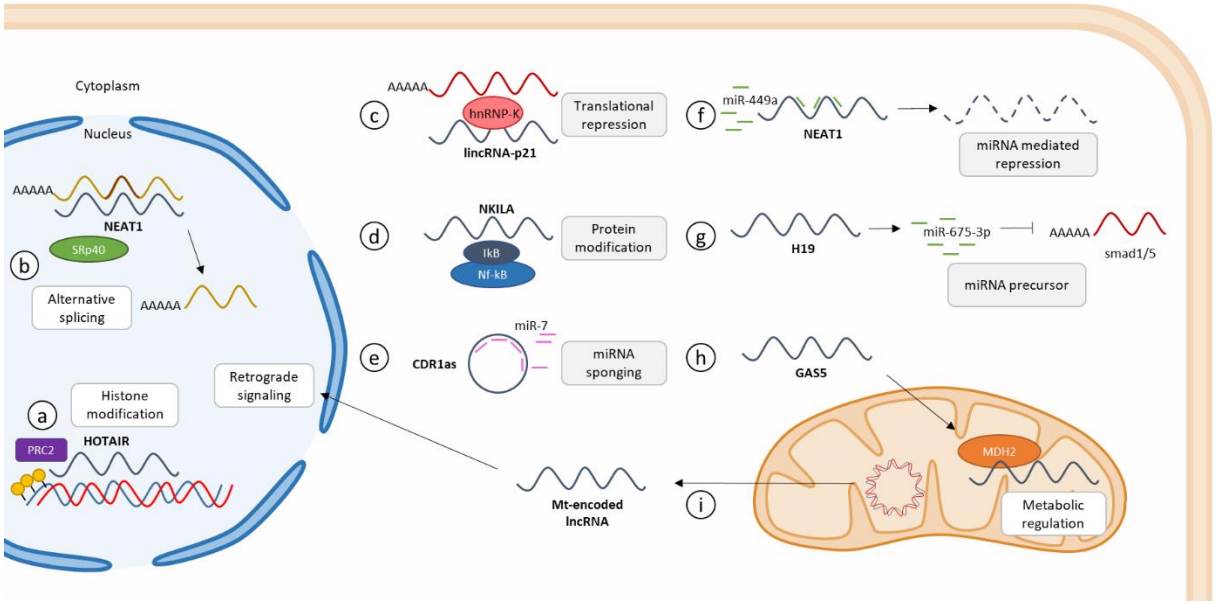

Figure 1-3 Representative examples for general functional mechanisms of lncRNA regulation in different cellular compartments. a: Transcriptional regulation by HOTAIR-mediated histone methylation via PRC2. **b:** NEAT1 scaffolding SRp40 together with mRNAs leading to regulation of alternative splicing. **c:** lincRNA-p21 functions as transcriptional repressor, binding hnRNP-K together with an mRNA. **d:** NKILA binding the NF-κB complex inhibits phosphorylation of IkB leading to loss of NFkB activation. **e:** CircRNA CDR1as contains miR-7 target sequences, functioning as miRNA sponge. **f:** NEAT1 is degradated after miR-449a binding. **g:** LncRNA H19 serves as a precursor RNA for several miRNAs, such as miR-675-3p. **h:** GAS5 is able to enter the mitochondria, binding MDH2 protein influencing the TCA flux and cellular metabolism. **i:** mitochondrial genome encoded lncRNAs can traffic between mitochondria and nucleus, functioning in retrograde signaling. Modulated after (Karger et al. 2021)

Nuclear lncRNAs for example are known to regulate gene expression e.g. through chromatin modification, such as the HOX antisense intergenic RNA (HOTAIR). HOTAIR is highly expressed in NSCLC tissue and recruits the PRC2 complex, leading to histone methylation and transcriptional repression (Tsai et al. 2010). Nuclear paraspeckle assembly transcript 1 (NEAT1) is localized in nuclear speckles, and associates with SRp40, affecting alternative splicing of transcripts (Cooper et al. 2014). Cytoplasmatic RNAs can affect gene expression on the post-transcriptional and post-translational level. LncRNA 1/2-sbs-RNA binds to BACE1-AS-mRNA, increasing its stability and enhancing expression while lincRNA-p21 binds to a target mRNA sequence, and enhances interaction with the post-transcriptional repressor RCK and FMRP, consequently inhibiting translation (Rashid, Shah, and Shan 2016). Other lncRNAs can interact with proteins and influence protein modification. For example, lncRNA NKILA binds to the NF-κB complex and represses phosphorylation of IκB, thus inhibiting NF-κB activation (Liu, Sun, et al. 2015). Additionally, lncRNAs and miRNAs can influence each other due to their possible sequence complementarity. For instance, lncRNAs can contain binding sequences and function as miRNA sponges, serving as endogenous

competitors for miRNA–mRNA binding, thereby interfering with the miRNA-targeted degradation of a specific mRNA (Hansen et al. 2013). As endogenous competitors, LncRNAs can have the form of a circular RNA (circRNA), a newly identified class of RNAs that are predominantly localized in the cytoplasm of cells. CircRNA CDR1as for instance, contains 74 binding sequences for miR-7 (Memczak et al. 2013). On the other hand, miRNAs can regulate the stability of lncRNAs by binding to them and causing degradation. This is the case with miR-449a in lung cancer, which binds to NEAT1 to inhibit the lncRNA-function (Hansen et al. 2013). It has also been found that lncRNA transcripts can serve as precursors for miRNAs, such as lncRNA H19, which gives rise to miR-675-5p and miR-675-3p that inhibit smad1 and smad5, among others (Dey, Pfeifer, and Dutta 2014). More recently, several mitochondrial lncRNAs were identified as regulators of cellular metabolism. Some examples are nuclear-encoded lncRNA growth arrest specific 5 (GAS5) that enters the mitochondria, binds to MDH2, and regulates TCA flux under stress conditions (Sang et al. 2021), or even mitochondrial genome-encoded lncRNAs, which are mostly described as sending retrograde signals to the nucleus (Zhao, Sun, et al. 2018).

1.4.2.2 Antisense lncRNAs

The category of overlapping lncRNAs describes, as mentioned before, lncRNAs which are encoded in the genome overlapping another protein coding gene. These overlapping lncRNA genes can be transcribed on the same strand (sense) or the opposite strand (antisense) to the protein-coding gene (Liu et al. 2021). Antisense lncRNA transcripts have often been described to be localized in the nucleus and regulate gene expression on transcriptional level e. g., through interaction with the promotor region and recruitment of chromatin-modulating proteins, thereby influencing transcriptional activity (Kopp and Mendell 2018). *Cis*-acting lncRNAs regulate expression of their antisense protein-coding gene and *trans*-acting antisense lncRNAs regulate gene expression of genes in other genomic locations (Pelechano and Steinmetz 2013). However, antisense lncRNAs can also be located in the cytoplasm where they regulate through various other mechanisms, such as binding to mRNAs and influencing the RNA stability, inducing alternative splicing process, or acting as a “miRNA sponge” by binding miRNAs to inhibit their function (Zhou et al. 2021).

1.4.2.3 Role of lncRNAs in Cancer

Given the abilities of lncRNAs to control all kinds of processes within the cell, it is not surprising that disruption can lead to aberrant gene expression and is associated with multiple diseases, especially cancer. In previous years, more and more lncRNAs have been found to

regulate the occurrence and progression of many aspects of tumors by targeting genomic mutations, DNA damage repair, metabolic disorders, EMT or cancer cell stemness.

Accumulation of DNA damage plays an important role in cancer development. By regulating proteins that are involved in DNA damage repair or stress response, lncRNAs can influence the mutational burden of cells. For example, lncRNA MEG3 activates p53 to trigger its tumor suppressive function (Zhou et al. 2007) or lncRNAs CUPID1 and CUPID2, which are associated with progression of breast cancer, modulate the DNA damage response (Betts et al. 2017). Another hallmark of cancer, cellular metabolic disorders, can be regulated by lncRNAs. It has been shown that under energy stress, lncRNA NBR2 activates AMPK via direct binding, and absence of this lncRNA leads to changed metabolism and subsequently enhances tumor cell proliferation (Liu et al. 2016). Furthermore, Metastasis Associated Lung Adenocarcinoma Transcript 1 (MALAT1) has been extensively investigated for its function in tumorigenesis in NSCLC by promoting EMT and enhancing tumor progression and metastasis through the miR-124/STAT3 axis (Ji et al. 2003; Peranzoni et al. 2018; Zhou et al. 2015). Additionally, HOTAIR is known to promote metastasis, such as in breast cancer, liver cancer, and pancreatic cancer by activating the SMAD cascade signaling pathway, which induces EMT (Gupta et al. 2010; Padua Alves et al. 2013; Kim et al. 2013; Ren et al. 2018). Cancer stemness is another important factor for tumor metastasis since cancer cells with high stemness are able to survive and colonize other tissues. Several studies have shown that lncRNAs are involved in signaling pathways associated with stemness. In liver cancer cells, two lncRNAs, lncBRM and lncSOX4, have been shown to participate in self-renewal of liver cancer cells through the YAP1 and the STAT3 pathway (Chen, Huang, et al. 2016; Zhu et al. 2016). Altogether, lncRNAs have been shown to play a pivotal role in tumorigenesis, tumor progression and metastasis.

1.4.2.4 Role of lncRNAs in Immunity, Inflammation and the TME

Although lncRNAs have been extensively investigated through the years, their role in immunity and inflammatory response is still not completely understood. The immune system consists of various cell types that mediate responses to infections while maintaining tissue homeostasis (Chen, Ao, and Yang 2019; Mowel et al. 2018). Several studies revealed that lncRNAs can influence proliferation, differentiation, and activation of immune cells such as monocytes, macrophages, dendritic cells (DCs), neutrophils, T cells and B cells.

LncRNA-DC for instance, specifically expressed in DCs, can bind to STAT3, preventing the binding of phosphatase SHP1, therefore promoting STAT3 phosphorylation. Knockdown of lncRNA-DC was shown to impair DC differentiation *in vitro* and *in vivo*, indicating that lncRNAs can function as key immunomodulators (Wang et al. 2014). Furthermore, linc-Ccr2-5'AS is a Th2 associated lncRNA that regulates expression of the Th2 genes in immune cells

and has the ability to influence recruitment of Th2 cells to the lung (Gutschner et al. 2013). Additionally, RNA sequencing analysis revealed a large number of lncRNAs specifically expressed in CD8+ and CD4+ T cells (Pang et al. 2009; Xia et al. 2014), suggesting a potential role in those cells. LncRNA Lethe has been shown to be highly expressed in mouse embryonic fibroblasts, influencing NF-κB-dependent inflammatory response (Rapicavoli et al. 2013).

Within the TME, lncRNAs can act as modulators and communicators between immune cells and tumor cells. CASC2c was identified to regulate macrophage infiltration and polarization in glioblastoma by negatively regulating the expression of coagulating factor X (Zhang et al. 2018). MYC-regulated lncRNA NEAT1 was found to promote diffuse large B cell lymphoma proliferation via the miR-34b-5p-GLI1 axis (Qian et al. 2020). Furthermore, lnc-EGFR was shown to promote differentiation of T reg cells by inhibiting CTL activity, enhancing tumor progression of hepatocellular carcinoma (Jiang et al. 2017). Additionally, lncRNAs were recently identified to play a role in immunotherapy. For instance, lncRNA Tim3 was shown to inhibit T cell response in hepatocellular cancer, leading to tumor immune suppression (Ji et al. 2018), and AFAP1-AS1 was shown to be co-expressed with PD-1 lymphocytes in nasopharyngeal carcinoma, leading to poor overall survival (Tang et al. 2017). However, the majority of ncRNA-research still focuses on miRNAs, while the field of lncRNAs still needs further investigation.

1.4.2.5 LncRNAs in TAMs of Lung Cancer

LncRNAs seem to be regulated in all types of immune cells as well as cancer cells. Nevertheless, only a handful of lncRNAs are described to play a role specifically in macrophages in the TME of lung cancer (Karger et al. 2021). These lncRNA transcripts include GAS5, X-inactive Specific Transcript (Xist), GNAS Antisense RNA 1 (GNAS-AS1), LincRNA-p21 and Linc00662. Among them, GAS5 is the only one described to have a tumor suppressive function with high expression in M1-like macrophages, leading to induction of pro-inflammatory response and anti-tumor activity. On the other hand, high expression of Xist, GNAS-AS1, LincRNA-p21 or Linc00662 in macrophages led to induction of the M2-like macrophage phenotype by upregulation of anti-inflammatory signals and promotion of tumor functions such as proliferation and migration. Although the underlying mechanisms still need to be further investigated, it seems that lncRNAs play a crucial role in TAMs of lung cancer.

1.4.2.6 Clinical applications and therapeutic potential of lncRNAs

Recent studies reveal the potential of RNA therapeutics as new strategy to target diseases such as COVID 19. Considering the diverse roles of lncRNAs, RNA based therapies may represent promising approaches as therapeutic options for diseases with poor outcome

with available treatment options. Until now, there are several approaches to target ncRNAs *in vivo*: small interfering RNAs (siRNAs), antisense oligonucleotides (AO) such as short hairpin RNAs (shRNAs) or LNA GapmeRs triggering RNase H mediated RNA degradation, or CRISPR/Cas9 genome editing. Small molecules such as siRNAs or AOs can be applied directly or delivered using viral vectors. Some of these methods are tested in clinical trials for diverse pathologies, such as neurological disorders or cardiovascular complications (Jiang et al. 2019; Quemener et al. 2020; Rinaldi and Wood 2018). For example, the AO based therapeutic Nusinersen was approved by the FDA to treat spinal muscular atrophy, degrading incorrect mRNA-splice forms of the survival motor neuron (SMN) gene (Rinaldi and Wood 2018; Goodkey et al. 2018). The LNA GapmeR-based AO MRG-110 is targeting miR-92a-3p and currently being tested in a phase 2 clinical trial as anti-inflammatory drug (Abplanalp et al. 2020; Poller et al. 2018). Also for cancer several clinical trials are ongoing, e.g. targeting G12D-mutated KRAS mRNA in advanced pancreatic cancer, targeting STAT3 mRNA in metastatic NSCLC or targeting HSP27 mRNA in lung cancer, metastatic bladder cancer or prostate cancer (Winkle et al. 2021). In addition, viral vector-mediated gene delivery has been tested extensively in clinical trials and did not show any safety issues or adverse effects (Ambrosi et al. 2019).

Several ncRNAs are tested as targets in clinical trials as well, however, many of those focus only on miRNAs. A search for lncRNAs in cancer at ClinicalTrials.gov reveals only a few ongoing clinical trials mainly associated with a search for biomarkers. Additionally, those trials are still in the early recruiting phase, representing how novel the field of lncRNA therapeutics still is. However, expression modulation of some lncRNAs is already investigated in several mouse models. For example, knockdown of MALAT1 by treatment with antisense AOs in lung and breast cancer mouse models revealed a reduction in metastasis *in vivo* (Gutschner et al. 2013; Arun et al. 2016). Combination of MALAT1 AO together with Bortezomib even showed high anti-tumor activity and high levels of cytotoxic effect in multiple myeloma (Amodio et al. 2018). LncRNA HOTAIR targeted by AO in ovarian and breast cancer mouse models led to reduced tumor formation and improved the survival (Ozes et al. 2017). Decreased tumor growth was also found when targeting lncRNA DANCR in a breast cancer model, AC104041.1 in head and neck squamous cell carcinoma (HNSCC) or LINC01296 in NSCLC (Li, Ding, et al. 2020; Vaidya et al. 2019; Xu et al. 2019).

The field of therapeutics with lncRNA-targets is still in the developing phase, although there are many promising targets involved in different processes of tumor development that would be worth investigating in the future. For instance, MALAT1 was described as frequently upregulated in NSCLC increasing proliferation, invasion as well as cisplatin resistance (Gutschner et al. 2013; Guo et al. 2015; Fang et al. 2018). LncRNA HOTAIR showed high expression in lung cancer and increases proliferation and invasion as well as resistance to

cisplatin, gefitinib and crizotinib chemotherapy as well as radiation therapy (Liu et al. 2013; Zhai et al. 2016; Jiang et al. 2018; Yang et al. 2018; Chen et al. 2015). Several other lncRNAs, such as H19, PVT1, ANRIL, LINC00473, LINC00963 (also MetaLnc9), or BANCR also have been reported to be upregulated in lung cancer tissue while promoting tumorigenesis (Huang et al. 2018; Guo et al. 2018; Naemura et al. 2015; Chen, Li, et al. 2016; Yu et al. 2017; Jiang et al. 2015). Additionally, some tumor suppressive lncRNAs are known to be downregulated in lung cancer, e.g. PICART1 that suppresses proliferation and induces apoptosis (Zhao, Cheng, et al. 2018), or PANDAR, which is also involved in apoptosis induction (Han et al. 2015). Other downregulated lncRNAs, such as MEG3 or GAS5 have been shown to be involved in sensitivity to therapeutic approaches (Liu, Wan, et al. 2015; Lambrou, Hatziagapiou, and Zaravinos 2020).

In conclusion, non-coding RNAs are important in tumor development, progression and cancer therapeutics. Nonetheless, the field of lncRNAs in tumors with regard to the tumor microenvironment is still very new and needs to be further investigated.

2 Aims of the study

The composition of the TME and the interaction between tumor cells and infiltrating immune cells play crucial roles in tumor progression and metastasis. TAMs are one of the most abundant cell types within the TME and, based on their immune response, gene expression, and metabolic profile, can be divided into tumor inhibiting M1-like macrophages and tumor promoting M2-like macrophages. Understanding the regulation and activation process of TAMs within the TME is extremely important to understand cancer biology and harness TAMs for novel anti-cancer strategies.

The available literature clearly shows that lncRNAs have major regulatory influence on macrophage activation as well as lung tumor progression. However, the underlying mechanisms involved in this regulation within the TME are still not fully understood. For this investigation, we set the following central aims to conduct this study (Figure 2-1):

1. Identification and validation of macrophage-specific lncRNA expression pattern in tumor promoting M2-like macrophages and TAMs
2. *In vitro* manipulation of identified lncRNAs in macrophages by different genetic strategies (knockdown/overexpression)
3. Influence of lncRNA manipulation on macrophage activation process
4. Elucidation of the underlying molecular mechanisms and signaling pathways
5. Understanding the influence of identified lncRNAs on tumor development and progression *in vitro* and in *in vivo* mouse tumor models
6. Establishment of human tumor precision cut lung slices as an *ex vivo* model to determine the clinical relevance of the study in a human system

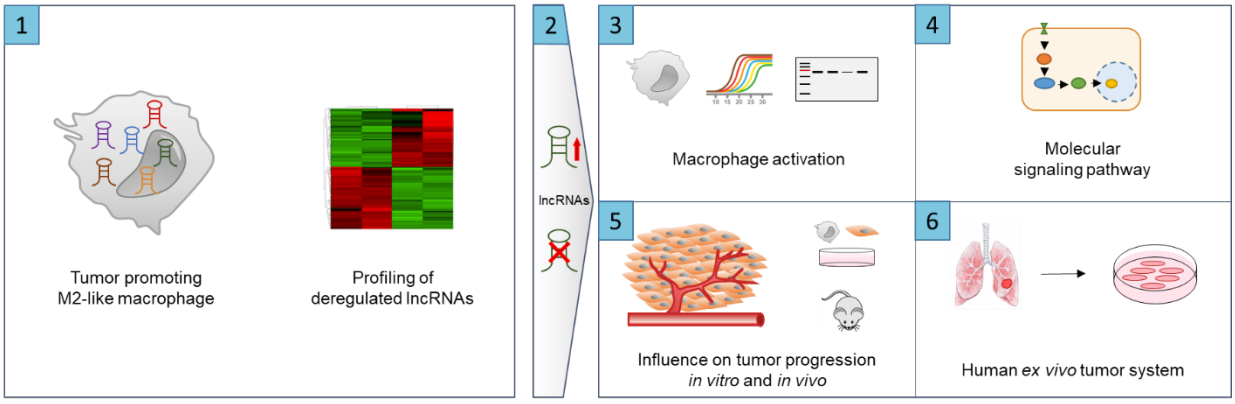

Figure 2-1 Aims of the study

3 Materials and Methods

3.1 Cell biological methods & cell culture

3.1.1 Cell cultivation

All cell lines were purchased from the American Type Culture Collection (ATCC®; Table 3-1) and incubated at 37 °C in an atmosphere of 5 % CO_2. Cells were grown in appropriate medium in 75 cm² cell culture flasks and routinely split every 2–3 days using Trypsin/EDTA.

For long-term storage cells were stored in liquid nitrogen storage tanks. For this, cells were harvested by centrifugation and the cell pellet was resuspended in 1 ml freezing medium (90 % FCS, 10 % DMSO). Thawing of cells was done by transferring the cryotube to a 37 °C water bath and adding the thawed cell suspension to the pre-warmed medium. The cells were centrifuged and the cell pellet was seeded into a new 75 cm² flask.

Table 3-1 Used cell lines.

Cell line	ATCC-No.	Media	Histological subtype
A549	ATCC® CRM-CCL-185™	DMEM	Lung Adenocarcinoma
A427	ATCC® HTB-53™	RPMI 1640	Lung Adenocarcinoma
H1650	ATTC® CRL-5883™	RPMI 1640	Lung Adenocarcinoma
THP1	ATTC® TIB-202™	RPMI 1640	Acute monocytic leukemia
HEK293T	ATTC® ACS-4500	DMEM	Embryonic kidney

3.1.2 Human macrophage generation

For generation of primary human macrophages, peripheral blood mononuclear cells (PBMCs) were isolated from buffy coats obtained from the blood bank of the Universities Giessen and Marburg Lung Center by density gradient centrifugation using Ficoll-Paque media. For this, Leucosep Centrifuge Tubes (Greiner Bio-one) were used and the blood samples together with 15 ml Ficoll-Paque media were centrifuged for 35 min at 440 g without brakes. The white layer above the filter in the separated sample containing the mononuclear cells was transferred into a new 50 ml Falcon and PBMCs were treated with erylysis buffer two times followed by two washing steps with PBS. The cell pellet was resuspended in an appropriate amount of serum free RPMI medium and the cells seeded into 6-well plates (Sarstedt, Nümbrecht, Germany). After two hours, the medium was exchanged with macrophage medium (RPMI, 2 % human serum). The following three days medium was changed every day, then every two days, to allow monocyte-to-macrophage differentiation. The density of macrophages were roughly 1×10^5 cells per well in 6-well plates.

THP1 monocytes were seeded into 6-well plates (1 × 10^6 cells/well) and treated with phorbol 12-myristate-12 acetate (PMA, 10 ng/ml) for 24 hours, which was then changed to PMA-free medium, allowing them to differentiate to macrophages for another 24 hours.

3.1.3 Macrophage polarization

PBMC derived and THP1 macrophages were activated into M1-like phenotype by stimulation of M0 macrophages with LPS (100 ng/ml; Sigma-Aldrich, Taufkirchen, Germany) and IFNγ (100 U/ml; Roche, Basel, Switzerland). PBMC derived macrophages were activated to M2-like phenotype by stimulation of M0 macrophages with IL-4 (20 ng/ml; VWR, Radnor, USA), while THP1 macrophages were activated to M2-like phenotype by treatment with of IL-4 (20 ng/µl) together with IL-13 (10 ng/ml; VWR, Radnor, USA).

Cells were incubated for 24 hours at 37 °C and 5 % CO_2 before harvest or further analysis. The samples were used for RNA Isolation (methods section 3.3.1) or whole cell extracts (methods section 3.3.5).

3.1.4 Co-culture

Co-culture of macrophages with A549 was performed using a transwell system with a 6-well layout (Sarstedt, Nümbrecht, Germany). First, 5 × 10^5 A549 cells were seeded into transwells with a pore size of 0.4 µm and left to attach to the membrane. After 20 min, transwell inserts were placed in 6-well plates containing macrophages and incubated for 24 hours (Figure 3-1).

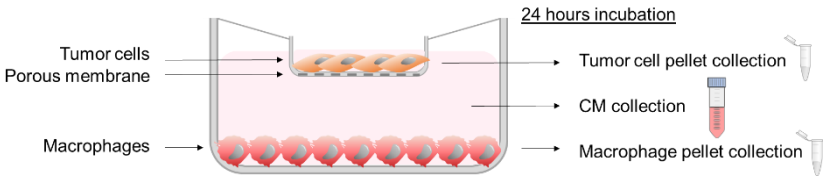

Figure 3-1 Schematic representation of indirect co-culture of macrophages with A549 cells.

A549 cells and macrophages were seeded separately as controls. After 24 hours, the supernatant (conditioned media, CM) was harvested, centrifuged, and stored at -80 °C for further experiments. Additionally, each cell type was harvested separately for RNA (methods section 3.3.1) or protein (methods section 3.3.5) isolation.

3.1.5 Transient cell transfection

Transfection of macrophages with different siRNAs (Table 3-2) or antisense LNA GapmeRs (Table 3-3) was done using the HiPerFect Transfection Reagent (Qiagen, Hilden,

Germany) in an OptiMEM serum-free medium (Sigma-Aldrich, Taufkirchen, Germany). The transfection mix was vortexed shortly and incubated for 5–10 min on RT. Meanwhile, macrophage medium was replaced with fresh medium and after incubation time, transfection mix was added dropwise on top of the cells. After 24–48 hours, CM was harvested and cells used for RNA (methods section 3.3.1) or protein isolation (methods section 3.3.5).

Table 3-2 Custom siRNAs used for knockdown of the respective gene.

Target RNA	siRNA ID	Cat. No.	Source	Final conc.
ADPGK-AS1	n513852	4392420	ThermoFisher Scientific	25 nM
MRPL15	s26457	4392421	ThermoFisher Scientific	25 nM
MRPL35	s27942	4392421	ThermoFisher Scientific	25 nM
IDH	s7119	4390824	ThermoFisher Scientific	25 nM
Negative control	-	4390843	ThermoFisher Scientific	25 nM

Table 3-3 Custom antisense LNA GapmeRs used for knockdown of the respective lncRNA.

Target RNA	Product No.	Cat. No.	Source	Final conc.
ADPGK-AS1	339511	LG00204486-DDA	Qiagen	25 nM
Negative control	339516	LG00000002-DFA	Qiagen	25 nM
	Catalog No.	**siRNA-ID**		
ADPGK-AS1	n513852	4392420	Invitrogen	25 nM
Negative control	4390843	-	Invitrogen	25 nM

3.1.6 Lentiviral stable transfection

Transduced THP1 cell lines were generated using a lentiviral vector (pLV-puro-CMV) containing the cDNA of ADPGK-AS1 purchased by VectorBuilder (#VB181004-1001qb; Chicago, USA). An empty vector was cloned as described in methods section 3.3.6 and used as negative control. Transduced A549 cells were generated using a GFP-containing pCDH-CMV plasmid, which was previously described (El-Nikhely et al. 2020).

Lentiviral particles were produced by co-transfection of HEK293T cells with lentiviral plasmid (psPAX2) and packing plasmid (pMD2.G) using TurboFect transfection reagent (Fermentas, Waltham, USA). Supernatants containing the viral particles were collected after 48–72 hours after transfection. THP1 cells were cultured in 6-well plates and transduced with the lentivirus in the presence of 6 µg/ml polybrene (Sigma-Aldrich, Taufkirchen, Germany). Medium was replaced with fresh medium containing Puromycin (Gibco, Texas, USA) 24 hours after infection.

3.1.7 Fluorescence *in situ* hybridization

RNA Fluorescence *in situ* hybridization (FISH) was used to visualize the location of lncRNA transcripts within a cell. Therefore, custom LNA detection probes modified with a red fluorescent dye were designed (Table 3-4).

Cells were grown on coverslips (Neuvitro, #H-18-1.5-PDL), rinsed briefly in 1x PBS and fixed in 4 % PFA for 7 min at RT. Fixative was removed by washing three times in 1x PBS for 1 min on a shaker. Permeabilization was performed in PBS containing 0.5 % Triton X-100 and 5 mM VRC on ice for 10 min with three following washing steps for 5 min in 1x PBS. Prior hybridization cells were rinsed once in 2x SSC buffer. Hybridization mixture was heated to 80 °C for 90 sec prior usage and hybridization was performed overnight in a slide moat (Boekel Scientific) at 37 °C in humid conditions. After incubation, cells were washed four times in 2x SSC buffer with 50 % (v/v) Formamide for 20 min at 37 °C. Coverslips were then mounted in mounting medium containing 4′,6-diamidino-2-phenylindole (DAPI). Short term, slides were stored at 4 °C, for long term storage slides were moved to -20 °C. Fluorescence signal was analyzed and representative pictures were taken by ZEISS Imager.Z1 or Leica SP8 confocal microscope.

Table 3-4 Custom antisense LNA detection probes for FISH

Target RNA	Product no.	Design-ID	Modification	Source
β-actin	300500	247370-1	5'-TYE665	Qiagen
Target RNA	**Product no.**	**Catalog no.**	**Modification**	**Source**
ADPGK-AS1	339500	LCD0165475-BKP	5'-TYE665	Qiagen

20x SSC-Buffer: 3 M Sodium Chloride, 0.3 M Sodium Citrate, pH 7.0 in DEPC treated H_2O
Hybridization mix: 10 % (v/v) Dextran sulfate, 2 mM RNase Inhibitor, 0.02 % (w/v) RNAse-free BSA, 400 µg *E.coli* tRNA, 50 % (v/v) Formamide, 2x SSC buffer, 100 µM RNA detection probe

3.1.8 Luciferase assay

We co-transfected macrophages to 6-well plates using of a Firefly luciferase construct containing the ADPGK promotor (Appendix Figure 2, see methods section 3.3.6) together with a Renilla luciferase construct and incubated the cells for 24 hours. Afterwards, we quantified luciferase activities using the dual-luciferase reporter assay system (Promega, Madison, USA) according to manufacturer's protocol using a luminescence plate reader (Tecan infinite M200 PRO). The ratio of Firefly luciferase signal to Renilla luciferase signal was calculated as previously described (Sarode, Zheng, et al. 2020).

3.2 Functional assays for cells

3.2.1 Cell proliferation assay

For proliferation assessment, 10,000 A549 cells/well or 5,000 H1650 cells/well were seeded in a 96-well plate for 24 hours, followed by starvation in serum-free medium for

24 hours. Different macrophage conditioned media (100 µl/well) were added to the cells for 24 hours and proliferation was assessed using a bromodeoxyuridine (BrdU) based cell proliferation kit (Roche, Basel, Switzerland) according to manufacturer's instructions. The BrdU assay is a colorimetric immunoassay and can be used for cell proliferation based on the measurement of BrdU incorporation during DNA synthesis. BrdU labeling solution was added to the cells and incubated for additional 90 min. For fixation, the labelling medium was removed and 200 µl/well FixDenat was added for 30 min at RT. After fixation, solution was removed by thoroughly flicking and tapping, 100 µl/well of anti-BrdU-POD solution (1:100) was added and incubated for 2 hours at RT in the dark. Antibody conjugate was removed by flicking off, wells were washed three times with 300 µl/well washing solution. Subsequently, 100 µl/well of substrate solution was added and cell proliferation was determined by measuring absorbance at 370 nm with reference wavelength at 492 nm (Tecan Infinite M200 PRO).

3.2.2 Migration assay

3.2.2.1 Boyden chamber Transwell assay

One method to analyze the migratory behavior of cells is the transwell assay. For this, we seeded 50,000 cells (A549 and H1650) in 100 µl serum free medium on membranes with pores of 8.0 µm size on the inside of cell culture inserts (Falcon™, Eschborn, Germany). After 15 min at RT cells were settled on the membranes and inserts were transferred in a 24-well plate containing 700 µl of different conditional media. The plate was incubated in a cell culture incubator for 6 hours before stopping the assay. Membranes were washed in 1x PBS and remaining cells on the inside of the insert were wiped with a cotton swab. Cells that were migrated through the pores to the outside of the inserts were fixed for 3 min in methanol and stained in 10 % crystal violet for 10 min. Inserts were washed again in ddH_2O, membranes were cut out using a scalpel and mounted on microscope slides with Pertex (Medite GmbH, Burgdorf, Switzerland). Slides were dried at RT before scanning with the NanoZoomer digital slide scanner (Hamamatsu Photonics, Japan). Numbers of migrated cells were determined using the Image-based Tool for Counting Nuclei (ITCN) plugin for ImageJ software.

3.2.2.2 Scratch assay

For scratch assay, 100,000 A549 cells/well were seeded in a 24-well plate (Sarstedt, Nümbrecht, Germany). When confluent, a "scratch" was created with a 10 µl pipet tip, cells were washed three times with 1x PBS to remove the debris and then 1–2 ml of different CM was added. To obtain the same field during the image acquisition, marks were created on the downside of the plate and used as references. After reference points were made, the plate was placed immediately under a phase-contrast microscope and images of the scratch were

captured. After 15–24 hours incubation time at 37 °C and 5 % CO_2, images were taken again with matching reference points. Gap closure was analyzed using the ImageJ software.

3.2.3 Cell death detection assay

Apoptosis rate of cells was measured by using the Cell Death Detection ELISA^{PLUS} kit (Roche, Basel, Switzerland) according to manufacturer's protocol. Here, 8,000 A549 cells/well or 10,000 H1650 cells/well were seeded in a 96-well plate and starved overnight in serum-free medium. The next day, 200 µl/well of different conditional media was added and incubated for 24 hours. Cells were then centrifuged 10 min at 500 g, supernatant was discarded and 200 µl/well of 1x lysis buffer was added for 30 min. After lysis, cells were centrifuged again for 10 min at 500 g to pellet the cell debris and 20 µl of the supernatant was transferred to a provided streptavidin coated microplate well. To each well, 80 µl of freshly prepared Immunoreagent was added and incubated on a shaker (~300 rpm) in the dark for 2 hours. The solution was removed by thoroughly tapping and washed three times by rinsing each well with 200 µl Incubation buffer. Washing solution was removed and 100 µl/well ABTS solution was added. Analysis was performed by measuring absorbance at 405 nm with a reference wavelength at 490 nm (Tecan Infinite M200 PRO).

3.3 Molecular biology & biochemical methods

3.3.1 RNA Isolation

3.3.1.1 Extraction Kit

Total RNA was isolated from cells using the RNeasy® Mini/Micro Kit (Qiagen) according to the procedure described by the manufacturer.

3.3.1.1 TRIzol Reagent

Tissues were lysed in 1 ml TRIzol (Qiagen, Hilden, Germany) and homogenized twice using Precellys® Ceramic Kit 1.4 (Peqlab, Erlangen, Germany) and Precellys homogenizer. Adherent cells were washed with PBS and directly lysed by adding TRIzol (Qiagen, Hilden, Germany). Lysates were transferred into a tube and homogenized by pipetting up and down several times with a 1 ml pipet. 200 µl Chloroform per 1 ml TRIzol was added, the tube was vortexed for 15 seconds, incubated for 2 min at RT and then centrifuged at 12.000 rpm for 15 min at 4 °C. The upper aqueous phase was then transferred into a new tube. To precipitate the RNA, 500 µl Isopropanol (100 %) per 1 ml TRIzol was added and the tube inverted 4–5 times followed by 10 min incubation time at RT. Precipitated RNA was pelleted by

centrifugation at 12,000 rpm, 4 °C for 15 min. The pellet was washed with 70 % ethanol (v/v). The dried pellet was resuspended in an appropriate amount of RNase free water. RNA concentration and purity were determined in a spectrometer (Table 3-5, ThermoFisher Scientific, Waltham, USA) and RNA was long-term stored at -80 °C.

Table 3-5 RNA measurement using a spectrometer

Concentration	1 OD(260 nm) = 40 µg RNA/ml
Purity	OD(260 nm/280 nm) = ~2.0

3.3.2 Reverse transcription

For reverse transcription of RNA into complementary DNA (cDNA) the High capacity cDNA reverse transcription kit (Applied Biosystems, Massachusetts, USA) was used according to manufacturer's protocol. The following reagents and protocol were used as described in Table 3-6 and Table 3-7. After the reaction the cDNA was diluted with sterile water and used as a template for quantitative real-time PCR (methods section 3.3.3).

Table 3-6 Reaction mix and temperature program used for reverse transcription.

Reagent	Volume [µl]
RNA template	1 µg in 10 µl
10x RT Buffer	2
10x RT Random Primer	2
dNTPs (100 mM)	0.8
MultiScribe Reverse Transcriptase (50 U/µl)	1
RNase Inhibitor (20 U/µl)	1
RNase free water	3.2

Table 3-7 Reverse transcription program

Time	Temperature
10 min	25 °C
120 min	37 °C
5 min	85 °C
∞	4 °C

3.3.3 Quantitative real time polymerase chain reaction (qRT-PCR)

The quantitative real-time PCR (qRT-PCR) method allows the relative quantification of the expression level of specific target genes between different samples. For qPCR, target gene specific oligonucleotides (Appendix Table 10-1) were designed and SYBR green was used as a reporter. This fluorescent dye intercalates with double-stranded DNA which enhances its fluorescence intensity. Thus, the signal increases during the specific amplification of the DNA

and can be detected. The reaction mix was prepared as described in Table 3-8 and qPCR was performed in a StepOnePlus Real-Time PCR cycler (Applied Biosystems, Massachusetts, USA).

Table 3-8 qPCR reaction mix.

Reagent	Volume [µl]
Template cDNA (1:20 dilution)	4
SYBR green mix (Applied Biosystems)	5
Forward primer (10 µM)	0.5
Reverse Primer (10 µM)	0.5

Experiments were performed in at least duplicates and quantitation was done using the comparative $\Delta\Delta C_T$-method. For that, data were normalized to the housekeeping gene (HPRT1) and the resulting ΔC_T values were compared to a control sample (e.g. non-tumor cells). The relative expression level was then calculated according to the following formula: $R = 2^{-\Delta\Delta CT}$.

3.3.4 RNA-sequencing analysis

For RNA sequencing, we isolated RNA from M1 and M2 polarized PBMC-derived macrophages using the miRNeasy micro Kit (Qiagen, Hilden, Germany). This was combined with on-column DNase digestion (DNase Set, Qiagen) to avoid genomic DNA contamination. RNA integrity was analyzed with BioAnalyzer 2100 (Agilent, Santa Clara, USA) and LabChip GX Touch 24 (PerkinElmer). We used total RNA (2 µg) for Truseq Stranded mRNA Library preparation following the low sample protocol and performed sequencing on the NextSeq500 instrument (Illumina) using v2 chemistry with 2 × 75 bp single-end setup.

The resulting raw reads were assessed for quality, adapter content, and duplication rates with FastQC (Andrews S. 2010, FastQC: a quality control tool for high throughput sequence data. Available online at: http://www.bioinformatics.babraham.ac.uk/projects/fastqc). Trimmomatic version 0.39 was employed to trim reads after a quality drop below a mean of Q15 in a window of 5 nucleotides (Bolger et al., Trimmomatic: a flexible trimmer for Illumina sequence data). Only reads longer than 15 nucleotides were cleared for further analyses. Trimmed and filtered reads were aligned versus the Ensembl human genome version hg38 (GRCh38) using STAR 2.7.9a with the parameters "--outFilterMismatchNoverLmax 0.1--outFilterMatchNmin 20--alignIntronMax 200000" (Dobin et al., STAR: ultrafast universal RNA-seq aligner). The number of reads aligning to genes was counted with featureCounts 2.0.2 tool from the Subread package (Liao et al., featureCounts: an efficient general purpose program for assigning sequence reads to genomic features). Only reads mapping at least partially inside exons were admitted and

aggregated per gene. Reads overlapping multiple genes or aligning to multiple regions were excluded. A combined raw count matrix was produced and the batch corrected per donor (batch 1: *_1, batch 2: *_2, batch 3: *_3) using CountClust (Dey KK, Hsiao CJ, Stephens M (2017), Visualizing the structure of RNA-seq expression data using grade of membership models, PLoS Genetics). The batch-corrected matrix was used for differential expression analysis using DESeq2 version 1.30.1 (Love et al., Moderated estimation of fold change and dispersion for RNA-seq data with DESeq2). Differentially expressed genes of M2/M1 were analyzed at log2 fold change >0.59 or <−0.59 and Benjamini-Hochberg adjusted P-value <0.05. The Ensemble annotation was enriched with UniProt data (release 08.03.2018) based on Ensembl gene identifiers (Activities at the Universal Protein Resource (UniProt). RNAseq was performed at the MPI core facility by Dr. Stefan Guenther. Bioinformatics analysis was done by Carsten Künne.

3.3.5 Protein Isolation

Tissue was lysed in RIPA buffer and homogenized as described in 3.3.1.1. Cells were washed with PBS, then harvested in RIPA buffer (SantaCruz Biotechnologies, Dallas, USA) containing proteinase Inhibitor, phenylmethylsulfonyl fluoride (PMSF) and sodium orthovanadate. Cell suspension was incubated for 15 min on ice and vortexed approximately every 3 min. Afterwards, cells were centrifuged for 15 min at 12,000 rpm and protein-containing supernatant was transferred into a fresh 1.5 ml Eppendorf Tube. Proteins were stored at -80 °C until further use.

The protein content was quantified by a modified Lowry assay using DC™ Protein Assay (Bio-Rad, Munich, Germany). Series dilution of bovine serum albumin (BSA) ranging from 0.125–2 µg/µl were used as protein standard. Samples from tissues were diluted 1:10 and samples from cells were diluted 1:5. The developed blue color was measured at 750 nm using Tecan Infinite M200 PRO microplate reader (Tecan Group Ltd, Switzerland).

3.3.6 Western blotting

Protein samples were mixed with 5x SDS sample loading buffer and boiled for 3–5 min at 95 °C. Samples were then loaded on 10–12 % SDS PAGE gels. Afterwards, gels were electrophoretically transferred to nitrocellulose or PDVF membranes (Bio-Rad, Hercules, USA) and incubated in blocking dilution (5 % non-fat milk or 5 % BSA in TBS-T) for 1 hour on RT with agitation. Membranes were incubated with primary antibody overnight at 4 °C, washed three times in TBS-T and then incubated for 1 hour with the corresponding HRP-coupled secondary antibody. Membranes were developed by addition of WesternBright™ ECL or Sirius (Advansta, California, USA) solution and imaged using the iBright 1500 system (Invitrogen,

ThermoFisher Scientific, Massachusetts, USA). Used antibodies are listed in Appendix Table 10-3.

TBS-T: 20 mM (Tris), 150 mM NaCl, 0.1 % (w/v) Tween®-20 detergent

3.3.7 Cloning

The empty vector plasmid for lentiviral transduction (Appendix Figure 1) as well as the pCDNA 3.1+ plasmid containing the ADPGK-AS1 cDNA sequence and the pGL3 luciferase plasmid containing the ADPGK promotor (Appendix Figure 2) was cloned as described in the following steps.

Restriction enzymes cut DNA at a specific sequence. Most commonly used restriction enzymes recognize and cleave a 4–7 nucleotide long sequence that is often palindromic. Analytical or preparative digestions were performed in the recommended restriction buffers. Table 3-9 gives an example of a digestions with two enzymes. After incubation of 1–4 hours at the enzyme specific temperature, the samples were analyzed by agarose gel electrophoresis and purified if necessary.

Table 3-9 Restriction enzyme digestion mix

Reagent	Volume
Plasmid DNA	1–2 µg
10x Restriction buffer	2 µl
Restriction enzyme 1 (10 U/µl)	1 µl
Restriction enzyme 2 (10 U/µl)	1 µl
ddH_2O	ad 20 µl

In order to generate the empty vector control for the pLV-CMV-ADPGK-AS1 plasmid purchased from VectorBuilder, the plasmid was incubated with NotI and PacI (NEB, Frankfurt Main, Germany) to cut out the ADPGK-AS1 cDNA sequence. After restriction, the mix was separated by agarose gel electrophoresis and the leftover plasmid backbone was purified from the gel using the GenElute Kit (Sigma-Aldrich, Taufkirchen, Germany) according to manufacturer's protocol. Empty plasmid backbone was incubated with T4 DNA polymerase (NEB, Frankfurt Main, Germany) to generate blunt ends. Afterwards, these ends were phosphorylated using the T4 polynucleotide kinase (PNK; NEB, Frankfurt Main, Germany) with addition of 10 µM ATP. Finally, ends were ligated using the T4 DNA ligase (NEB, Frankfurt Main, Germany) for 1 hour at RT in its respective buffer.

For cloning of the ADPGK-AS1 cDNA sequence into the pCDNA 3.1+ vector, PCR was done with primers flanking the ADPGK-AS1 cDNA, containing restriction sites for Acc65I

(forward primer) and NotI (reverse primer). The primer sequences can be found in Appendix Table 10-2 and the PCR reaction mix is described in Table 3-8. Simultaneously, the pCDNA 3.1+ backbone was incubated with restriction enzymes Acc65I and NotI (NEB, Frankfurt Main, Germany). The linearized plasmid as well as the PCR product were separated in an agarose gelelectrophoresis and respective bands were isolated using the GenElute Kit (Sigma-Aldrdich, Taufkirchen, Germany). ADPGK-AS1 cDNA with Acc65I and NotI compatible ends (insert) were ligated into the linearized pCDNA 3.1+-Acc65I-NotI-cut plasmid (vector) with a molar ratio from vector to insert of 1:2–1:5 using the T4 DNA ligase (NEB, Frankfurt Main, Germany).

For cloning of the ADPGK promotor region into the pGL3 basic plasmid for luciferase-based assays, primers flanking the promotor region containing restriction sites of XhoI and HindIII (Appendix Table 10-2) were used for PCR (Table 3-10) with A549 genomic DNA as template. Simultaneously, pGL3 basic plasmid was digested with XhoI and HindIII (NEB, Frankfurt Main, Germany). Both PCR product and linearized pGL3 plasmid were analyzed using agarose gelelectrophoresis, respective bands were purified and vector with insert were ligated as described before.

Table 3-10 PCR reaction mix

Reagent	Volume [µl]
DNA template	up to 1 µg
10x Reaction buffer	
25 mM $MgCl_2$	3
10 mM dNTPs	1
10 µM forward primer	2
10 µM reverse primer	2
Phusion polymerase	0.5
ddH_2O	ad 50

3.3.8 Transformation and isolation of plasmid DNA

Generated plasmids were amplified using competent *E. coli* (10-beta; NEB, Frankfurt Main, Germany), which were thawed shortly on ice and incubated with 0.2–1.0 µg plasmid DNA for 30 min on ice. Incorporation of DNA was achieved by heat shock at 42 °C for exactly 30 sec, followed by incubation on ice for 5 min. 950 µl of bacterial outgrowth medium without antibiotics was added and bacteria were cultured for 1 hour at 37 °C on a shaker. The cells were plated on LB agar plates supplemented with the respective antibiotic for the transformed plasmid and colonies were grown overnight at 37 °C. Single colonies on the plate were picked with a pipette tip and added to LB medium supplemented with the respective antibiotic in bacterial growth flasks. Bacterial culture was grown overnight at 37 °C on a shaker and

subsequently was used for plasmid isolation using the Mini, Midi or Maxi Kit (Qiagen, Hilden Germany) according to manufacturer's protocol and resuspended in TE buffer (10 mM Tris-HCl, 1mM EDTA, pH 8.0). Concentration of plasmid DNA was quantified by measuring the optical density (OD, Table 3-11). Plasmid DNA was stored at -20 °C.

Table 3-11 RNA measurement using a spectrometer

Concentration	1 OD(260 nm) = 50 µg dsDNA/ml
Purity	OD(260 nm/280 nm) = ~2.0

3.3.9 Subcellular Fractionation

A subcellular fractionation is a method to separate the cytoplasm and nucleus. For this, cells were washed with cold PBS and transferred into a 1.5 ml Eppendorf Tube. The cell pellet was resuspended in 200 µl of buffer A and incubated on ice for 15 minutes. After adding 15 µl IGEPAL (10 % v/v) the samples were vortexed for 10 seconds and centrifuged for 10 minutes at 4.000 rpm. The supernatant containing the cytoplasmatic fraction was transferred into a new 1.5 ml Eppendorf Tube and lysed in TRIzol. The pellet containing the nuclei was washed once with buffer A and then also lysed in TRIzol with half the amount of volume that was added to the cytoplasmatic fraction. For fractionation of cytoplasm and mitochondrial fraction, mitochondrial isolation Kit (Abcam, #ab110170) was performed using 2.0-ml dounce homogenizer (VWR, Radnor, USA) according to the manufacturer's instructions.

Buffer A: 10 mM HEPES (pH 7.9), 10 mM KCl, 0.1 mM EDTA, 0.1 mM EGTA, 1 mM, β-Mercaptoethanol, one drop PMSF

3.3.10 RNA Pulldown

3.3.10.1 In vitro transcription

RNA Pulldown is a method for identification of interacting proteins. RNAs were transcribed *in vitro* by using pCDNA3.1+ plasmids containing the respective lncRNA sequence (see cloning, 3.3.6), which was linearized with a ScaI (single cutter, not present in ADPGK-AS1 cDNA sequence) beforehand. *In vitro* transcription was performed using the NEB HiScribe T7 Quick High Yield RNA Synthesis Kit according to manufacturers' protocol. The transcribed RNA was then isolated using the RNeasy Mini Kit (methods section 3.3.1.1) and stored at -80 °C until used in further experiments.

3.3.10.2 Biotinylation

For pulldown of the RNA with streptavidin beads, *in vitro* transcribed RNA needs to be conjugated with biotin. Biotinylation was performed using the 3'-end biotin labeling Kit from Pierce according to manufacturers' protocol. Afterwards, RNA was again isolated, eluted in 20 µl RNase free water and then used for RNA folding.

3.3.10.3 RNA folding

In vitro transcribed biotinylated RNAs need to be folded in a correct way to obtain the specific secondary structure. For this, 3 µg RNA was adjusted with RNA folding Buffer to 100 µl and heated up to 90 °C for 2 min. Subsequently, samples were incubated 3 min on ice and 25 min on RT. The samples can be stored at -20–-80 °C or shortly kept on ice before proceeding with the pulldown (3.3.10.4).

RNA folding Buffer: 20 mM Tris-HCl pH 7.5, 100 mM KCl, 10 mM $MgCl_2$, 20 U RNase Inhibitor

3.3.10.4 RNA pulldown

RNA pulldown was performed by incubation of 10 pmol biotinylated RNA with macrophage whole cell lysate (preparation see 3.3.5) in a head over tail rotator on 4 °C for 3 h–overnight. Formed RNA-protein complexes were then crosslinked by UV light exposure for 90 sec. 80 µl streptavidin beads were equilibrated by washing three times with dilution buffer, then added to the samples and further incubated for 1 hour at 4 °C on a head over tail rotator for pulldown of the crosslinked RNA-protein-complexes. After incubation, the beads were washed four times for 10 min in 500 µl dilution buffer at 4 °C on a head over tail rotator. The last washing step was performed in dilution buffer without addition of detergents or proteinase inhibitor and beads were transferred into a new 1.5 ml Eppendorf tube. Samples were centrifuged, supernatant was discarded and the beads were frozen at -80 °C for subsequent mass spectrometry. Mass spectrometry was carried out by Dr. Ilka Wittig at the functional proteomics facility, Goethe University Frankfurt.

As a control, TRIzol was added and RNA isolation with following cDNA synthesis and qPCR for the respective lncRNAs was performed.

Dilution Buffer: 20 mM Tris-HCl pH 7.4, 150 mM NaCl, 2 mM EDTA pH 8.0, 0.5 % Triton X-100, Proteinase Inhibitor, PMSF

3.3.11 Metabolome measurement (LC-MS/MS)

Cell samples were lysed in ice-cold 85 % methanol (10 µL/mg) with two freeze-thaw cycles. Medium samples were directly processed. The homogenate or culture medium was centrifuged (15,000 g, 5 minutes, 4 °C). An equal volume of supernatant was collected, an isotope labeled internal standard mix was added, and the samples were evaporated to dryness in a Concentrator Plus (Eppendorf, Wesseling-Berzdorf, Germany). Samples were reconstituted in 50 µL water + 0.5 % formic acid, transferred to autosampler vials and subsequently analyzed via liquid chromatography coupled to tandem mass spectrometry (LC-MS/MS). Negative ionization ESI-LC MS/MS was performed on an Agilent 1290 Infinity LC system (Agilent, Waldbronn, Germany) coupled to a QTrap 5500 mass spectrometer (Sciex, Darmstadt, Germany). Ion source parameters were as follows: CUR 30 psi, CAD medium, Ion Spray Voltage - 4500 V, TEM 400 °C, GS1 45 psi, GS2 25 psi. TCA metabolites were identified with authentic standards and/or via retention time, elution order from the column and 1-2 transitions. For quantification, specific MRM transitions for every compound were normalized to appropriate isotope labeled internal standards. Reversed-phase LC separation was performed by using a Waters Acquity UPLC HSS T3 column (150 mm × 2.1 mm, 1.8 µm). Compounds were eluted with a flow rate of 0.4 ml/min and with the following 10 min gradient: 2 % B for 1.5 min, a 3 min gradient to 100 % B, a cleaning and equilibration step. Solvent A consisted of 100 % water containing 0.5 % formic acid and solvent B consisted of 100 % methanol containing 0.5 % formic acid. Column oven temperature was set to 40 °C, and the autosampler was set to 6 °C. Injection volume was 2.5 µL. Measurements were done at the metabolomics core facility at the University Hospital Frankfurt/Goethe University by Dr. Stephan Klatt and Dr. Sven Zukunft.

3.3.12 *In vitro* transcription with following *in vitro* translation

For *in vitro* transcription and translation, pCDNA3.1+ plasmids were used containing the cDNA of ADPGK-AS1. The TnT quick-coupled transcription/translation system (Promega, Madison, USA) and transcend nonradioactive translation detection system was used to *in vitro* transcribe and translate the full-length lncRNA from the T7 promoter of a pcDNA3.1+ plasmid per the manufacturer's instructions. Following completion of the transcription/translation reaction, 1 µL of the reaction product was added to 15 µL of SDS sample buffer, heated for 2 min to 100°C to denature the proteins, and then loaded onto a 4–12 % 1-mm 15-W NuPage SDS–polyacrylamide gel (Life Technologies). Protein products labeled with the biotinylated Transcend tRNA were detected with Western Blue reagent (Promega, Madison, USA) per the manufacturer's instructions. The luciferase T7 control DNA plasmid supplied with the TnT quick-coupled transcription/translation system was used as a positive control.

3.3.13 Seahorse

To measure oxygen consumption rate, 80,000 THP1 cells per well were seeded in RPMI medium containing PMA on a 96-well seahorse XF cell culture plate (Agilent, Santa Clara, USA). After 24 hours, medium was replaced with fresh medium without PMA and again incubated for 24 hours. Afterwards, oxygen consumption rate was analyzed using the Agilent Seahorse XF Analyzer.

3.3.14 Enzyme activity assay

Enzyme activity staining on tissue sections was carried out as described before (Miller et al. 2017). Specific buffers were prepared as follows: For lactate dehydrogenase (LDH) or IDH assay the buffer was 0.1 Tris-Maleate buffer pH 7.5, for succinate dehydrogenase (SDH) activity assay it was 0.1 M Tris-HCl buffer pH 8.0. In the enzyme specific buffers, 10 % polyvinyl alcohol was dissolved at 60 °C under stirring until the mixture was clear. Enzyme specific assay media was prepared including negative control reactions with additional 200 mM sodium oxamate (LDH inhibition), 100 mM oxaloacetic acid (IDH inhibition) or 250 mM malonic acid (for SDH inhibition). Assay medium containing the enzyme-specific substrates was applied to cover the whole tissue section/cell slide. Enzyme reactions were carried out at RT for around 15 min or until high staining was visible and stopped by removal of the incubation medium by washing with PBS. Tissue sections/cell slides were mounted directly or used for following antibody staining.

3.3.15 ATP determination

For determination of ATP production, ATP Determination Kit (ThermoFisher Scientific, Waltham, USA) was used according to manufacturer's instructions. 1×10^6 THP1 cells were seeded into 6-well plates and differentiated to macrophages. 90 µl of THP1 macrophage whole cell extract was mixed with 10 µl reaction solution containing D-luciferin and a Firefly luciferase. Subsequently, luminescence was measured using a fluorescence plate reader (Tecan Infinite M200 PRO).

3.3.16 Mitochondrial membrane potential

1×10^6 THP1 cells were seeded into 6-well plates and differentiated to macrophages prior analysis of mitochondrial membrane potential using the JC-1 mitochondrial membrane potential assay kit (Abcam, Cambridge, UK) according to manufacturer's instructions. Cells were collected, washed in 1x dilution buffer, and resuspended in JC-1 working solution. After 30 min incubation time at 37 °C in the dark, cells were washed with 1x dilution buffer and

resuspended in 1x supplemented dilution buffer. 200,000 THP1 cells/well were seeded into a dark 96-well plate and analyzed with a fluorescent plate reader (Tecan Infinite M200 PRO) with an excitation wavelength at 535 ± 17.5 nm and emission wave length at 530 ± 15 nm. Afterwards, cells were transferred in a transparent well-plate, shortly centrifuged and JC-1 staining analyzed with a fluorescence microscope (Keyence, Osaka, Japan).

3.3.17 MitoSOX ROS staining

Reactive oxygen species (ROS) formation in THP1 macrophages was determined using the MitSOX™ red mitochondrial superoxide indicator (Invitrogen, Waltham, USA) according to manufacturer's instructions. THP1 macrophages were grown on cover slips and treated with 5 µM MitoSOX reagent working solution for 10 min at 37 °C. Subsequently, coverslips were washed three times with warm 1x PBS, then imaged using a fluorescence microscope (Keyence, Osaka, Japan).

3.3.18 Cytokine array

Cells were seeded in 6-well plates and after 24 hours of culture, supernatant was harvested and centrifuged to discard remaining cell debris. For Cytokine array (R&D systems, Minneapolis, USA) 500 µl of supernatant was used and the array was performed according to manufacturers' protocol. ImageJ was used for quantification and analysis.

3.4 Histological techniques

3.4.1 Haematoxylin & Eosin (H&E) staining

H&E staining is based on two different chemicals. Haematoxylin stains cell nuclei in a dark purple, whereas Eosin stains cytoplasm as well as extracellular matrix in different shades of pink. For H&E staining of cryo sections, tissue sections were thawed for 10 min on RT and then fixed for 20 min in Aceton/Methanol (1:1) at -20 °C. After additional 10 min at RT, slides are washed 5 min in distilled water and then stained with Haematoxylin (Mayer) for 20 min. Slides are washed again for 5 min in flowing water, placed in Ethanol (96 %) for 1 min, then stained with Eosin for 4 min. Afterwards, slides are rinsed with water and placed two times for 2 min in Ethanol (96%), then two times Ethanol (99,8 %) for dehydration. Slides are placed three times for 5 min in Xylol, then mounted with coverslips using Entellan mounting medium (Merck Millipore, Germany).

3.4.2 Immunohistochemistry/Immunofluorescence

Immunofluorescence staining visualizes proteins in eukaryotic cells or tissue. For this, cells on cover slips (200,000 THP1 macrophages), frozen tissue sections or fresh precision cut lung slices (PCLS) were used. All steps are carried out on a shaker.

Cells on cover slips and tissue sections were fixed with 4 % PFA for 10 min at RT. PCLS were fixed in 1 % PFA overnight at 4 °C. After fixation, cells, slides, and tissues were washed three times with 1x PBS for 5 min, then permeabilized with 0.3 % Triton X-100/PBS for 10 min (cells, tissue sections) or 30 min (PCLS) at RT and blocked in 5 % bovine serum albumin (BSA)/PBS for 1 hour at RT. Subsequently, first antibody (in 1 % BSA/PBS) was added to the cells, sections or tissues and incubated at 4 °C overnight. After washing three times in 1x PBS, secondary fluorochrome-conjugated antibody (in 1 % BSA/PBS) was incubated for 1 hour at RT and then again washed three times in 1x PBS. Finally, cells and tissue sections were mounted with mounting medium containing DAPI and stored at 4 °C until imaging. For PCLS, DAPI was stained separately for 15 min at RT using DAPI (10 mg/ml; Invivogen, San Diego, USA) in a 1:500 dilution in 1x PBS. After washing two times with 1x PBS, PCLS was stored in 1x PBS at 4 °C until imaging. Imaging was done using either wide field microscopy (Keyence, Osaka, Japan) or confocal microscopy (LSM 710, Zeiss, Jena, Germany; SP8, Leica, Wetzlar, Germany). All used antibodies can be found in Appendix Table 10-3.

3.5 Precision cut lung slices

For preparation of precision cut lung slices (PCLS), human lung lobes (healthy or lung tumor-bearing) were filled through an open bronchus/artery with 1 % low melting agarose (Sigma, Missouri, USA) in DMEM/F12 medium without any additive. All tissues were obtained from the Universities Giessen and Marburg Lung Center (UGMLC) and use for experiments was approved from ethics committee (AZ 58/15). After inflation of the whole lobe the entry opening was closed and the lobe placed on ice to cool down and solidify the agarose. The filled lung lobe is cut in smaller pieces and embedded in 4 % agarose in 1x PBS, then cut into 300–400 µm thick sections using a VT1200S vibratome (Leica, Wetzlar, Germany). Slices are cultured in PCLS culture medium (DMEM F12 with 10 % FCS, 1 % Penicillin/Streptomycin, and 0.1 % Amphotericin) and further used for experiments.

3.5.1 Seeding of cells on PCLS

PCLS was distributed in an appropriate density in 8-well chambers or 48-well plates. Medium was removed and 60,000–100,000 A549-GFP cells in 30 µl per PCLS were seeded

carefully on top. When co-seeded with THP1, an equal number of THP1 cells were resuspended in 30 µl medium containing PMA and added on top of the PCLS.

Cells were allowed to settle down by incubation under the cell culture hood with closed lids to prevent drying. After 30–60 min, either macrophage CM or PCLS culture medium was added, and PCLS were used for experiments. Treated PCLS were cultured 24–48 hours before fixing with 1 % PFA overnight at 4 °C. After fixation, PFA was removed and PCLS were stored in 1x PBS at 4 °C until further use.

3.5.2 EdU staining

For detection of proliferation, 20 µM of 5-ethynyl-2'-deoxyuridine (EdU) was added to the PCLS and incubated overnight in the cell incubator. EdU is a thymidine nucleoside analog and is incorporated into the DNA during replication. After incubation, PCLS was fixed in 1 % PFA overnight at 4 °C, permeabilized in 0.3 % Triton X-100/PBs for 30 min at RT, and incorporated EdU was stained following the instruction of the Click-iT™ EdU cell proliferation kit (ThermoFisher Scientific, USA). PCLS was either used for further immunofluorescence staining as described in 3.4.2 or directly imaged using Leica SP8 confocal microscopy.

3.5.3 TUNEL assay

Fixed PCLS were permeabilized with 0.3 % Triton X-100/PBS for 30 min at RT. Apoptotic cells were stained using the *in situ* cell death detection kit (Roche, Basel, Switzerland) following manufacturer's protocol. Stained cells were imaged with Leica SP8 confocal microscopy.

3.6 Animal experiments

3.6.1 Mouse lines

NOD.Cg-Prkdcscid Il2rgtm1Wjl/SzJ: NSG

Also known as NOD-scid IL2Rgammanull, NOD-scid IL2Rgnull, NSG, NOD scid gamma

These mice are most often referred to using their branded name "NSG™" and are severely immunodeficient. The mice carry two mutations on the NOD/ShiLtJ genetic background: severe combined immune deficiency (*scid*) and a complete null allele of the IL2 receptor common gamma chain ($IL2rg^{null}$). The *scid* mutation is in the DNA repair complex protein *Prkdc* and renders the mice B and T cell deficient. The $IL2rg^{null}$ mutation prevents cytokine signaling through multiple receptors, leading to a deficiency in functional NK cells. The severe immunodeficiency allows the mice to be humanized by engraftment of human

CD34+ hematopoietic stem cells (HSC), peripheral blood mononuclear cells (PBMC), patient derived xenografts (PDX), or adult stem cells and tissues. The immunodeficient NSG mice enable research in human immune function, infectious disease, diabetes, oncology, and stem cell biology.

We maintained all mice under specific pathogen-free conditions and handled them in accordance with the guidelines of European Union Commission on Laboratory animals. NSG mice were obtained from Jackson Laboratory (Bar Harbor, USA). All the animal experiments were performed at the Max Planck Institute for Heart and Lung Research (Bad Nauheim, Germany), and were approved by local authorities (Proposal Number B2/1225, Regierungspräsidium Darmstadt, Hessen, Germany).

3.6.2 Subcutaneous mouse model of lung cancer

This model was used to monitor primary tumor growth of A549 cells under the influence of different macrophage phenotypes. Briefly, 1×10^6 A549 cells together with 1×10^6 macrophages (PBMC derived, *in vitro* polarized and transfected with antisense LNA GapmeRs) were subcutaneously injected (24g needle, 0.55 x 25 mm, Neolus) into NSG mice. Tumor growth was measured every 4 days with a digital caliper. At day 40, mice were sacrificed and tumor, lung, liver and spleen were harvested and analyzed regarding weight, FACS, immunohistochemistry or molecular biology techniques.

3.7 Statistical analysis

Statistical analysis was performed with Prism 8 Software (GraphPad Software Inc., San Diego, USA). Student's *t* test (two-tailed) was used to compare two groups. For more than two groups, differences among the groups were determined by one-way ANOVA with Tukey's posttest for unpaired non-parametric variables. Data are expressed as mean ± SEM; statistical significance was set at $p \leq 0.05$. Significance level is noted as follows: **$p \leq 0.05$, **$p \leq 0.01$, ***$p \leq 0.001$.

4 Results

4.1 M2 macrophages show tumor promoting capabilities and induces specific lncRNA expression profile

4.1.1 Characterization of macrophage phenotypes

Macrophages are very plastic and known for their ability to be activated into M1-like or M2-like phenotype that vary in gene expression, metabolic regulation and their influence on tumor cells. PBMC-derived macrophages can be polarized into M1-like by treatment with LPS and IFNɣ or into M2-like by stimulation with IL-4. Since these phenotypes look morphologically similar, effective polarization was checked by expression analysis of M1 marker genes such as TNFα, IL-8, CCR7, IL-1β, IL-12 and M2 marker genes such as CD206, CSF-1R, IL-10 and ALOX15 (Fig 4-1 a). Further, A549 cells treated with CM of these M1-like and M2-like macrophages showed increased apoptosis with M1-like CM (Figure 4-1 b) and higher proliferation, increased migration and gap closure with M2-like CM (Figure 4-1 c-e).

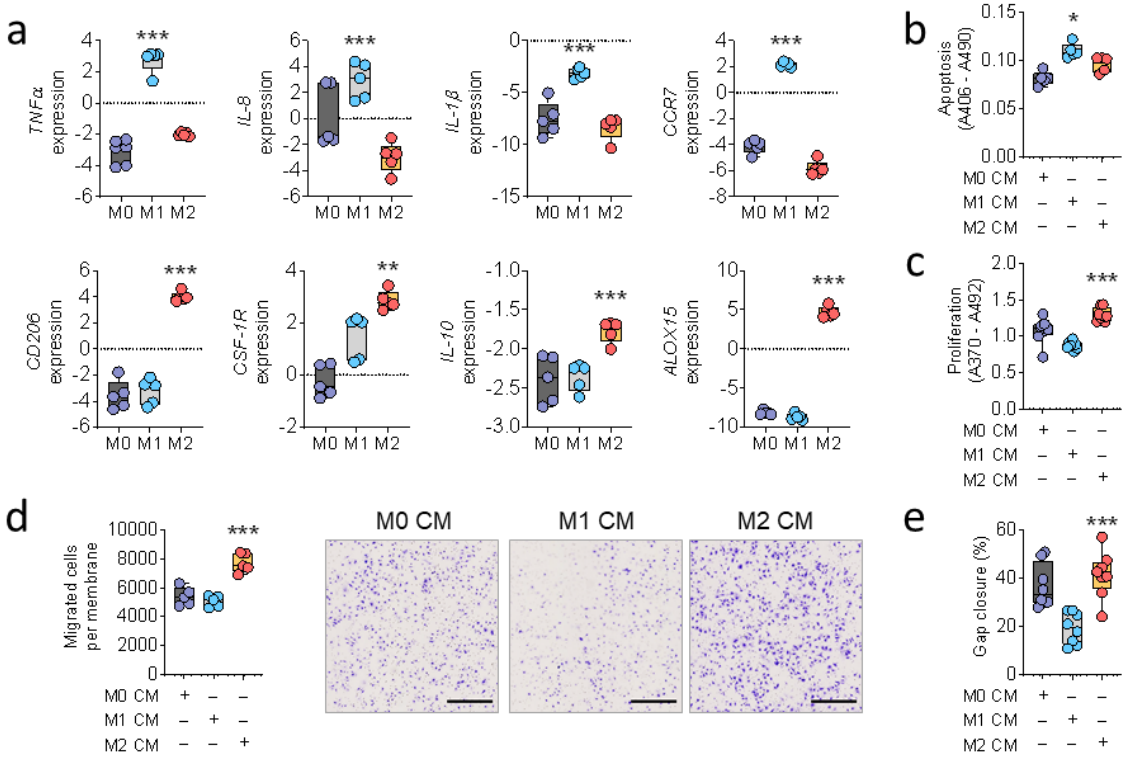

Figure 4-1 PBMC-derived macrophage phenotypes can be distinguished by distinct marker gene expression and have an influence on tumor cell functional assays. a: mRNA expression analysis of macrophage activation marker in macrophages treated either with LPS/IFNɣ (M1-like) or IL-4(/IL-13) (M2-like) or untreated (M0). n = 5 **b-e:** Cell death detection (apoptosis) assay, BrdU incorporation (proliferation) assay, boyden chamber transwell (migration) assay and wound healing assay of A549 cells treated with macrophage M0, M1-like or M2-like CM. scale bar = 400 µm, n = 5 Data are represented as mean ± SEM, **p≤0.01, ***p≤0.001 compared to M1-like or M2-like

In addition, we used a human monocytic cell line (THP1), differentiated them into macrophages and activated them to the respective phenotypes with cytokines. Our results (Figure 4-2 a-d) demonstrate that the THP1 cell line behaves similarly to primary PBMC-derived macrophages and can be used to study the different macrophage phenotypes in context of the lung tumor microenvironment.

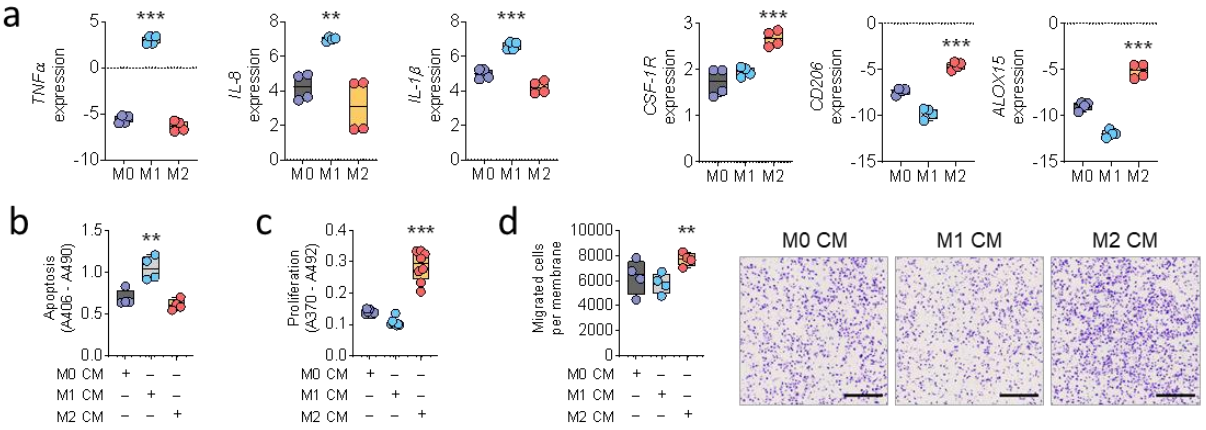

Figure 4-2 THP1 macrophage phenotypes. a: mRNA expression analysis of macrophage activation marker in macrophages treated either with LPS/IFNɣ (M1-like) or IL-4/IL-13 (M2-like) or untreated (M0). n = 4 **b-d:** Cell death detection (apoptosis) assay, BrdU incorporation (proliferation) assay and boyden chamber transwell (migration) assay of A549 cells treated with macrophage M0, M1-like or M2-like conditioned medium. n = 4. scale ba r= 400 µm. Data are represented as mean ± SEM, **p≤0.01, ***p≤0.001 compared to M1-like or M2-like

4.1.2 RNA sequencing analysis show deregulated long non-coding RNAs in M1 and M2 macrophages

To find out which lncRNAs could be involved in macrophage activation process, RNA from PBMC-derived and activated M1-like and M2-like macrophages was isolated and RNA sequencing was performed. Whole transcriptome analysis revealed 18,032 expressed genes in both phenotypes, of which 13,487 genes were protein-coding and 4,545 genes non-coding (Figure 4-3 a). Non-coding genes were further subdivided into long non-coding RNAs (≥200 bp), out of which 407 were differentially expressed genes (DEGs), and other non-coding RNAs (<200 bp), such as miRNAs or snoRNAs. Due to our aim of studying tumor associated macrophages, which inherit mainly the M2-like phenotype, we further focused on M2-like upregulated lncRNAs. The top 40 upregulated lncRNAs in M2-like macrophages were analyzed regarding several criteria (Figure 4-3 b-c) including transcript size, histone marks at the promotor region and the available literature. We chose six upregulated lncRNA candidates and validated the expression in M2-like macrophages via qPCR using two different primer pairs (Figure 4-3 d).

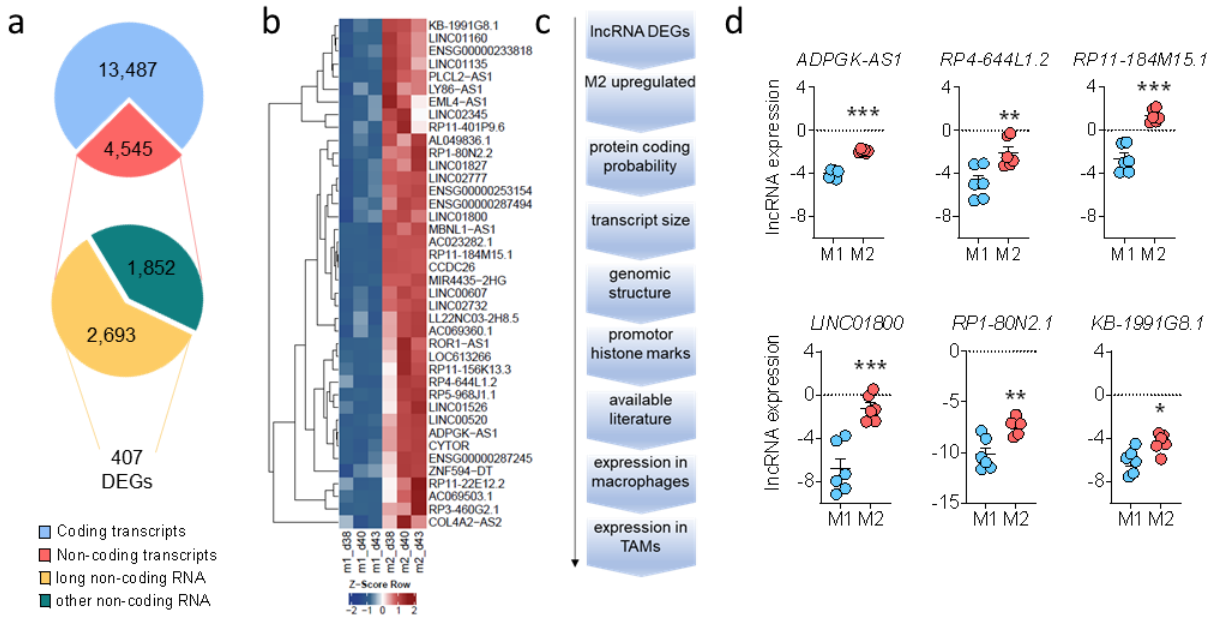

Figure 4-3 RNA sequencing of M1-like and M2-like macrophages reveal aberrant lncRNA gene expression in macrophage phenotypes. a: Pie charts of transcripts in M1-like (LPS/IFNɣ) and M2-like (IL-4) macrophages categorized into coding and non-coding transcripts based on Ensembl gene types and the respective differentially expressed genes (DEGs) resulting from RNA sequencing analysis. **b:** Heatmap of top 40 upregulated lncRNAs in M2-like macrophages (red) compared to M1-like macrophages (blue). **c:** Criteria of further candidate restriction **d:** Expression validation of M2-like upregulated candidate lncRNAs in M1 like or M2 like macrophages. n = 6, *p≤0.05, **p≤0.01, ***p≤0.001 compared to M1. Data are represented as mean ± SEM

4.1.3 LncRNA ADPGK-AS1 is upregulated in tumor promoting M2 macrophages

Next, we analyzed and compared the candidates regarding their protein coding probability, expression pattern in various cancer cell lines, and expression in different macrophage systems, to select a suitable candidate to proceed with for further characterization. However, in the following figure, only the results for our final selected candidate, lncRNA ADPGK-antisense RNA 1 (ADPGK-AS1), are shown.

LncRNA ADPGk-AS1 was found to be non-protein coding, as predicted by calculation of protein coding probability and coding potential score (Figure 4-4 a) based on its cDNA sequence. Here, β-actin mRNA sequence served as a control for a coding gene, while the sequence of lncRNA MALAT1 served as the non-coding control. Additionally, *in vitro* transcription of the ADPGK-AS1 cDNA with following *in vitro* translation confirmed the non-coding ability, as no additional protein bands (>10 kDa) were detected in coomassie stained SDS gels (Figure 4-4 b). Further, we have several macrophage systems available in our lab including *in vitro* activated THP1 and PBMC-derived macrophages, co-cultured macrophages to generate *in vitro* TAMs, as well as TAMs isolated from lung cancer tissue in comparison to macrophages isolated from healthy lung tissue. Here, we validated the expression of ADPGK-AS1 in the different systems and we found that ADPGK-AS1 was highly expressed in *in vitro*

polarized M2-like macrophages derived from human PBMCs as well as THP1 cells (Figure 4-4 c-d). Additionally, ADPGK-AS1 was highly expressed in macrophages isolated and sorted from human lung cancer tissue compared to macrophages isolated from healthy lung tissue (Figure 4-4 e), suggesting that this lncRNA plays a role in TAMs and possibly lung cancer development or progression.

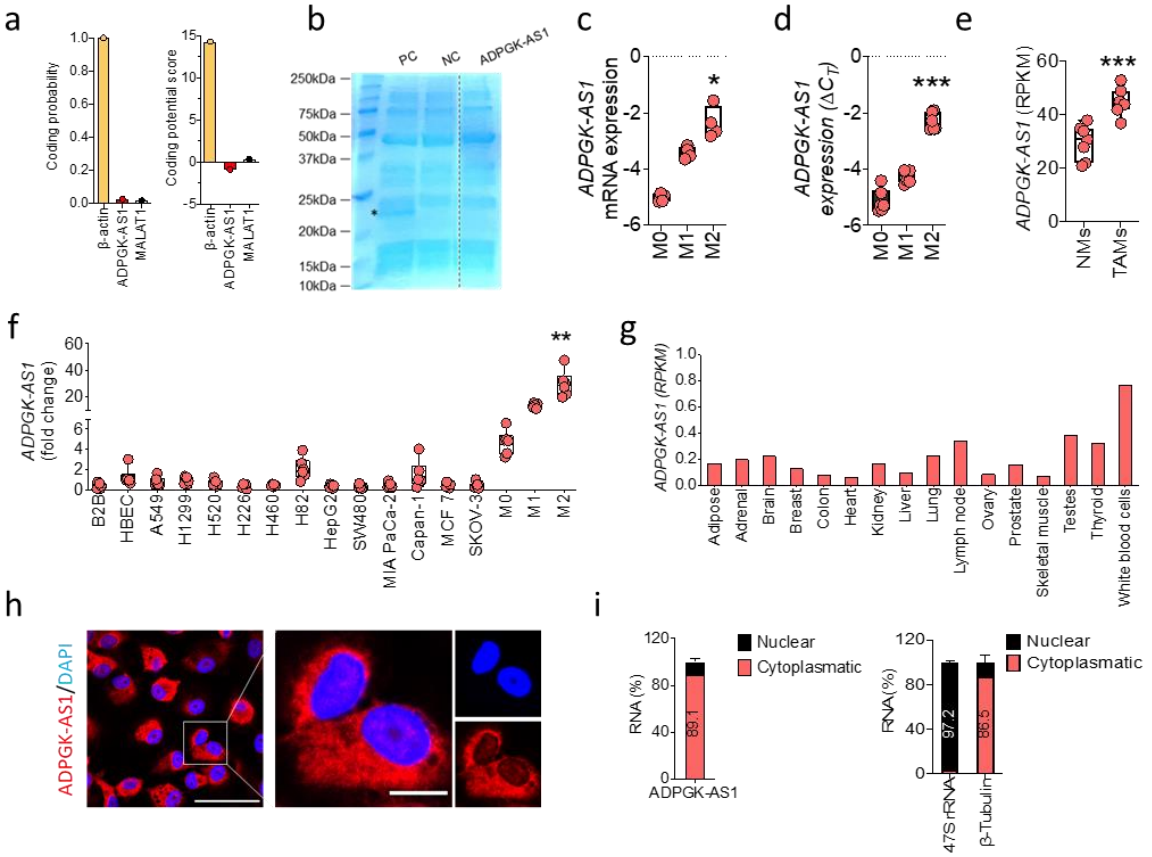

Figure 4-4 LncRNA ADPGK-AS1 is upregulated in tumor promoting macrophages and is localized in the cytoplasm. a: Coding probability and coding potential score using the cDNA sequence of ADPGK-AS1, β-actin as example for a protein-coding sequence and MALAT1 as example for a non-coding transcript. **b:** Transcription with following translation of ADPGK-AS1 to exclude coding function of proteins >10 kDa. *represents positive control (PC); negative control (NC). **c-d:** RNA expression of ADPGK-AS1 in primary and THP1 derived macrophages untreated (M0), M1-like or M2-like phenotype. n = 4, *p≤0.05, ***p≤0.001 compared to M1 **e:** Expression analysis of ADPGK-AS1 in TAMs sorted from healthy lung tissue (normal macrophages; NMs) or lung tumor tissue (TAMs). n = 7, ***p≤0.001 compared to NMs **f:** RNA expression analysis of ADPGK-AS1 in cell lines and macrophage phenotypes. n = 6, **p≤0.01 compared to healthy cell line B2B. **g:** RNA expression of ADPGK-AS1 based on Illumina Seq dataset (Source: UCSC genome browser, July 2021) **h:** Representative images of fluorescence in situ hybridization of ADPGK-AS1 (red) and nuclei (blue) in M2-like macrophages. scale bar = 50 µm (left), 10 µm (right) **i:** RNA expression analysis of ADPGK-AS1, 47S rRNA (nuclear control) and β-Tubulin (cytoplasmic control) in M2-like macrophages after subcellular fractionation. n = 6. Data are represented as mean ± SEM

Furthermore, ADPGK-AS1 was found to be expressed throughout different cell lines, such as healthy lung (B2B, HBEC), lung cancer (A549, H1299, H520, H226, H460, H82), hepatocellular carcinoma (HepG2), colon adenocarcinoma (SW480), pancreatic cancer (MIA PaCa-2, Capan-1), breast cancer (MCF-7) and ovarian adenocarcinoma (SCOV-3) (Figure 4-

4 f). However, ADPGK-AS1 expression was highly upregulated in white blood cells, particularly macrophages and their activated phenotypes (Figure 4-4 f-g). Due to the fact that lncRNAs are often expressed tissue and cell type specific, we hypothesized that upregulated expression of ADPGK-AS1 in macrophages compared to other cell types could be due to a specific function of this lncRNA in these cells. Therefore, we chose ADPGK-AS1 as suitable candidate for further characterization.

Next, we analyzed the location of the ADPGK-AS1 transcript in macrophages since localization of lncRNAs within the cellular compartments can already give a hint about their possible function. To do this, we used fluorescence *in situ* hybridization (FISH) in M2-like macrophages with specific fluorescence coupled antisense probes (Figure 4-4 h). The staining showed that ADPGK-AS1 is predominantly distributed in the cytoplasm of the cells. This was confirmed by subcellular fractionation of cytoplasm and nucleus with following RNA isolation and qPCR-based expression analysis (Figure 4-4 i). Here, 89.1 % of the ADPGK-AS1 transcript was detected in the cytoplasmic fraction. β-Tubulin served as a cytoplasmic control and 86.5 % of the transcript was detected in the cytoplasm. Since pre-ribosomal RNA is exclusively within the nucleus (Aubert et al. 2018), 47S pre-rRNA was the nuclear control. More than 97 % of 47S pre-rRNA was detected within the nuclear fraction.

4.2 LncRNA ADPGK-AS1 enters the macrophage mitochondria and interacts with mitochondrial ribosomal proteins

As antisense lncRNA, ADPGK-AS1 is encoded in the genome antisense to the ADPGK protein coding gene. Although the majority of antisense lncRNAs are known to regulate gene expression of their antisense protein coding gene in *cis*, ADPGK-AS1 is not localized in the nucleus (Figure 4-4). Therefore, we concluded that ADPGK-AS1 is acting through a different mechanism than direct gene expression regulation. To identify possible protein interaction partners, we performed an RNA pulldown assay with following mass spectrometry. For this, ADPGK-AS1 was *in vitro* transcribed, biotinylated and pulldown was prepared using streptavidin beads together with M2-like macrophage whole cell extract (Figure 4-5 a). After pulldown, RNA from beads was isolated and qPCR confirmed pulldown of the correct RNA transcript compared to the control (lower C_T-value, Figure 4-5 b). Particularly, mass spectrometry revealed a high number of mitochondrial ribosomal proteins (MRPs) interacting with ADPGK-AS1 (Figure 4-5 c), such as MRPL35, MRPL15, MRPL23, MRPS33 and MRPL47. Further, we were able to confirm the interaction of ADPGK-AS1 with the two top candidates MRPL35 and MRPL15 (Figure 4-5 d-e). Notably, both MRPL35 and MRPL15 have been found to be overexpressed in lung tumor tissue compared to normal lung and to correlate with poor patient survival (Figure 4-5 f-g).

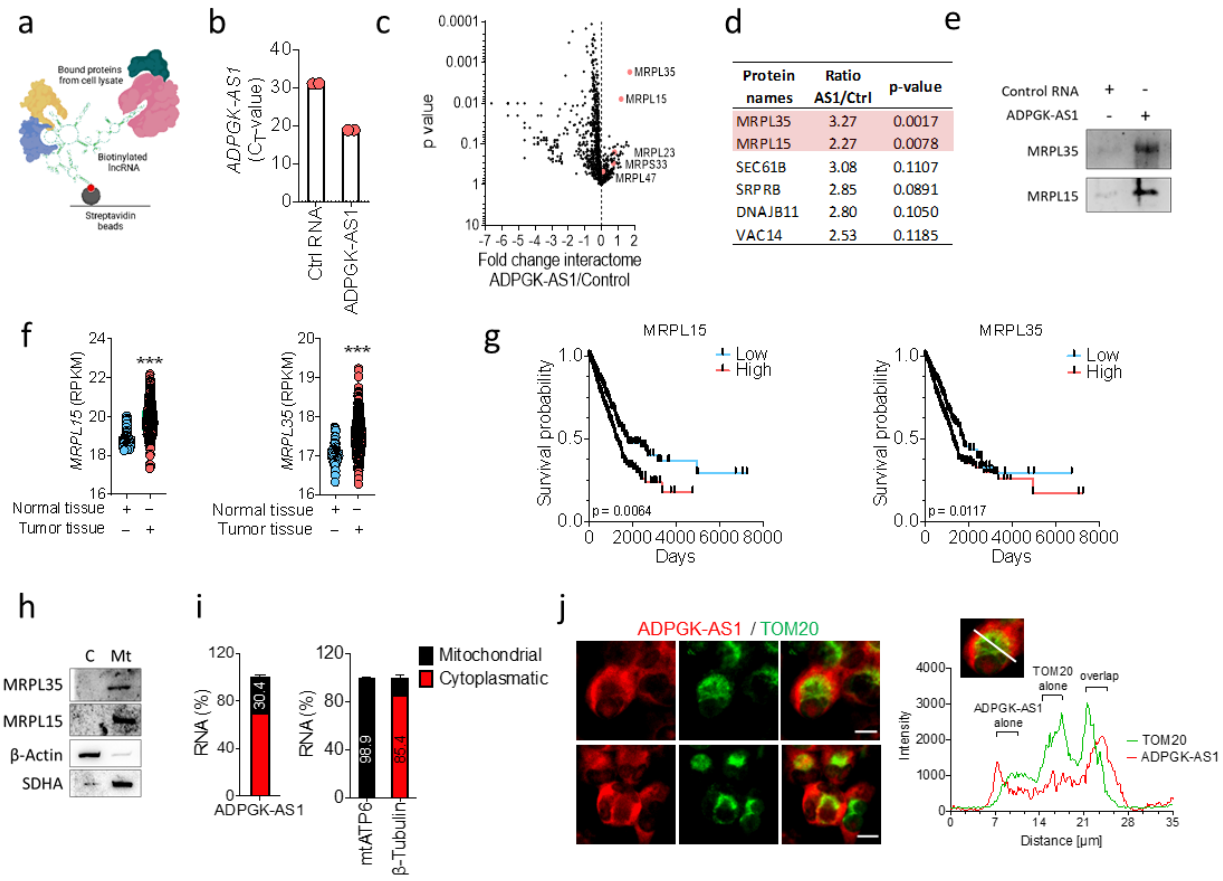

Figure 4-5 ADPGK-AS1 enters the mitochondria and interacts with mitochondrial ribosomal proteins. a: Schematic overview of RNA pulldown method. **b:** RNA pulldown validation of bound ADPGK-AS1 transcript using eluted RNA from streptavidin beads. n = 2 **c:** Volcano plot showing the protein interactome of ADPGK-AS1 after RNA pulldown compared to a control RNA. n = 5. **d:** Top candidates of interacting proteins. **e:** Representative immunoblot of validation of interacting proteins MRPL15 and MRPL35 after ADPGK-AS1 pulldown. **f:** Expression of MRPL15 and MRPL35 in normal lung tissue (n = 59) and tumor tissue (n = 524). ***p≤0.001 compared to normal tissue. **e:** Kaplan-Meier estimate of survival probability among patients with lung adenocarcinoma (GDC TCGA dataset) classified according to levels of MRPL15 and MRPL35 as high (above mean value, red) or low (below mean value, blue). **h-i:** Fractionation of cytoplasm (C) and mitochondria (Mt) in macrophages with following protein or RNA isolation and location analysis of MRPL15, MRPL35 as well as ADPGK-AS1. n = 3 **j:** Co-staining of ADPGK-AS1 (red) and mitochondrial marker TOM20 (green) in macrophages and fluorescence intensity profile of both signals through macrophage cells. scale bar = 10 µm. Data are represented as mean ± SEM

Next, subcellular fractionation of mitochondria and cytoplasm revealed that MRPL15 and MRPL35 are exclusively localized within the mitochondrial fraction (Figure 4-5 h). Therefore, we analyzed the localization of ADPGK-AS1 in more detail. Interestingly, after fractionation of macrophages into cytoplasmic and mitochondrial fraction, around one third (30.4 %) of ADPGK-AS1 RNA was detected in the mitochondrial fraction (Figure 4-5 i). Additionally, co-staining of ADPGK-AS1 and mitochondrial marker TOM20 in macrophages showed overlapping areas of both signals, further indicating that ADPGK-AS1 is able to translocate into the mitochondria (Figure 4-5 j). Taken together, these results suggest that ADPGK-AS1 in macrophages is mainly localized in the cytoplasm of the cells, but can enter the mitochondria and bind to mitochondrial proteins.

4.3 ADPGK-AS1 overexpression increases macrophage mitochondrial mass and influences mitochondrial dynamics

To assess the function of ADPGK-AS1 in macrophages regarding mitochondrial metabolism, we generated a stable overexpression cell line. Overexpression (OE) of ADPGK-AS1 in macrophages was confirmed by qPCR as well as with fluorescence *in situ* hybridization (FISH) using fluorescence-labelled probes specific for ADPGK-AS1 (Figure 4-6 a-b).

Interestingly, mitochondrial staining with MitoTracker and TOM20 (Figure 4-6 c-d) showed increased signal in ADPGK-AS1 OE cells, possibly due to a higher number of mitochondria. Isolation of macrophage mitochondrial (mt) DNA and analysis of mtDNA to genomic DNA ratio, as well as gene expression analysis of the mitochondrial encoded genes NADH-ubichinone oxidoreductase (ND1, ND2, ND4), ATP synthase membrane subunits (ATP6, ATP8), cytochrome C oxidase (CO1, CO2) and cytochrome B (CyB), further confirmed an increase of mitochondrial number in ADPGK-AS1 OE macrophages (Figure 4-6 e-f). Additionally, high expression of mitochondria-associated proteins, such as TOM20, αb-crystallin, PCG-1 or cytochrome C was observed in ADPGK-AS1 OE macrophages, including the previously identified interaction partners MRPL15 and MRPL35 (Figure 4-6 g).

Interestingly, ADPGK-AS1 overexpressing macrophages seem to have enhanced mitochondrial fission, which was seen on protein level by upregulation of fission-associated proteins Drp1 or pAMPK and downregulation of mitochondrial fusion-associated proteins such as Mfn1 and Opa1 (Figure 4-6 h). In addition, confocal imaging of these macrophages revealed a high number of small, fragmented mitochondria in ADPGK-AS1 overexpressing cells compared to control cells, in which the mitochondria built a longer network (Fig- 4-6 i). Mitochondrial length was also measured and quantified, confirming these observations. To find out whether these changes in mitochondrial morphology were linked with a changed macrophage phenotype, we analyzed polarized THP1 macrophage phenotypes regarding their mitochondrial shape (Figure 4-6 j). Interestingly, we found that M1-like macrophages had an increase of longer, fused mitochondria, while M2-like macrophages showed high number of smaller mitochondria, similar to those detected in ADPGK-AS1 OE macrophages. Unstimulated M0 macrophages had a mixture of both mitochondrial phenotypes. Taken together, these results suggest that high expression of ADPGK-AS1 in macrophages leads to enhanced mitochondrial fission process and therefore a higher number of mitochondria in these macrophages.

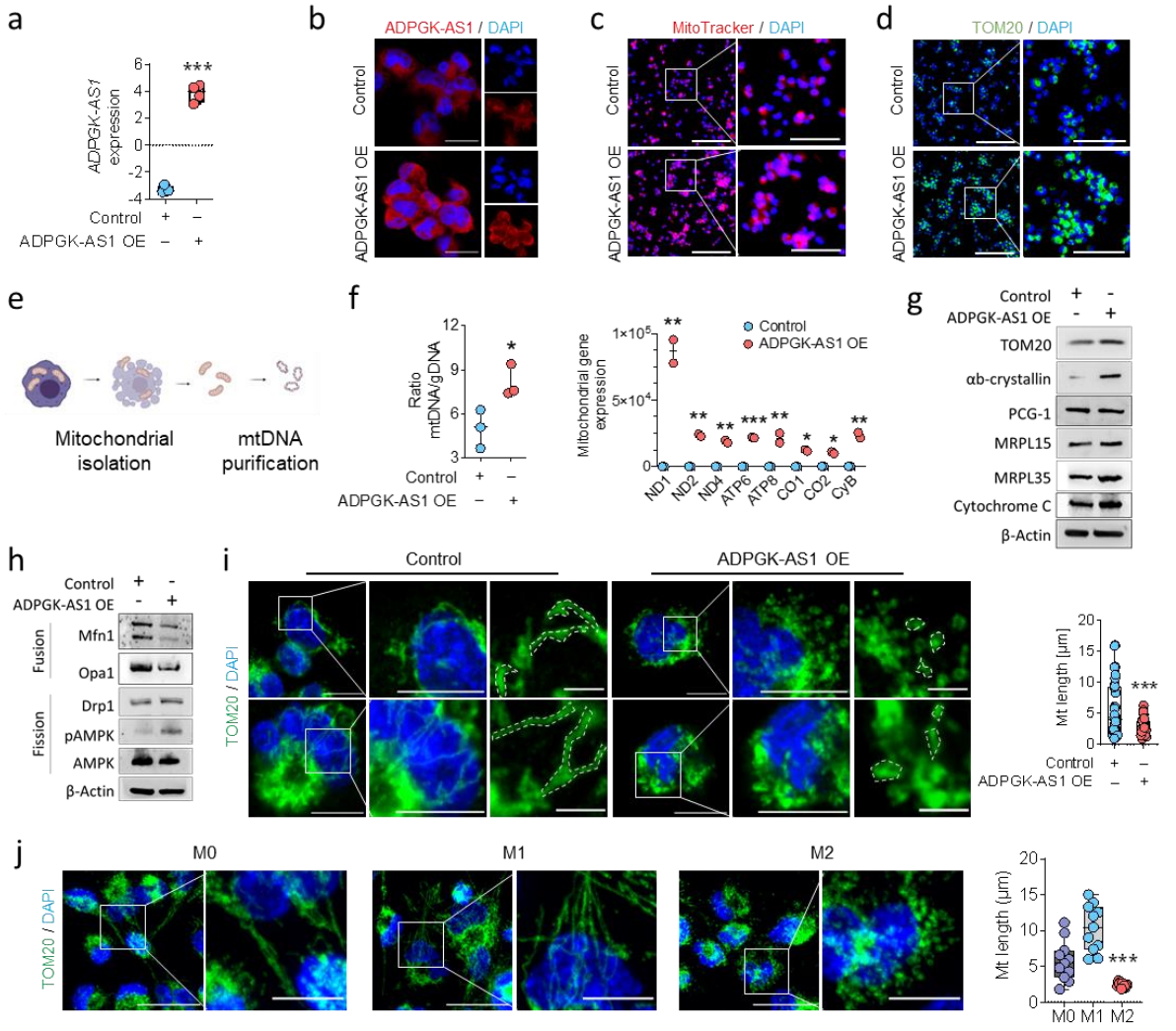

Figure 4-6 ADPGK-AS1 overexpression leads to increased number of mitochondria and induces mitochondrial fission in macrophages. a: RNA expression of ADPGK-AS1 in THP1 control and ADPGK-AS1 overexpressing (OE) cells. n = 4, ***p≤0.001 compared to control **b:** Representative FISH images of ADPGK-AS1 in THP1 control and ADPGK-AS1 OE macrophages. scale bar = 25 µm **c-d:** Representative images of mitochondria by staining with MitoTracker (red) and TOM20 (green) in THP1 Control and APDGK-AS1 OE macrophages, DAPI (blue). scale bar = 200 µm (left), 100 µm (right, magnification) **e:** Schematic representation of mitochondrial (mt) DNA isolation. **f:** Ratio of mt to genomic DNA content (left panel) in THP1 control and ADPGK-AS1 OE macrophages, and gene expression analysis of mitochondrial encoded genes (right panel). n = 3, *p≤0.05, **p≤0.01, ***p≤0.001 compared to control **g:** Representative immunoblot for mitochondrial proteins in THP1 Control and ADPGK-AS1 OE cells. **h:** Representative immunoblot of proteins involved in mitochondrial fission and fusion process. **i:** Representative images of THP1 control and ADPGK-AS1 OE macrophages stained with mitochondrial marker TOM20 (green) and DAPI (blue) with quantification of average mitochondrial length. scale bar = 10 µm (left and middle), 3 µm (right). n = 30, ***p≤0.001 compared to control. **j:** Representative images of THP1 macrophages polarized to M1-like, M2-like or untreated (M0) stained with mitochondrial marker TOM20 (green) and DAPI (blue) and quantification of average mitochondrial length. Scale bar = 30 µm, 10 µm (magnification). n = 11. ***p≤0.001 compared to M1. Data are represented as mean ± SEM

4.4 ADPGK-AS1 modulation induces metabolic changes in macrophages

Next, we examined how the previously shown effects on macrophage mitochondria through ADPGK-AS1 overexpression influence the metabolic state. We were able to detect enhanced ATP production as well as increased basal and ATP-linked respiration in ADPGK-AS1 OE macrophages (Figure 4-7 a-b). On the contrary, LDH enzyme activity was downregulated, as well as glucose-6-phosphate dehydrogenase (G6PD) enzyme activity, indicating decreased metabolic activity in the pentose phosphate (Figure 4-7 c-d). Enhanced TCA cycle activity was confirmed by increased SDH and IDH activity, both important enzymes of the TCA cycle (Figure 4-7 e-f).

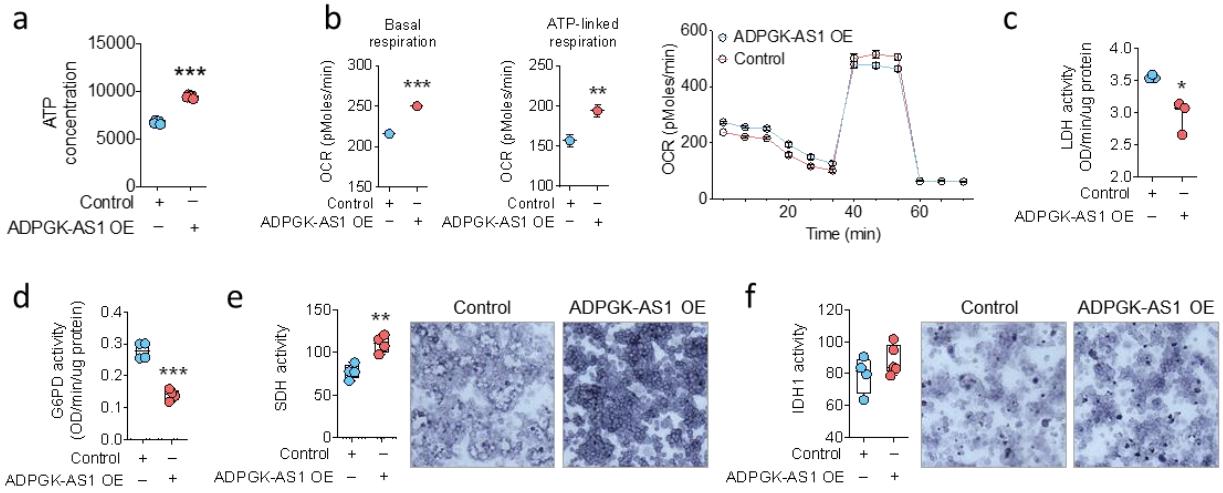

Figure 4-7 ADPGK-AS1 overexpression leads to macrophages metabolic switch. a: ATP production in THP1 control and ADPGK-AS1 OE cells. n = 5 **b:** Oxygen consumption rate (OCR), basal and ATP-linked respiration measured by seahorse method in THP1 control and ADPGK-AS1 OE macrophages. n = 8 **c-d:** Enzyme activity assay of lactate dehydrogenase (LDH, n = 3), Glucose-6-phosphate-dehydrogenase (G6PD), succinate dehydrogenase (SDH) and isocitrate dehydrogenase (IDH1) with representative brightfield images in THP1 control and ADPGK-AS1 OE macrophages. n = 4, *p≤0.05, **p≤0.01, ***p≤0.001 compared to control. Data are represented as mean ± SEM (a, c-f) or as mean ± SD (b)

Subsequently, we analyzed the macrophages regarding their mitochondrial metabolic composition. For this, we used Control and ADPGK-AS1 OE macrophages as well as primary M2-like (ADPGK-AS1^{high}) macrophages and performed siRNA- or antisense LNA GapmeR-mediated knockdown (KD) of ADPGK-AS1 (Figure 4-8 a-b). We were able to see an upregulation of several TCA metabolites such as citrate, fumarate, malate or α-ketoglutarate (αKG) in ADPGK-AS1 OE macrophages, which were significantly downregulated after ADPGK-AS1 KD (Figure 4-8 c-d). Additionally, macrophages with high expression of ADPGK-AS1 showed high mitochondrial membrane potential (Figure 4-8 e-f), as seen by JC-1 aggregate formation (Sivandzade, Bhalerao, and Cucullo 2019), confirming the previously

described enhanced ATP production. We were able to reverse this effect, by siRNA-mediated downregulation of ADPGK-AS1 in ADPGK-AS1 OE cells, diminishing mitochondrial membrane potential. In addition, ADPGK-AS1 seems to play a role in ROS formation. Visualization of ROS using MitoSOX staining showed decreased amounts of ROS in ADPGK-AS1 OE macrophages, which were restored after ADPGK-AS1 KD (Figure 4-8 g). Collectively, these results suggest a broad metabolic adaption in macrophages after ADPGK-AS1 expression modulation, increasing mitochondrial metabolic signaling pathways, changing the availability of metabolites (Figure 4-8 h).

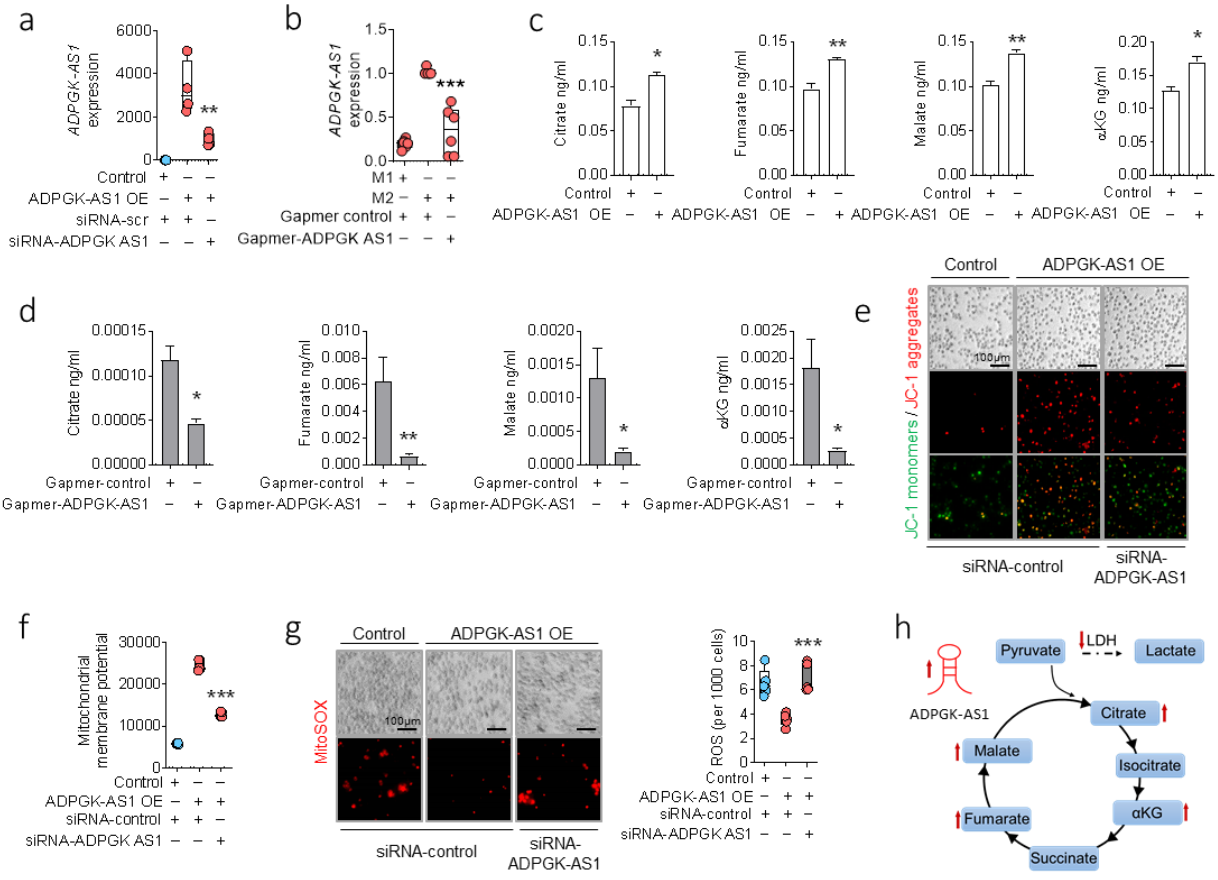

Figure 4-8 ADPGK-AS1 induces broad metabolic changes in macrophages. a-b: expression analysis of ADPGK-AS1 in THP1 control and ADPGK-AS1 OE macrophages (n = 4) and primary M1-like/M2-like macrophages (n = 6) after transfection with siRNA or antisense LNA GapmeRs specific against ADPGK-AS1 or a negative control. **p≤0.01, ***p≤0.001 compared to negative control **c-d:** Analysis of deregulated metabolites in cell lysates of THP1 ADPGK-AS1 OE macrophages or PBMC-derived M2-like ADPGK-AS1 knockdown macrophages compared to the respective control using mass spectrometry. n = 3, displayed as ratio of lysate to supernatant. *p≤0.05, **p≤0.01 compared to control **e:** Representative images of JC-1 monomers (green) and aggregates (red) in THP1 control and ADPGK-AS1 macrophages transfected with siRNA against ADPGK-AS1 or a negative control. **f:** Measurement of JC-1 aggregate emission at 590 nm in THP1 control and ADPGK-AS1 OE macrophages transfected with siRNA. n = 5, ***p≤0.001 compared to negative control **g:** Representative images and quantification of ROS accumulation in THP1 control and ADPGK-AS1 OE cells transfected with siRNA against ADPGK-AS1 or a negative control. n = 5, ***p≤0.001 compared to negative control **h:** Schematic summary of previous shown findings regarding metabolite availability and enzyme activity in macrophages with high ADPGK-AS1 expression. Data are represented as mean ± SEM

4.5 Role of lncRNA ADPGK-AS1 in macrophage-tumor-cell crosstalk

4.5.1 Macrophages upregulate ADPGK-AS1 and adapt their metabolic signaling pathways after crosstalk with tumor cells

During tumor development, macrophages and tumor cells are in close contact. Due to this crosstalk via cytokines, chemokines and metabolites, the unique tumor microenvironment is shaped. Mitochondrial metabolism has been shown to be a crucial player in tumor progression as well as a very important player in macrophage activation state (Kelly and O'Neill 2015; Ma, Wang, and Jia 2020). To understand the role of ADPGK-AS1 within this interplay, co-culture of macrophages with lung tumor cells was performed (Figure 4-9 a). After 24 hours of co-culture, macrophage marker expression suggest an M2-like activation status (Figure 4-9 b) as seen by downregulation of TNFα and IL-8 and upregulation of CD206 and CSF-1R. Additionally, ADPGK-AS1 expression was significantly induced after co-culture with tumor cells compared to macrophage controls (Figure 4-9 c), indicating a role of ADPGK-AS1 in macrophages in the context of lung cancer. Furthermore, we analyzed the metabolites in the cell lysate of co-cultured macrophages and found increased levels of metabolites associated with the TCA cycle (Figure 4-9 d-e), such as fumarate, malate, citrate and succinate. This metabolic profile is similar as to the one previously found in the THP1 ADPGK-AS1 OE cells (Figure 4-8 c-d), again highlighting a role of ADPGK-AS1 in adaptation of macrophage metabolic signaling pathways.

Next, we analyzed the metabolites in the supernatant of the co-culture and found that, amongst others, the levels of αKG, gluconic acid and prostaglandin E2 (PGE2) were highly upregulated (Figure 4-9 f). To find out if ADPGK-AS1 expression is regulated by one of these metabolites, we treated macrophages with αKG, gluconic acid, PGE2 or lactate. Interestingly, only αKG was able to induce ADPGK-AS1 expression in macrophages (Figure 4-9 g). To further analyze whether αKG could be involved in the upstream signaling pathway of ADPGK-AS1 expression, we transfected A549 cells with siRNA against IDH, which is the enzyme mainly responsible for αKG production (Figure 4-9 h). Macrophages that were treated with CM of IDH knockdown (KD) A549 cells showed reduced upregulation of ADPGK-AS1 expression compared to macrophages treated with A549 control-CM (Figure 4-9 i). Taken together, these results suggest that ADPGK-AS1 expression in macrophages could be induced during macrophage-tumor-cell crosstalk by tumor cell secreted αKG.

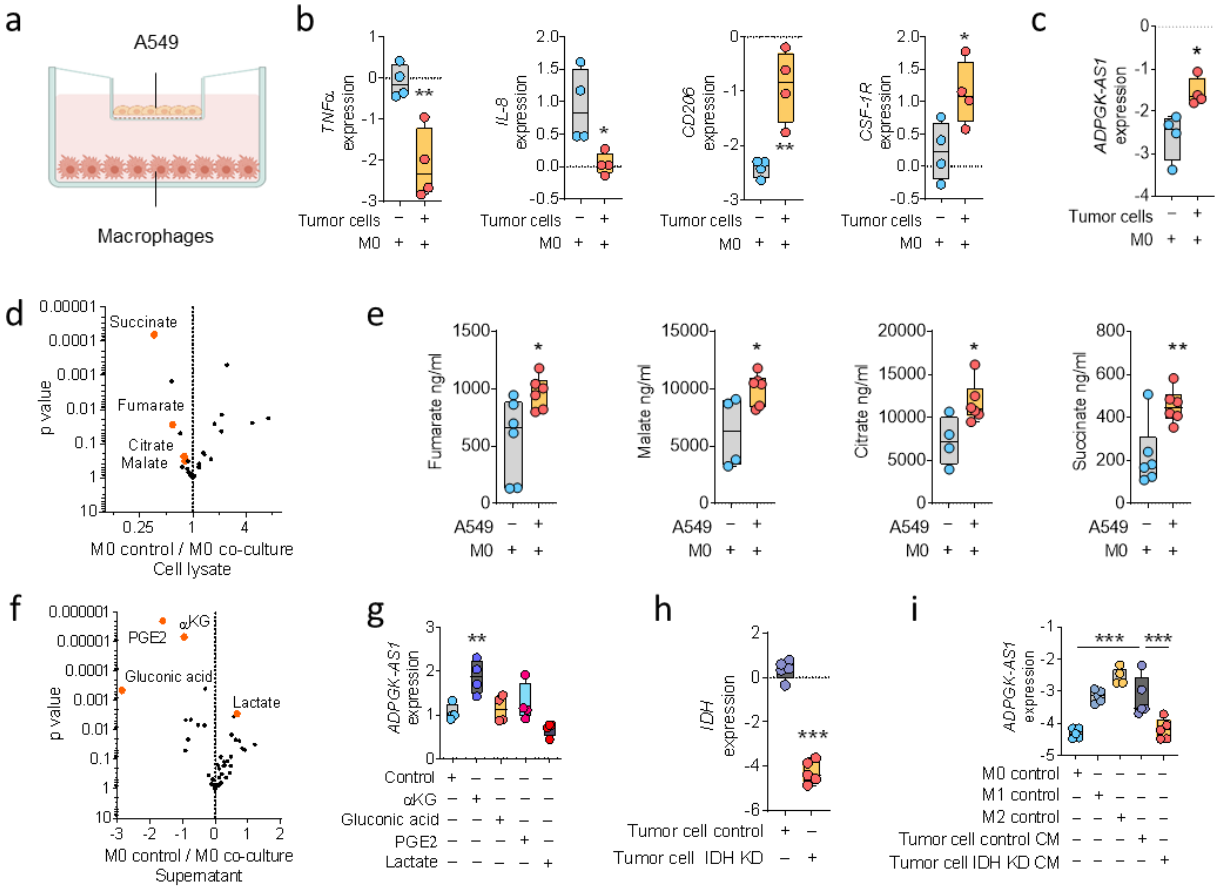

Figure 4-9 ADPGK-AS1 is regulated in macrophage-tumor cell crosstalk. a: Schematic overview of experimental setup of indirect co-culture of tumor cells (A549) and macrophages. **b:** mRNA expression analysis of M1 (TNFα, IL-8) and M2 (CSF-1R, CD206) macrophage marker genes in co-cultured macrophages. n = 4, *p≤0.05, **p≤0.01 compared to macrophage control (M0) **c:** RNA expression of ADPGK-AS1 in macrophages co-cultured with A549. n = 4, *p≤0.05 compared to M0 **d:** Volcano plot showing deregulated metabolites in cell lysates of co-cultured macrophages or macrophage controls. n= 6 **e:** Mass spectrometry analysis of TCA cycle metabolites (fumarate, malate, citrate, succinate) in co-cultured macrophages or macrophage controls. n = 6, *p≤0.05, **p≤0.01 compared to macrophage control **f:** Volcano plot showing deregulated metabolites in supernatant of macrophage-A549-co-culture compared to macrophage controls. n = 6 **g:** RNA expression of ADPGK-AS1 in macrophages treated with different metabolites for 24 hours. n = 5, **p≤0.01 compared to control **h:** RNA expression of IDH in A549 cells with an IDH knockdown (KD) compared to A549 control cells. n = 5, ***p≤0.001 compared to A549 control **i:** RNA expression of ADPGK-AS1 in macrophages polarized to M1-like, M2-like, untreated (M0) or treated with conditioned medium (CM) of A549 cells transfected with siRNA against IDH (IDH KD) or a negative control. n = 5. ***p≤0.001 compared to Tumor cell control CM. Data are represented as mean ± SEM

4.5.2 Treatment of macrophages with α-KG partially mimics the effect of ADPGK-AS1 overexpression

To further understand the upstream signaling pathway of ADPGK-AS1 we analyzed the cytokine secretion profile of THP1 ADPGK-AS1 OE and control macrophages (Figure 4-10 a). We found that inflammatory cytokines IL-1β and IFNɣ were downregulated and the anti-inflammatory cytokine IL-10 was upregulated in the supernatant of ADPGK-AS1 OE macrophages compared to the control (Figure 4-10 b). Macrophages treated with αKG also showed downregulation of IL-1β and upregulation of IL-10 expression (Figure 4-10 c),

deceiving the cytokine regulation as seen in the ADPGK-AS1 OE cells. Also, A549 cells treated with CM of the macrophages showed increased migration with CM of αKG-treated macrophages (Figure 4-10 d), further indicating that αKG-treatment of macrophages mimics overexpression of ADPGK-AS1 in macrophages.

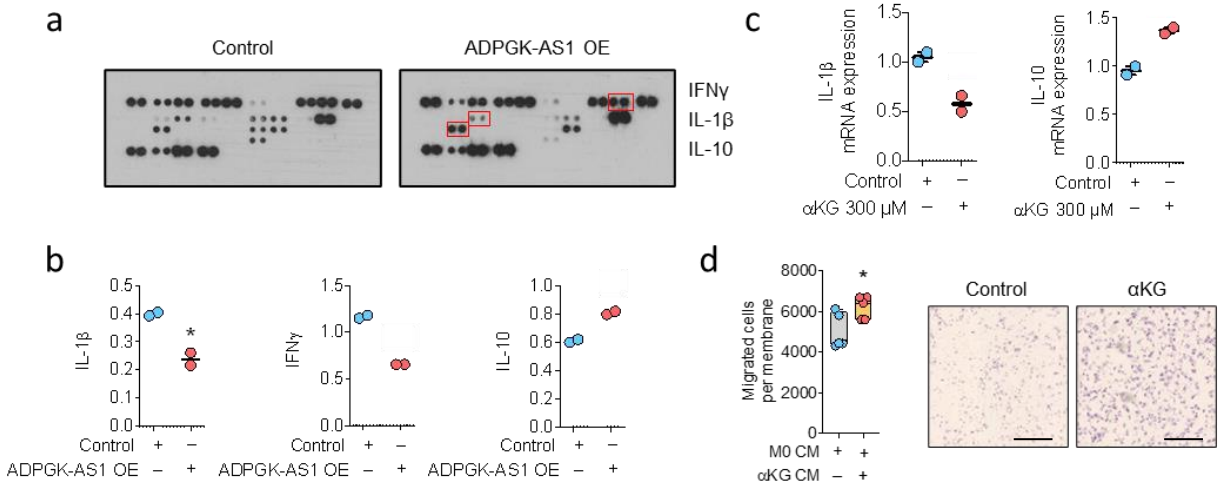

Figure 4-10 αKG may function as upstream activator of ADPGK-AS1 signaling pathway. a-b: Cytokine array and quantification with respect to the reference of THP1 control and ADPGK-AS1 overexpressing macrophages. n = 2 **c:** mRNA expression analysis of IL-1β and IL-10 in macrophages treated with αKG for 24 hours. n = 2 **d:** Boyden chamber transwell assay with representative membrane images of A549 treated with CM of macrophages with and without treatment of αKG. n = 5, scale bar = 400µm, *p≤0.05 compared to M0 CM. Data are represented as mean ± SEM

4.6 ADPGK-AS1 regulates macrophage activation and induces tumor cell apoptosis and migration *in vitro*

4.6.1 Knockdown and overexpression of ADPGK-AS1 in macrophages

As shown in Figure 4-4 and Figure 4-8, ADPGK-AS1 is expressed in co-cultured macrophages, FACS sorted TAMs from lung cancer patients, and *in vitro* polarized M2-like macrophages. Thus, we hypothesized that ADPGK-AS1 plays a significant role in macrophage activation and influences the effect on tumor cell functions. To analyze this further, we examined the macrophages regarding their marker gene expression in context of ADPGK-AS1 overexpression and knockdown.

For this, we used our THP1 ADPGK-AS1 OE macrophages (Figure 4-11 a) to analyze the effect of a high lncRNA-expression in macrophages without further stimulation. We were able to see downregulation of M1-like macrophage marker genes such as TNFα and IL-8 and downregulation of M2-like macrophage marker genes such as CSF-1R and CD206, indicating that ADPGK-AS1 expression alone is sufficient to induce an M2-like phenotype (Figure 4-11 b-c). This was further confirmed by treatment of A549 and H1650 cells with CM of THP1 control

and ADPGK-AS1 OE cells, leading to decreased apoptosis (Figure 4-11 e) and enhanced migration (Figure 4-11 f) with ADPGK-AS1 OE CM, while tumor cell proliferation was not significantly changed (Figure 4-11 d). These results demonstrate that ADPGK-AS1 is able to induce a tumor promoting macrophage phenotype.

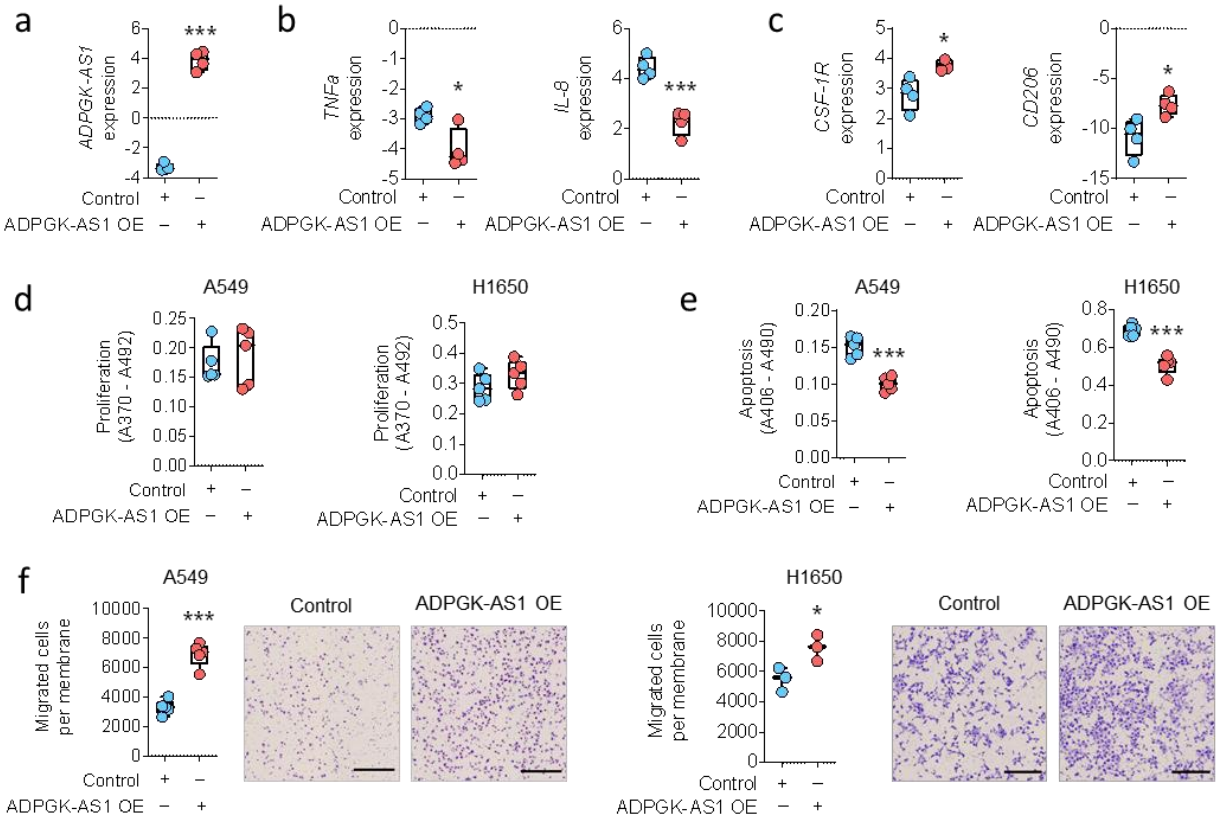

Figure 4-11 ADPGK-AS1 overexpression leads to M2-like macrophage activation state and influence tumor cell proliferation, apoptosis, and migration. a: RNA expression analysis of ADPGK-AS1 in THP1 control and ADPGK-AS1 overexpressing (OE) macrophages. n = 4 **b-c:** mRNA expression analysis of macrophage marker genes (TNFα, IL-8, CSF-1R, CD206) in THP1 control and ADPGK-AS1 OE macrophages. **d:** BrdU incorporation (proliferation) assay of A549 and H1650 cells treated with conditioned media (CM) of THP1 control and ADPGK-AS1 OE macrophages. n = 5 **e:** Cell death detection (apoptosis) assay of A549 and H1650 cells treated with CM of THP1 control and ADPGK-AS1 OE macrophages. n = 5 **f:** Boyden chamber transwell (migration) assay with representative membrane images of A549 and H1650 cells treated with CM of THP1 control and ADPGK-AS1 OE cells. scale bar = 400µm. n = 5, *p≤0.05, ***p≤0.001 compared to control. Data are represented as mean ± SEM

To test the therapeutic potential of ADPGK-AS1 in context of lung cancer, we used primary M1-like and M2-like macrophages and performed an antisense LNA GapmeR-mediated knockdown of ADPGK-AS1 in M2-like macrophages (Figure 4-12 a). Here, we were able to see the *vice versa* effect from before with an upregulation of M1-like macrophage marker gene expression TNFα and IL-8, while expression of M2-like macrophage marker genes CD206 and CSF-1R were downregulated in M2-like macrophages after ADPGK-AS1 knockdown compared to the negative control (Figure 4-12 b-c). CM of these cells slightly decreased proliferation of lung cancer cells A549 and H1650 (Figure 4-12 d), and significantly

upregulated tumor cell apoptosis (Figure 4-12 e) while tumor cell migration was reduced (Figure 4-12 f) in both lung cancer cell lines. Collectively, these results demonstrate that ADPGK-AS1 plays a crucial role in macrophage activation process, in which its overexpression enhances and downregulation reduces the tumor promoting M2-like phenotype, influencing tumor cell apoptosis and migration.

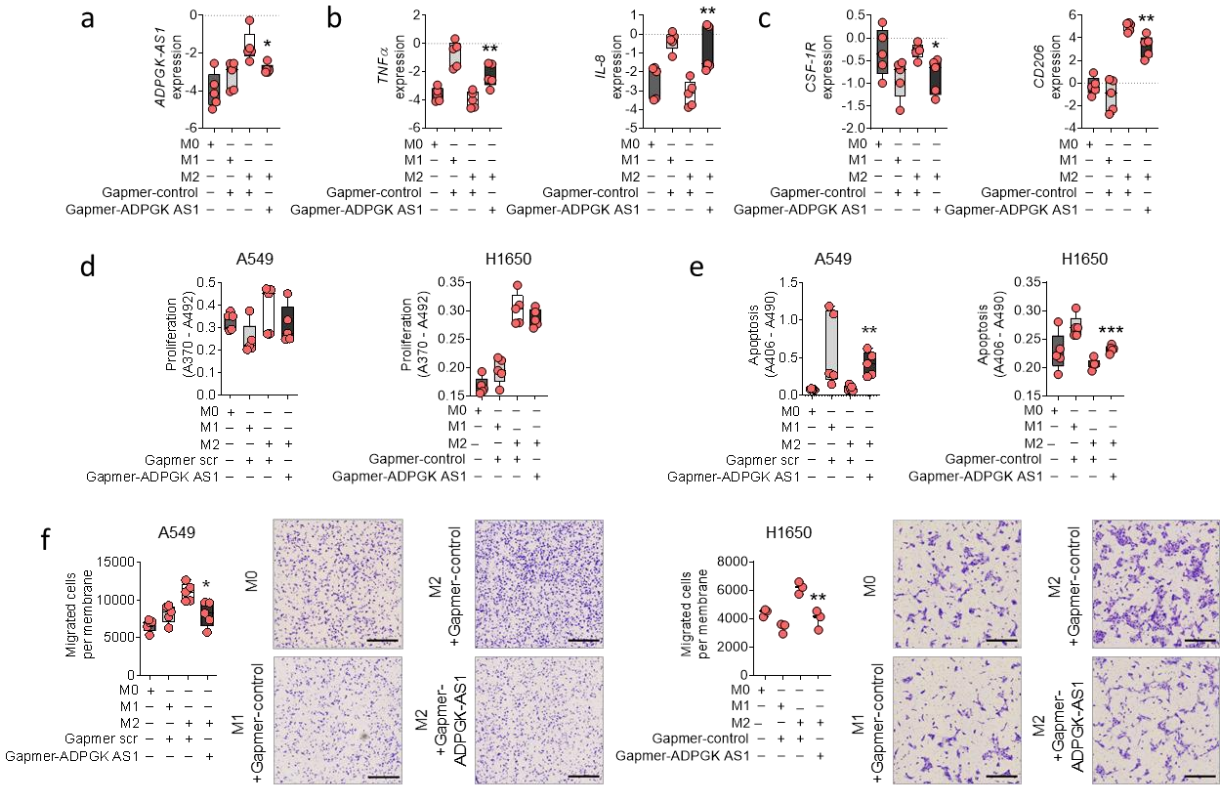

Figure 4-12 ADPGK-AS1 knockdown switches M2-like pro-tumorigenic macrophages into M1-like anti-tumorigenic macrophage phenotype. a: RNA expression analysis of ADPGK-AS1 in primary M1-like and M2-like macrophages transfected with antisense LNA GapmeRs specific against ADPGK-AS1 or a negative control. n = 5 **b-c:** mRNA expression analysis of macrophage marker genes (TNFα, IL-8, CSF-1R, CD206) in primary M1-like and M2-like macrophages transfected with antisense LNA GapmeRs specific against ADPGK-AS1 or a negative control. n = 5 **d-f:** BrdU incorporation (proliferation) assay, cell death detection (apoptosis) assay and boyden chamber transwell (migration) assay with representative membrane images of A549 and H1650 treated with conditioned media of primary M1-like and M2-like macrophages transfected with antisense LNA GapmeRs specific against ADPGK-AS1 or a negative control. scale bar = 400µm. n = 5, *p≤0.05, **p≤0.01, ***p≤0.001 compared to M2 negative control. Data are represented as mean ± SEM

4.6.2 ADPGK Inhibitor treatment does not show similar effect as ADPGK-AS1 knockdown in macrophages

As stated before, antisense lncRNAs are known to often regulate gene expression of their antisense protein coding gene, in this case ADPGK (Figure 4-13 a). To exclude a regulation, we analyzed ADPGK gene expression after ADPGK-AS1 OE and KD. Interestingly, ADPGK expression analysis revealed a slight increase in ADPGK-AS1 OE cells (Figure 4-13

b) and decrease of ADPGK in M2-like macrophages with an ADPGK-AS1 KD (Figure 4-13 d). We analyzed the binding sequence of the LNA GapmeRs used to knockdown ADPGK-AS1 and did not find any sequence similarity to the ADPGK transcript, indicating that the GapmeR itself is not responsible for the detected downregulation of ADPGK expression. Finally, we excluded whether ADPGK-AS1 plays a role in direct gene regulation of ADPGK. For this, the ADPGK promotor region was used for a luciferase-based assay in THP1 control and ADPGK-AS1 OE cells. Notably, Luciferase activity under influence of the ADPGK promotor was not changed in both cell types, showing that ADPGK-AS1 does not have the potential to directly induce ADPGK expression (Figure 4-13 c).

Next, we treated M2-like macrophages with different concentrations of 8-Bromo-AMP (8-Br-AMP), a known inhibitor for ADPGK (Grudnik et al. 2018). Upon treatment, we did not observe a change in ADPGK-AS1 expression, ADPGK or any macrophage marker gene e.g. IL-8 or CD206 as in 8-Br-AMP treated cells (Figure 4-13 e). Also, CM of inhibitor treated M2-like macrophages did not influence A549 migration (Figure 4-13 f). Collectively, these results show that ADPGK-AS1 does not directly regulate ADPGK gene expression.

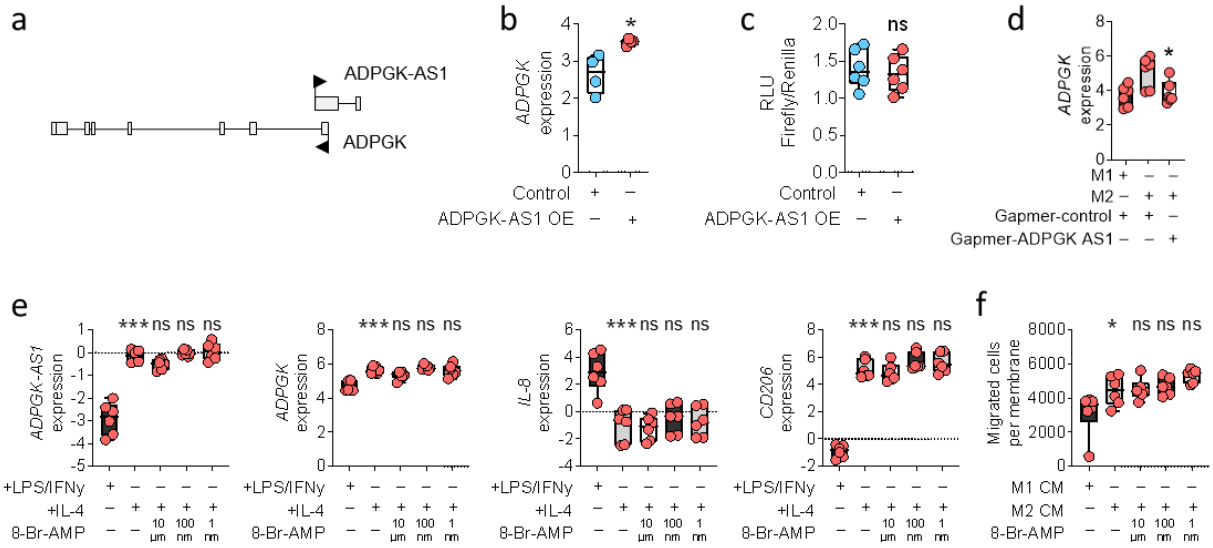

Figure 4-13 Macrophage phenotype and tumor cell function modulation is not regulated via ADPGK. a: Scheme of gene locus encoding the ADPGK and ADPGK-AS1 gene. **b:** mRNA expression of ADPGK in THP1 control and ADPGK-AS1 OE macrophages. n = 4, *p≤0.05 compared to control **c:** Luciferase based assay analyzing direct gene expression regulation of the ADPGK promotor in THP1 control and ADPGK-AS1 OE cells. n = 5 **d:** mRNA expression of ADPGK in primary M1-like and M2-like macrophages transfected with antisense LNA GapmeRs against ADPGK-AS1 or a negative control. n = 6, *p≤0.05 compared to M2 control **e:** RNA expression analysis of ADPGK-AS1, ADPGK and macrophage marker IL-8 and CD206 in M1-like or M2-like macrophages treated with different concentrations of ADPGK inhibitor 8-Br-AMP. n = 6, ***p≤0.001 compared to M1 **f:** Boyden chamber transwell assay of A549 cells treated with conditioned media of M1-like or M2-like macrophages treated with different concentrations 8-Br-AMP. n = 6, *p≤0.05 compared to M1. Data are represented as mean ± SEM

4.7 ADPGK-AS1 influences lung tumor growth *in vivo* and *ex vivo*

In the previous chapters lncRNA ADPGK-AS1 has now been extensively described as a modulator of macrophage metabolism, activator, and regulator of TAM-mediated lung cancer progression *in vitro*. However, tumor development and progression are a complex process within the tissue, involving various cell types. To confirm the potential of ADPGK-AS1 downregulation as a novel approach in lung cancer therapy, we wanted to analyze this lncRNA in a syngeneic mouse tumor model.

4.7.1 Search of ADPGK-AS1 mouse orthologue

For experimental convenience, we first searched whether ADPGK-AS1 is conserved throughout species. Unfortunately, we were not able to find an annotated ADPGK-AS1 gene in mouse or another species, thus we needed to identify other criteria giving hints to a lncRNA-gene conservation (Figure 4-14). First, the gene locus of flanking protein coding genes can be analyzed regarding conservation. Next, evolutionary conserved regions can be searched by alignment and comparison of the human and e.g. mouse gene loci using the ECR genome browser. Furthermore, the secondary structure of a possible orthologue can be predicted and compared to the predicted human lncRNA-structure using e.g. the RNAfold-WebServer. Finally, the possible orthologue can be identified and annotated using the 5'/3'-RACE method.

Figure 4-14 Schematic overview of steps for annotation of a lncRNA-gene orthologue.

To identify an orthologue of the human ADPGK-AS1 gene, we first analyzed the gene locus regarding their flanking protein coding genes. Unfortunately, ADPGK-AS1 gene locus was not conserved in fruit fly (*Drosophila melanogaster*), zebrafish (*Danio rerio*) or mouse (*mus musculus*) (Figure 4-15 a). We went further and searched for evolutionary conserved regions. However, we were not able to find sequence similarities between the human ADPGK-AS1 exons and the respective genome regions in mouse, african clawed frog (*Xenopus laevis*) or zebrafish (Figure 4-15 b). Due to the lack of possible orthologue sequences, we did not continue with secondary structure prediction and rather searched for possibilities to investigate the role of the human ADPGK-AS1 in tumor development and progression in a humanized mouse model *in vivo* (section 4.7.2) or in context of intact lung structure *ex vivo* (section 4.7.3).

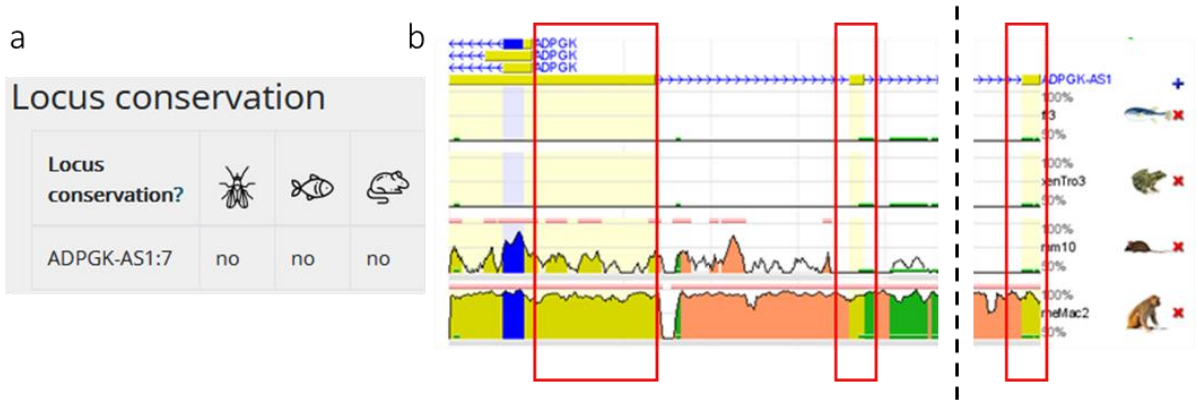

Figure 4-15 Exploration of an ADPGK-AS1 orthologue. a: Analysis of gene locus conservation (flanking protein coding genes) in different species. Source: lncipedia.org **b:** Sequence alignment of human ADPGK-AS1 genomic region with respective regions in other species in search of evolutionary conserved regions using ECR browser. Red boxes indicate human ADPGK-AS1 exon regions.

4.7.2 ADPGK-AS1 knockdown reduces tumor growth *in vivo*

Due to lack of an ADPGK-AS1 mouse orthologue, we took advantage of a humanized mouse model. NSG mice have a severely impaired immune profile, which allowed us to inject human tumor cells without triggering a rejection reaction. To test if this mouse model was appropriate for our purpose, we did an initial experiment in which we co-injected A549 tumor cells together with primary human macrophages polarized to M0, M1-like or M2-like phenotype. In this experiment, tumor growth in tumor cell control mice (without macrophages) and A549 co-injected with M0 macrophages were similar (Figure 4-16 a-c). When A549 cells were co-injected with M1-like macrophages, tumors were smaller compared to the control groups, and co-injection with M2-like macrophages led to development of the largest tumors. This confirms the published and known knowledge of M1-like and M2-like macrophages concerning their influence on tumor growth and shows, that this mouse model can be used to analyze human tumor growth affected by human macrophage phenotypes.

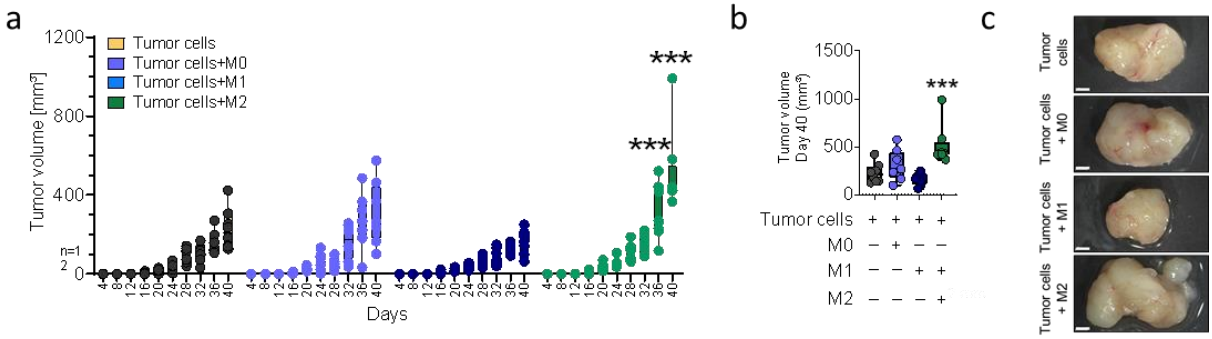

Figure 4-16 Macrophage phenotypes can influence the tumor growth *in vivo*. a-b: Subcutaneous (s. c.) co-injection of A549 cells human primary macrophages either unstimulated (M0), treated with LPS/IFNɣ (M1-like) or treated with IL-4 (M2-like) in immune-deficient NSG mice. Tumor volume was measured every 4 days and again quantified after 40 days after tumor isolation. n = 8 **c:** Representative images of s. c. tumors. scale bar = 2 mm, ***p≤0.001 compared to Tumor cells+M1. Data are represented as mean ± SEM

Next, we assessed the role of ADPGK-AS1 in macrophages during tumor progression. For this, we isolated primary macrophages and polarized them to M1-like or M2-like phenotype. These macrophages were then transfected with antisense LNA GapmeRs for ADPGK-AS1 or a negative control. Again, co-injection of A549 with M1-like control macrophages showed significantly decreased tumor growth compared to the A549 tumor cell control group. Co-injection together with M2-like macrophages transfected with the negative control again showed the highest tumor growth. However, after knockdown of ADPGK-AS1 in M2-like macrophages, this tumor growth was significantly reduced by around 50 % and even comparable to the M1-like control group, which showed only 40 % of the tumor size compared to the M2-like control group (Figure 4-17 a-b). Next, the analysis of tumor cell proliferation and apoptosis showed high proliferation and less apoptosis in M2-like control tumors, while tumors co-injected with M1-like control macrophages showed high apoptosis and reduced proliferation (Figure 4-17 c-d). In tumors developed in animals with co-injection of tumor cells and M2-like-ADPGK-AS1 knockdown macrophages, proliferation was reduced compared to M2-like control group, whereas levels of apoptotic cells were again increased. LDH activity assay, a marker for tumor invasiveness and metabolic activity, was very high in M2-like control tumors and again reduced in M2-like ADPGK-AS1 knockdown tumors (Figure 4-17 c + e). Taken together, these results suggest that the tumor promotive capability of M2 macrophages is reduced after ADPGK-AS1 knockdown and that this can reduce tumor growth *in vivo*. Reduction of ADPGK-AS1 expression (Figure 4-17 f) again confirmed the relationship of ADPGK-AS1 expression and tumor growth. In addition, we analyzed the expression of the identified ADPGK-AS1 protein interaction partner MRPL15 and MRPL35 in the tumors. Protein analysis revealed upregulated levels of MRPL35 in tumors co-injected with tumor cells and M2-like control macrophages compared to the M1-like control group as well as the tumor cell control groups. Interestingly, MRPL35 expression was reduced in animals co-injected with M2-like macrophages with an ADPGK-AS1 knockdown (Figure 4-17 g). However, protein levels of MRPL15 did not seem to be regulated between groups. Taken together, these results demonstrate a correlation of ADPGK-AS1 expression in macrophages with increased tumor growth and progression *in vivo*.

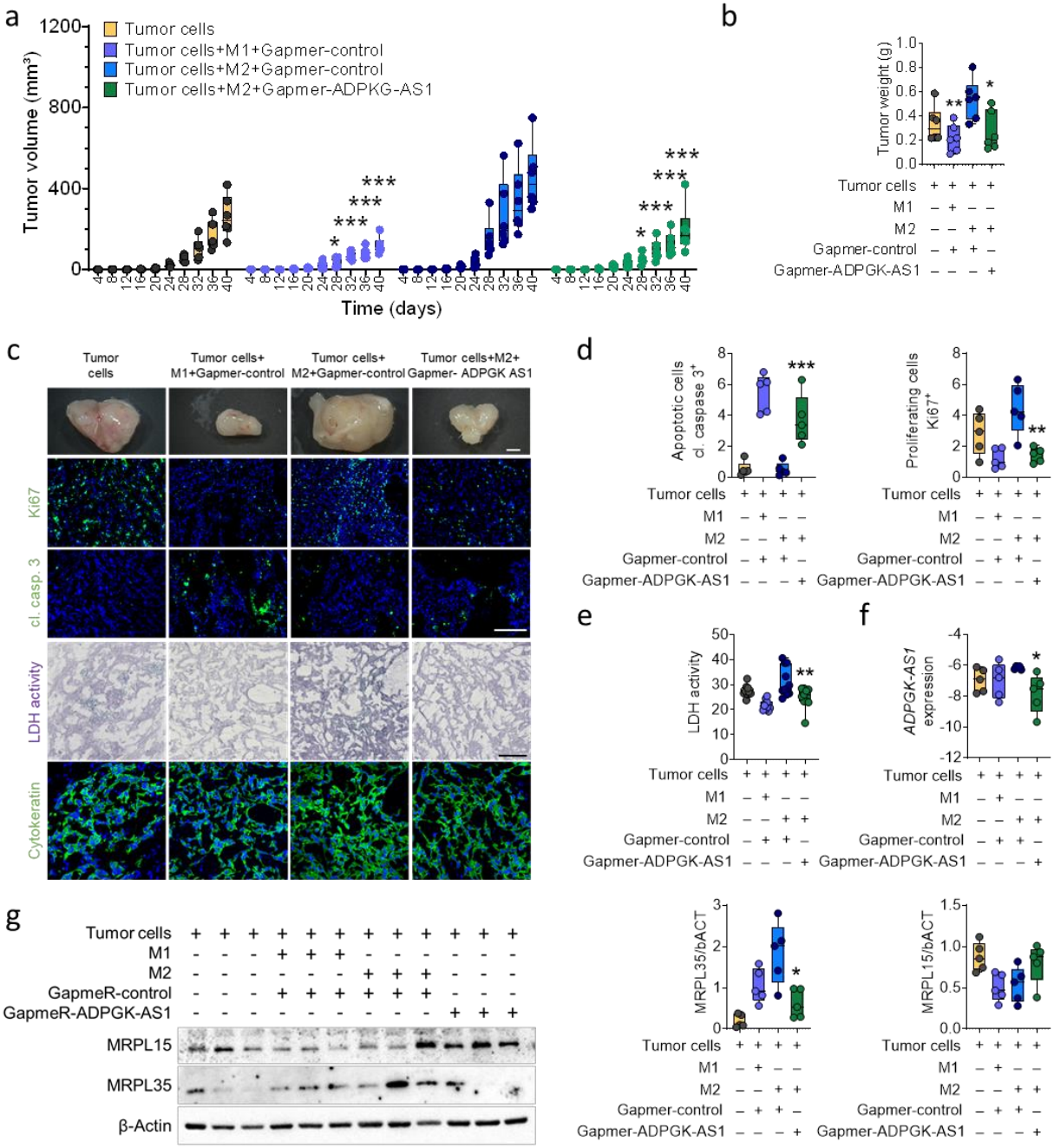

Figure 4-17 ADPGK-AS1 knockdown in macrophages reduces tumor growth *in vivo*. a: Time dependent tumor growth (volume, mm^3) within 40 days after subcutaneous (s. c.) co-injection of M1-like or M2-like macrophages transfected with antisense LNA GapmeRs against ADPGK-AS1 or a negative control. n = 6 **b:** Tumor weight after 40 days of co-injection. n = 6 **c:** Representative brightfield images (tumor size; scale bar = 2 mm), fluorescence images (Ki67, cleaved caspase 3; scale bar = 200 µm) and images of LDH activity (scale bar = 25 µm) together with Cytokeratin (tumor tissue) **d:** Quantification of Ki67 and cl. Casp. 3 staining in tumor sections. n = 5 **e:** Quantification of LDH activity staining in tumor sections. n = 10 **f:** RNA expression analysis of ADPGK-AS1 in isolated tumor tissue. n = 5 **g:** Representative immunoblot and quantification of MRPL15 and MRPL35 protein expression in isolated tumor tissue. n = 5, *p≤0.05, **p≤0.01, ***p≤0.001 compared to Tumor cells+M2 GapmeR-control. Data are represented as mean ± SEM

4.7.3 ADPGK-AS1 modulation in the *ex vivo* model of human precision cut lung slices

As shown in humanized mouse model *in vivo*, ADPGK-AS1 modulation influences the tumor growth. To further understand the role of ADPGK-AS1 in a real-life situation, we were in need to develop a new tumor model. For this, we established and optimized the method of human precision cut lung slices (PCLS) during this study. Here, a human (tumor-bearing or healthy) lung lobe is filled with agarose in the surgery theater to preserve the lung structure. Next, with the help of a pathologist, the tumor tissue and non-tumor tissue are separated and the tissue-agarose-blocks are sliced into ~400 µm thick sections, resulting in non-tumor tissue PCLS (healthy, hPCLS) and tumor tissue PCLS (tPCLS) (Figure 4-18 a).

For hPCLS, GFP labeled A549 cells were added and grown to mimic lung tumor development, which was then used for treatment options (Figure 4-18 b). After incubation time, A549 cells on the PCLS were analyzed regarding their number, proliferation, and apoptosis marker. Interestingly, tissue resident macrophages present in the donor lung were even seen to invade the A549- "tumor"- area, as shown by staining of CD68 positive cells (Figure 4-18 c).

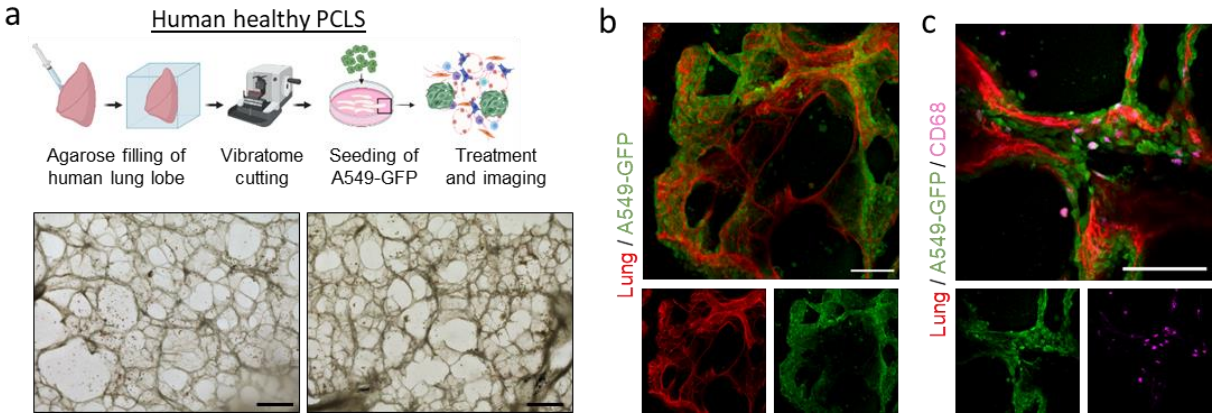

Figure 4-18 Tumor cell growth on non-tumor PCLS function as an *in vivo*-like lung tumor model. a: Schematic overview of healthy PCLS preparation and experimental design with representative brightfield images. scale bar = 500 µm. **b-c:** Representative fluorescence image of healthy PCLS (red, lung autofluorescence) seeded with A549-GFP cells (green) stained for $CD68^+$ cells (purple). scale bar = 150 µm.

To analyze the impact of ADPGK-AS1 downregulation in M2 macrophages on the tumor growth in this model, we seeded A549-GFP cells on hPCLS and treated them with different macrophage CM. Quantification of GFP positive tumor cells showed few numbers on hPCLS treated with M1-like control CM and a high number of A549 cells on PCLS treated with M2-like control CM (Figure 4-19 a-b). When ADPGK-AS1 was downregulated in M2-like macrophages, the number of GFP positive tumor cells strongly decreased on the hPCLS treated with this CM. Additionally, we treated the hPCLS with ADPGK-AS1 OE CM

macrophages. CM derived from ADPGK-AS1 OE macrophages was able to increase A549-GFP number compared to the control CM on hPCLS.

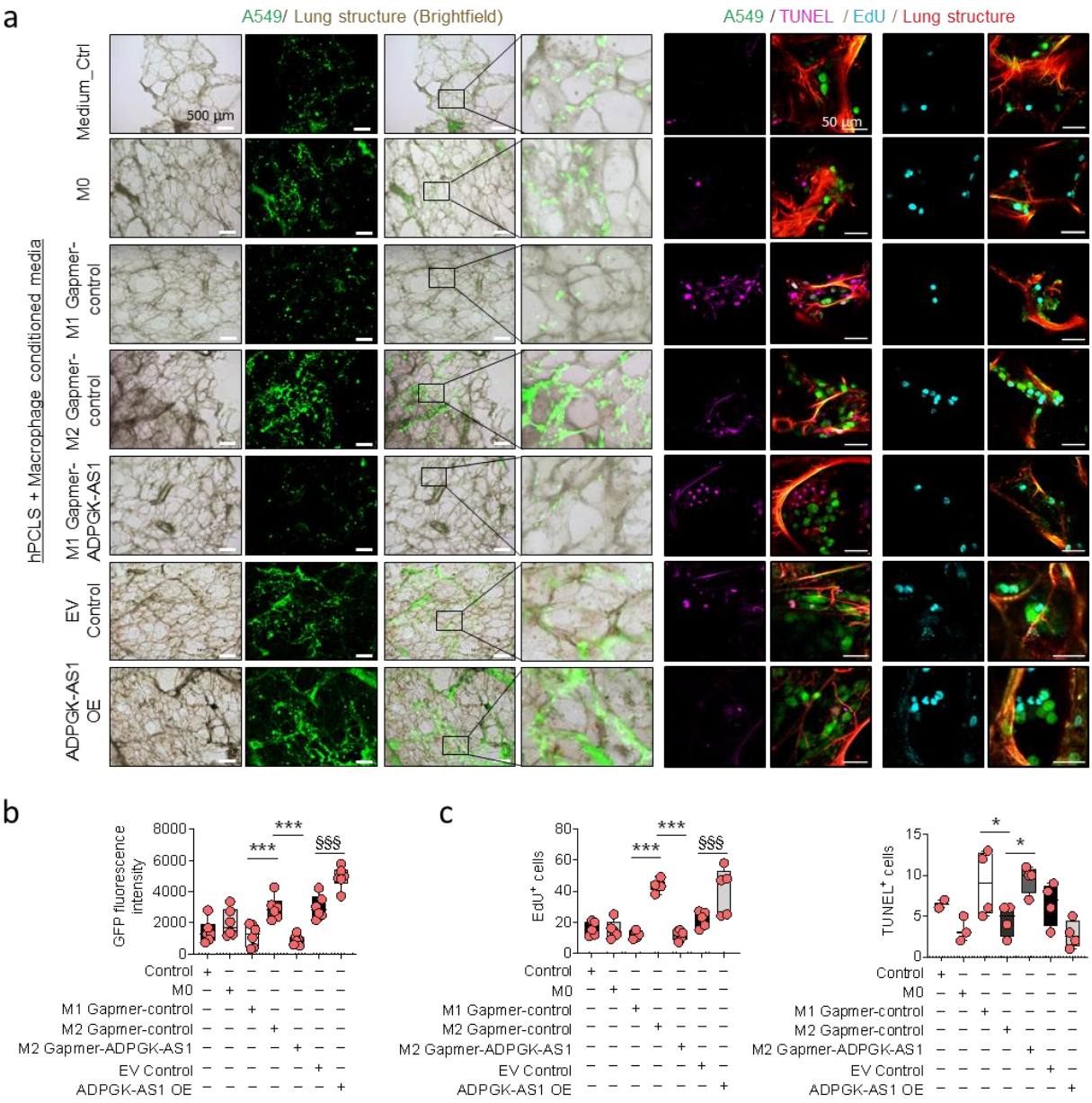

Figure 4-19 ADPGK-AS1 influences lung cancer cell growth and apoptosis *ex vivo*. a: Representative brightfield and fluorescence images of hPCLS (red, autofluorescence) with A549-GFP (green), apoptotic (magenta) and proliferative (cyan) cells in sections treated with CM of primary M1-like and M2-like macrophages transfected with antisense LNA GapmeRs against ADPGK-AS1 or a negative control, or CM of THP1 control and ADPGK-AS1 overexpressing macrophages. scale bar = 500 µm (left panel), 50 µm (right panel). **b-c:** Quantification of GFP^+ (A549), EdU^+ (proliferative) and $TUNEL^+$ (apoptotic) cells on hPCLS treated with CM of primary M1-like and M2-like macrophages transfected with antisense LNA GapmeRs against ADPGK-AS1 or a negative control, or CM of THP1 control and ADPGK-AS1 overexpressing macrophages. n = 6, *p≤0.05, ***p≤0.001 compared to M2 GapmeR control CM, §§§p≤0.001 compared to EV control CM. Data are represented as mean ± SEM

Further, analysis of proliferative (EdU^+) and apoptotic ($TUNEL^+$) cells showed expected results based on the *in vitro* data (Figure 4-19 a right panel, c). Proliferation marker were downregulated in hPCLS seeded with A549-GFP and treated with M1-like control CM as well as M2-like ADPGK-AS1 knockdown CM compared to the M2-like control CM and upregulated in sections treated with ADPGK-AS1 OE CM compared to the EV control CM. Apoptotic marker showed the opposite regulation, peaking in PCLS treated with M1-like control CM, followed by M2-like ADPGK-AS1 KD CM. These results confirm the anti-tumorigenic effect of an ADPGK-AS1 knockdown in M2-like macrophages in a humanized lung tumor model.

In addition to the hPCLS system, we also used tumor-bearing lung lobes to generate tPCLS (Figure 4-20 a). Tumor PCLS has the advantage of using real life lung cancer tissue in culture. After treatment of choice, the tPCLS were stained with cytokeratin as a marker for tumor area (Figure 4-20 b). Similarly to hPCLS all kinds of cell types including $CD68^+$ cells were found in tPCLS (Figure 4-20 c). Notably, these TAMs showed expression of different macrophage activation marker, such as IL-8 or ALOX15, reflecting the diversity of TAM phenotypes in the lung TME, interacting with the tumor ($cytokeratin^+$) cells (Figure 4-20 d).

Additionally, the tumor cells in the tPCLS showed high proliferation marker ($Cytokeratin^+/EdU^+$ cells, Figure 4-20 e), suggesting a good viability of the tissue sections. Hence, this human relevance method allowed us to treat human lung tumor tissue and analyze the effect of ADPGK-AS1 expression modulation to profile direct human relevance in context of lung cancer patients.

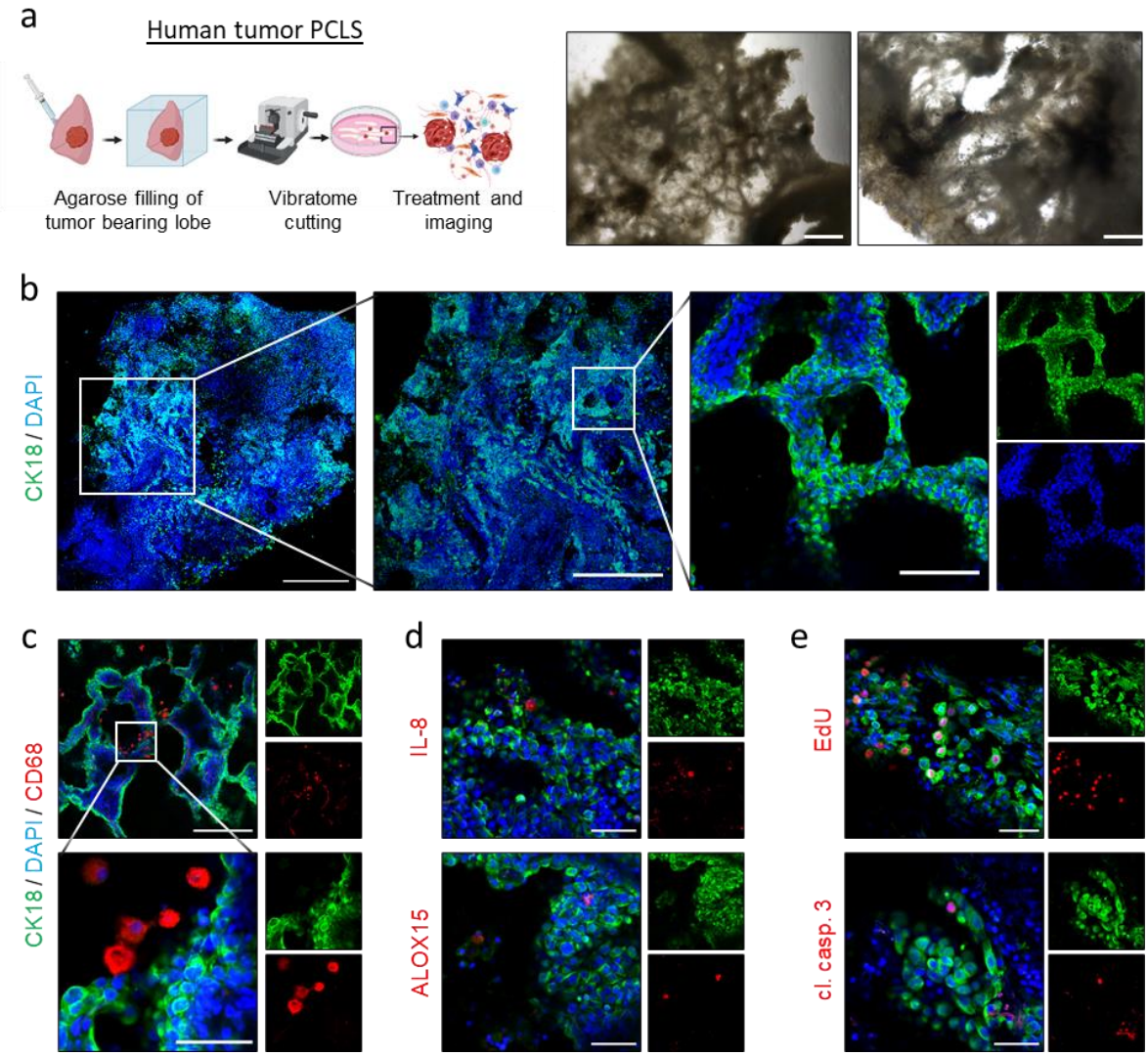

Figure 4-20 Human tumor precision cut lung slices (tPCLS). a: Schematic overview of PCLS preparation with representative bright field images. scale bar = 500 µm **b:** Representative fluorescence images of tPCLS stained with cytokeratin (green) for tumor cells and DAPI (blue) for nuclei. scale bar (from left to right) = 1 mm, 500 µm, 100 µm **c-e:** Representative images of tPCLS stained with cytokeratin (green) for tumor area, DAPI (blue) for nuclei, and marker for macrophages (CD68, IL-8, ALOX15), proliferation (EdU) and apoptosis (cleaved caspase 3) (red). scale bar = 250 µm (c, upper panel), 50 µm (c lower panel, d and e)

Next, we used the tPCLS to analyze ADPGK-AS1 regulation in tumor growth *ex vivo*. Here, we transfected tPCLS with antisense LNA GapmeRs specific against ADPGK-AS1 or a negative control. Additionally, we added THP1 control and ADPGK-AS1 OE macrophages to the tPCLS. After 24 hours incubation, we fixed the sections and stained them for proliferation and apoptosis marker and isolated RNA as well as protein. Staining analysis revealed a reduced number of proliferative (EdU^+) cells in tPCLS with an ADPGK-AS1 knockdown and increase of proliferative cells in sections with ADPGK-AS1 OE macrophages (Figure 4-21 a+c). Staining and quantification of apoptotic cells within the tPCLS revealed that treatment with GapmeR-ADPGK-AS1 increased tumor cell apoptosis, while apoptotic cells were reduced in tPCLS with ADPGK-AS1 OE macrophages (Figure 4-21 b-c). Further, ADPGK-AS1 OE and

GapmeR-ADPGK-AS1 CM treated tPCLS confirmed the down- and upregulation of ADPGK-AS1 (Figure 4-21 d). Next, protein isolation showed similar results as microscopic quantification (Figure 4-21 e), with proliferation marker (Cyclin D1, PCNA) being reduced after knockdown and increased with ADPGK-AS1 OE macrophages, while apoptotic marker (cleaved caspase 3) showed the opposite regulation to the proliferation marker. Additionally, ADPGK-AS1 interaction partner MRPL15 and MRPL35 were analyzed regarding their regulation. MRPL35 showed downregulation after ADPGK-AS1 knockdown and upregulation in tPCLS with ADPGK-AS1 macrophages. Furthermore, we saw changes of macrophage marker expression IL-8 and CD206, suggesting an influence of ADPGK-AS1 on TAM activation.

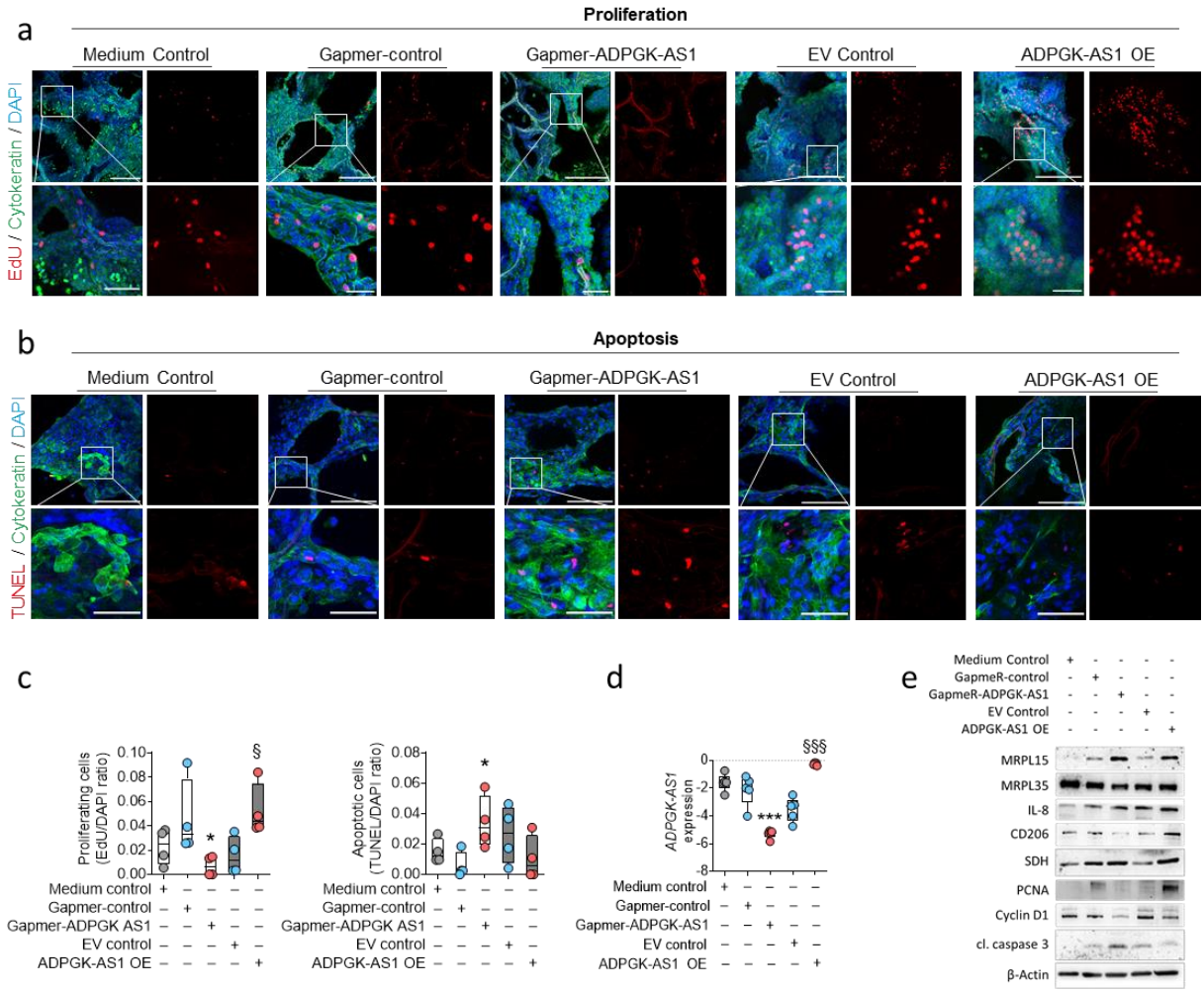

Figure 4-21 ADPGK-AS1 influences human lung tumor progression *ex vivo*. a-b: Representative images and quantification of tumor PCLS stained for proliferative (EdU$^+$) and apoptotic (TUNEL$^+$) cells (red) in relation to total cell number (DAPI+, blue) in tumor area (Cytokeratin$^+$, green). scale bar = 250 µm (upper row), 50 µm (lower row, magnification) **c:** Quantification of proliferative and apoptotic cells with regard to total cell number (DAPI$^+$ cells). n = 10, *p≤0.05 compared to GapmeR-control, §p≤0.05 compared to EV control **d:** RNA expression analysis ADPGK-AS1 in tumor PCLS treated with antisense LNA GapmeRs specific for ADPGK-AS1 or a negative control or seeded with THP1 control or ADPGK-AS1 OE cells. n = 5, ***p≤0.001 compared to GapmeR-control, §§§p≤0.001 compared to EV control **e:** Representative Immunoblot of proteins involved in proliferation (PCNA, cyclin D1), apoptosis (cl. caspase 3), metabolism (SDH), or macrophage activation (IL-8, CD206). Data are represented as mean ± SEM

5 Discussion

5.1 Long non-coding RNAs in macrophage phenotypes

TAMs have been known to be crucial players during tumor development and progression. Several studies have shown that TAM density correlates with a poor prognosis in lung cancer (Schmall et al. 2015; Zheng, Weigert, et al. 2020; Ruffell and Coussens 2015). Macrophages are able to dynamically adapt their phenotype to a more pro-inflammatory and anti-tumorigenic (M1-like) or anti-inflammatory and tumor promoting (M2-like) phenotype. This plasticity is orchestrated by a variety of cytokines, chemokines and metabolites within the TME (Ley 2017; Sarode, Schaefer, et al. 2020; Zheng, Mansouri, et al. 2020). Understanding the underlying molecular mechanisms is important for the development of new strategies in immunotherapy and targeted therapy.

Long non-coding RNAs (lncRNAs) can influence different cellular processes through various signaling pathways and many lncRNAs, such as MALAT1 or HOTAIR are known to be commonly deregulated in cancer (Wu et al. 2018; Jin et al. 2017; Wu et al. 2021; Tang and Hann 2018; Ji et al. 2003). When it comes to macrophage activation, several lncRNAs involved in phenotype regulation have been described, such as Xist, which is upregulated in anti-inflammatory M2-like macrophages or lncRNA GAS5, that is described as a tumor suppressor and upregulated in pro-inflammatory M1-like macrophages (Karger et al. 2021; Jia and Zhou 2020; Mohapatra et al. 2021). However, underlying molecular mechanisms often still need to be further elucidated.

In this study, we used RNA sequencing analysis and were able to identify numerous regulated lncRNAs. Amongst them, ADPGK-AS1 was shown to be upregulated in tumor promoting M2-like macrophages as well as in TAMs from lung cancer patients. ADPGK-AS1 has been previously described as highly expressed in several cancer types and cell lines, such as colon cancer, pancreatic cancer, osteosarcoma and breast cancer (Jiang and Wang 2020; Song et al. 2018; Yang et al. 2019; Luo et al. 2019; Zhang et al. 2020). Mechanistically, ADPGK-AS1 was suggested to act as an RNA sponge for miRNAs, such as miR-525, miR-3196 or miR-542-3p in the cytosol, leading to reduced tumor cell proliferation, migration, and invasion, e.g. via regulating ZEB1-mediated epithelial-to-mesenchymal transition (EMT). In macrophages, we were able to detect a cytoplasmic localization of ADPGK-AS1 as well. Notably, by the start of this project, there was no available literature about the functioning mechanisms of this lncRNA. Thus, to further analyze the signaling pathway, we decided to conduct RNA pulldown experiments to identify interacting proteins. Interestingly, identification of various mitochondrial ribosomal proteins (MRPs), as well as fractionation and co-staining led to the conclusion, that ADPGK-AS1 is not only present in the cytoplasm but has the ability to translocate into the mitochondria of macrophages, possibly playing a role in regulation of mitochondrial signaling pathways. Up to this date, a limited number of nuclear-encoded non-

coding transcripts haven been shown to be imported into mitochondria. LncRNA SAMMSON for example, is an oncogenic transcript in aggressive melanomas and stimulates mitochondrial function of actively proliferating tumor cells (Leucci et al. 2016; Vendramin et al. 2018). Also, several miRNAs, such as miR-1, miR-181c or miR-378 haven been shown to localize within the mitochondria, influencing mitochondrial mRNA stability (Zhang, Zuo, et al. 2014; Das et al. 2017; Jagannathan et al. 2015). Although several studies aimed to understand the specific mitochondrial import mechanisms by identification of crucial RNA sequences needed for the import (Jeandard et al. 2019), a general mechanism and all involved players have not yet been described in human. Furthermore, existence and function of mitochondria imported lncRNAs in macrophages is completely unknown. Hence, investigation of the ADPGK-AS1 function within the mitochondria in macrophages can be of help to elucidate some of those functions.

5.2 Mitochondrial metabolic regulation of ADPGK-AS1

Mitochondria are known as the “powerhouse of the cell” and are double membrane organelles containing the components of the electron transport chain (ETC), which is responsible for generation of a proton gradient and thereby conversion of ADP to ATP via the ATP synthase (Papa et al. 2012). Mitochondria contain their own small genome of 16,850 bp that codes for 2 rRNAs, 22 tRNAs and 13 mRNAs, which are transcribed and further translated via a mitochondrial-specific ribosomal complex (Sylvester et al. 2004). Mitochondrial ribosomes consist of a large 39S subunit and a small 28S subunit, comprised of a diverse set of MRPs, other proteins and rRNAs, and differ from both prokaryotic and eukaryotic cytosolic ribosomes e. g., in being less RNA rich than the other two (Spremulli 2016; Taanman 1999). More recently, MRPs have been shown to not only be involved in translation of mitochondrial genes, but also in regulation of several other cellular processes such as regulation of oxidative phosphorylation or induction of apoptosis (Huang, Li, and Zhang 2020). Additionally, while mutation of cytoplasmic ribosomal proteins are usually lethal during development, consequences of MRP mutations range from lethality to marginally impaired energy metabolism (Sylvester et al. 2004), again highlighting that the process of mitochondrial translation and the involvement of MRPs, or other functions of these proteins, are still not fully understood.

Interestingly, we were able to newly identify MRPL35 and MRPL15 as interaction partner of ADPGK-AS1 in macrophages. Both proteins are reported to be prognostic markers and upregulated in breast or colorectal cancer (Sotgia, Fiorillo, and Lisanti 2017; Zhang et al. 2019). In the present study, we were able to show that MRPL35 and MRPL15 are correlated with a short overall survival of lung cancer patients and are strongly increased with high ADPGK-AS1 expression in macrophages, suggesting a central role of ADPGK-AS1 and its interaction partner in association with lung cancer progression.

Furthermore, overexpression of ADPGK-AS1 resulted in an increased number of mitochondria with higher amount of mitochondrial DNA content, as well as increased proteins levels of MRPs and components of the ETC, such as cytochrome C. MRPL35 has been shown to play a key role in coordination of synthesis and assembly of cytochrome C in yeast, thereby directly regulating rates of oxidative phosphorylation (Box, Kaur, and Stuart 2017). Consistent with these findings, elevated MRPL35 and cytochrome C levels in our ADPGK-AS1 overexpressing macrophages resulted in increased ATP production and higher basal as well as ATP-linked respiration, suggesting overall enhanced number and more active mitochondria.

More recently, it has become clear that mitochondria are highly mobile organelles and that mitochondrial dynamics have an impact on cellular metabolism, but also cell division, differentiation, or cell death. The process of combining neighboring mitochondria is described as fusion and leads to a long, elongated mitochondrial network. Fusion of the outer membrane is regulated by Mitofusin (Mfn) proteins 1 and 2, while fusion of mitochondrial inner membrane is mediated by the optic atrophy 1 (Opa1) protein (Altieri 2019; El-Hattab et al. 2018; Xie, Li, and Jin 2020). Mitochondrial fission is the opposite process and describes the division of mitochondria into smaller fragments. Fission is mediated by dynamin-related protein 1 (Drp1) and, more upstream, enhanced by the AMPK pathway by phosphorylation of mitochondrial fission factor (MFF) (Herzig and Shaw 2018). Interestingly, we found that upon ADPGK-AS1 overexpression in macrophages, both Mfn1 and Opa1 were downregulated, while Drp1 and the AMPK pathway seem to be activated, suggesting induction of mitochondrial fission. This was confirmed by detecting a high number of small and fragmented mitochondria in ADPGK-AS1 overexpression macrophages. Mitochondrial dynamics are very important in quality control, i. e. regulation of mitophagy, but also in the maintenance of metabolic homeostasis. Although mitochondrial dynamics are in a way connected with their physiological functions, mitochondrial fission and fusion processes still need to be fully understood in context of immune response (Gao et al. 2017; Wai and Langer 2016). Interestingly, in this study we were able to link mitochondrial morphology with the macrophage phenotype. While enhanced mitochondrial fusion was observed in M1-like macrophages, M2-like macrophages were seen to have enhanced mitochondrial fission, similar to ADPGK-AS1 OE macrophages. Notably, mitochondrial morphology and dynamics have been previously described for different macrophage subtypes (Li, He, et al. 2020). In that study, the authors showed contradictory results with enhanced mitochondrial fission in M1-like activated macrophages and increased mitochondrial fusion in M2-like macrophages. However, this study was done in a murine system with bone marrow derived macrophages treated with M-CSF, while our data resulted from human THP1 macrophages treated with different cytokines. To that end, it must be noted that when it comes to metabolism, numerous factors can influence and change this complex signaling network within the cell, therefore it is crucial to compare the observed phenotypes

and results within one system. Taken together, these results suggest that high expression of ADPGK-AS1 in macrophages leads to enhanced mitochondrial fission process, therefore a higher number of mitochondria in these macrophages and a suggested phenotypic switch towards the M2-like macrophage phenotype.

In addition to mitochondrial morphology, ADPGK-AS1 expression modulation seems to change the metabolic availability in macrophages. Upregulation of TCA cycle metabolites, enhanced TCA cycle enzyme activity and increased mitochondrial membrane potential suggest that ADPGK-AS1 changes the macrophage metabolism towards enhanced oxidative phosphorylation (OXPHOS) and thereby, on a metabolic level, to the anti-inflammatory M2-like macrophage phenotype, which was previously described to rely on enhanced OXPHOS for energy production (Kelly and O'Neill 2015). Additionally, elevated ROS levels in macrophages are known to be important in host defense against pathogens and often upregulated in M1-like macrophages (Tan et al. 2016; Deng et al. 2019). Thus, the observed downregulation of ROS through ADPGK-AS1 further confirms activation of those macrophages to an anti-inflammatory M2-like phenotype. Interestingly, MRPL35 has been described to regulate production of ROS in colorectal cancer (Zhang et al. 2019), again suggesting that ADPGK-AS1 function is carried out through its interaction with MRPS, particularly MRPL35.

Collectively, these results demonstrate that high expression of ADPGK-AS1 induces mitochondrial fission, increases the number of mitochondria (mt), mt-DNA and mt-proteins, and enhances the amount of TCA cycle metabolites, thereby resulting in overall more active mitochondria in macrophages. Notably, only a few lncRNAs have been described in relation to mitochondrial function. For example, tumor suppressive lncRNA GAS5 was recently described to enter the mitochondria under stress conditions, forming a complex with TCA cycle enzyme malate dehydrogenase (MDH2), leading to cellular growth arrest (Sang et al. 2021). Another lncRNA; lncFAO was shown to bind mitochondrial proteins in mouse macrophages, enhancing inflammation resolution by activation of fatty acid oxidization (Nakayama et al. 2020). Besides these examples, the field of lncRNA-mediated mitochondrial regulation, especially in a human system, is only in the beginning. Nevertheless, it is gradually gaining more attention. The extend of mitochondrial metabolic modulation in human macrophages through ADPGK-AS1, particularly in tumor associated macrophages, is a good example to highlight the importance of this research area.

5.3 ADPGK-AS1 regulation in milieu of macrophage-tumor cell-crosstalk

Several studies have linked mitochondrial metabolism with tumor progression as well as macrophage activation states (Kelly and O'Neill 2015; Foo et al. 2021; Wang et al. 2021).

Additionally, accumulating evidences demonstrate that crosstalk between tumor cells and immune cells in the TME is one of the most important processes modulating tumor development, malignancy, immune cell infiltration, and tumor metastasis (Sarode, Schaefer, et al. 2020; Schmall et al. 2015; Wei et al. 2019; Sarode, Zheng, et al. 2020). Understanding these regulations on the molecular level is crucial when it comes to the development of promising new therapeutic approaches in targeted and immunotherapy. At the tumor site for instance, secreted colony stimulus factor 1 (CSF-1) and IL-6 is closely associated with TAM infiltration of tumor stroma in NSCLC (Pei et al. 2014), suggesting that tumor cells specifically recruit monocytes/macrophages into the tumor tissue. Monocytes/macrophage recruitment is further stimulated by TAMs secreting IL-8, leading to enhanced CSF-1 production (Wang et al. 2016), which is a vicious feedback loop. In addition, CCL2 is a prominent tumor cell secreted chemokine that is known to recruit (C-C motif) receptor 2 (CCR2)-expressing monocytes to the tumor tissue (Chen et al. 2018). Following the TAM recruitment, tumors are able to activate the macrophages to behave tumor-beneficial. Thus, a variety of secreted molecules such as IL-4, IL-10, IL-13, CSF-1, or TGF-β are present in the TME, pushing the TAM phenotype towards an M2-like activation (Van Dyken and Locksley 2013; Li et al. 2015; Standiford et al. 2011; Ambade et al. 2016). Furthermore, metabolic conditions in the TME, such as acidification due to high lactate production in hypoxic regions, can affect TAM polarization towards a pro-tumoral M2-like profile (de Goede, Driessen, and Van den Bossche 2020).

In our study, we used a macrophage-tumor cell co-culture model to investigate the crosstalk between those cell types. A549 cells, a human non-metastatic adenocarcinoma cell line, was chosen to represent lung cancer cells in this system. Notably, we observed M2-like activation of macrophages co-cultured with tumor cells, together with increased expression of lncRNA ADPGK-AS1 and upregulation of TCA cycle metabolites. “Teaching” of macrophages adjacent to tumor cells to acquire an M2-like tumor promoting phenotype thus reflects the macrophage changes induced by ADPGK-AS1 overexpression.

Additionally, we hypothesized that tumor cells secrete molecules that are able to induce ADPGK-AS1 transcription. As stated before, metabolic changes in TME can modulate TAM activation. Since we were able to show that ADPGK-AS1 expression in macrophages leads to metabolism-associated changes, we wanted to further focus on deregulated metabolites that may have the potential to regulate macrophage activation and gene transcription. Metabolite analysis of co-culture medium revealed a deregulation of several metabolites after macrophage-tumor cell crosstalk. Amongst them, αKG was highly increased in co-culture medium and was able to induce ADPGK-AS1 expression in macrophages. Therefore, it is possible that tumor cell derived αKG plays an upstream role in the ADPGK-AS1 pathway.

αKG is a two carboxylic group with a ketone group in the α-position and is mainly produced in the TCA cycle from isocitrate in a reaction catalyzed by the enzyme isocitrate

dehydrogenase (IDH) (Abla et al. 2020). In addition, αKG can be produced by glutaminolysis, in which glutamine is conversed in a two-step reaction to αKG and ammonia (Xiao et al. 2016). As most of the TCA cycle metabolites, αKG is able to shuttle between mitochondria and cytoplasm and crosses the mitochondrial membranes through the voltage-dependent anion channel (VDAC) and the αKG/malate antiporter (Monne et al. 2013). Besides its role as a TCA intermediate, αKG was shown to be involved in several other cellular processes by regulating activity of various enzymes or by being a substrate for other biosynthetic reactions (Abla et al. 2020). For instance, chromatin modifying enzyme Jumonji-domain containing histone demethylase (JmjC-KDM) uses αKG as a cofactor to remove methyl groups from histones (Kooistra and Helin 2012), shaping the epigenetic landscape and altering gene expression. In macrophages, it was suggested that increased amounts of αKG generated from glutaminolysis promotes the M2-like phenotype via the Jmjd3-depenedent metabolic and epigenetic reprogramming (Liu et al. 2017), increasing the expression of M2-like marker genes such as Arginase-1 (Arg1) and decreasing the expression of M1-like markers such as IL-1β, TNFα or IL-12. In our system, treatment of macrophages with αKG was able to confirm these results. Here, we detected downregulation of IL-1β and upregulation of M2-like marker IL-10, which is a similar expression pattern as in macrophages with ADPGK-AS1 overexpression. Additionally, CM of αKG-treated macrophages was able to enhance tumor cell migration, further suggesting an activation towards the M2-like phenotype and again mimicking the influence on tumor cells of macrophages with an ADPGK-AS1 overexpression.

Collectively, these results together with the detected upregulation of ADPGK-AS1 expression in macrophages after co-culture as well as after direct αKG treatment, suggest that tumor cell secreted αKG could be an upstream mediator of ADPGK-AS1 expression, further modulating them into a tumor promoting M2-like phenotype by downregulation of inflammatory cytokines and upregulation of anti-inflammatory cytokines through ADPGK-AS1. ADPGK-AS1 expression in macrophages seems to play a crucial regulatory role to generate a TAM-like phenotype through crosstalk with cancer cells, resulting in a metabolic switch to energy production via the mitochondrial respiratory chain. However, whether ADPGK-AS1 gene expression is enhanced due to αKG-mediated epigenetic changes in macrophages, remains to be further investigated in detail. Additionally, the role of αKG in different tumors and tumor cells remains to be not fully understood. IDH1 and IDH2 have been shown to be frequently mutated in different cancer types (Yan et al. 2009; Mardis et al. 2009), leading to a more malignant phenotype. However, in NSCLC, IDH mutations are not commonly observed (Rodriguez et al. 2020). The role of IDH and αKG, particularly in lung cancer, and its potential to modulate the immune inflammatory microenvironment, should be further elucidated.

5.4 ADPGK-AS1 regulates macrophage phenotype and influences lung tumor progression

The central role of ADPGK-AS1 in M2-like macrophage activation is further supported by a series of *in vitro*, *in vivo* and *ex vivo* experiments.

First, we wanted to determine whether the observed mitochondrial and metabolic changes in the macrophages influence the macrophage phenotype. Interestingly, high expression of ADPGK-AS1 in THP1 macrophages was able to enhance an activation towards the M2-like phenotype on transcriptional level as well as regarding tumor cell functional assays by decreasing apoptosis and increasing migration of lung cancer cell lines. This demonstrates, that overexpression of ADPGK-AS1 alone is sufficient, to induce a tumor promoting macrophage phenotype. On the other hand, downregulation of ADPGK-AS1 in PBMC-derived M2-like macrophages showed the complete opposite effect. Here, we saw increased expression of pro-inflammatory M1-like marker and downregulation of anti-inflammatory pro-tumorigenic M2-like marker. In addition, inhibition of ADPGK-AS1 in M2-like macrophages was able to induce tumor cell apoptosis, while tumor cell migration was reduced. Collectively, this demonstrates that ADPGK-AS1 plays a crucial role in the macrophage activation process and might serve as a target in the development of novel lung cancer therapeutics.

Although numerous antisense lncRNAs are described in the literature to function via regulating their antisense protein coding gene, we were able to exclude that ADPGK-AS1 directly induces ADPGK expression. Hence, the observed changes are not regulated via the ADPGK gene and seem to be an indirect, more downstream effect upon ADPGK-AS1 expression modulation, which goes in line with the previously shown cytoplasmic/mitochondrial localization of the lncRNA. The influence of ADPGK-AS1 up- or downregulation on the macrophage activation state seems to not be regulated via ADPGK, but is possibly a result of the previously shown influence of ADPGK-AS1 on macrophage mitochondrial signaling pathway.

The use of cell lines and primary macrophages is adequate and convenient to investigate whether the gene of interest influences cellular signaling pathways. Nonetheless these artificial 2D *in vitro* culture systems are too simple and lack the ability to display the full complexity of the heterogeneity of the TME. Thus, we also wanted to investigate the biological significance of ADPGK-AS1 during tumor development *in vivo*.

The majority of lncRNAs are poorly conserved throughout species (Johnsson et al. 2014), at least regarding sequence similarity. Some lncRNAs have been shown to have a conserved secondary structure, which makes it more challenging to identify those. Unfortunately, there is also no orthologue annotated for ADPGK-AS1 and our approach to find homologue sequences in mouse was also not successful. Therefore, we used the severely

immunosuppressed mouse line NOD-SCID IL2γ^{null} (NSG) for a humanized *in vivo* tumor model. NSG mice are T and B cell depleted, have a loss of C5 complement, a very low natural killer (NK) cell activity and impaired innate immunity. Additionally, human tumor engraftment was shown to be the most successful when using this mouse model compared to other immunosuppressed mouse lines (Puchalapalli et al. 2016). In our study, we used human primary macrophages activated towards the M1-like or M2-like phenotype and co-injected them to the NSG mice together with human lung cancer cells. As expected, we were able to detect the highest tumor growth in tumor cells co-injected with M2-like macrophages and reduced tumor growth in co-injection with M1-like macrophages. Therefore, we proceeded with this model and transfected the macrophages prior to co-injection to generate an ADPGK-AS1 knockdown in M2-like macrophages. Interestingly, we were able to see that inhibition of ADPGK-AS1 in M2-like macrophages was able to significantly reduce tumor growth by induction of apoptosis and reduction of proliferation compared to tumors developed under influence of M2-like negative control macrophages. LDH enzymatic activity, also often used as a clinical marker for malignant transformation in patients with cancer (Forkasiewicz et al. 2020), was highly increased in tumors co-injected with M2-like control macrophages compared to the M2-like ADPGK-AS1 knockdown group, highlighting the tumor promoting function of the M2-like macrophage phenotype, which is reduced after inhibition of ADPGK-AS1. Additionally, protein interaction partner MRPL35 was reduced in tumors developed under influence of macrophages with an ADPGK-AS1 knockdown. Collectively, these results confirm the *in vitro* data and show that ADPGK-AS1 could serve as a novel therapeutic target in lung cancer therapy.

In contrast to the 2D cell culture method, investigation of tumor development in NSG mice *in vivo* has the advantage of a natural 3D structure. However, besides the injected macrophages, we lack the most other immune cell types in this humanized mouse system that are usually present in the TME. In addition, some effects analyzed in a mouse system are not representative of human-specific events (Asghar et al. 2015; Pound and Ritskes-Hoitinga 2018; Rust 1982). Therefore, we aimed one step further and wanted to characterize the therapeutic potential of an ADPGK-AS1 knockdown in a less artificial, human system. For this, we established the *ex vivo* method of (tumor) precision cut lung slices, allowing us to directly culture and treat human lung tissue.

The idea of using tissue slices as a model system to study organ toxicology initially came up by Otto Warburg in the early 1920s, but the limited technology at the time resulted in a low viability and high variability in thickness of the tissue (Warburg 1923). Development of efficient microtomes was a significant step towards reproducibility and the start of today's known precision cut tissue slices (Krumdieck, dos Santos, and Ho 1980; Stadie 1944). PCLS

combine the advantage of a natural 3D *in vivo*-like structure and the presence of all important cell types present in the lung, with exception of recruited cells from the circulatory system (Liu et al. 2019; Preuss et al. 2021). In order to prevent the lung from collapsing, it is inflated with agarose solution to preserve the unique alveoli structure. Recently, the methodology to prepare PCLS with healthy lung tissue has been standardized (Hess et al. 2016; Neuhaus et al. 2017; Preuss et al. 2021), but preparation of human tumor PCLS has not been challenged yet. Due to the nature of tumors, the tissue in this area is very dense and usually not easy to be reached with the agarose. Nonetheless, we were able to optimize the method to produce viable human tumor PCLS that can be used in *ex vivo* experiments.

For this study, we used the tumor PCLS to knockdown ADPGK-AS1 or to introduce ADPGK-AS1 overexpressing macrophages. Interestingly, we were able to see that inhibition of ADPGK-AS1 in the tumor PCLS reduced tumor progression with an increase in tumor cell apoptosis and decrease in proliferation, together with a changed macrophage marker expression, suggesting that ADPGK-AS1 inhibition affects the TAM phenotype. On the other hand, ADPGK-AS1 OE macrophages led to increased proliferation and decreased apoptosis of the tumor cells. Collectively, these results suggest that treatment and expression modulation of ADPGK-AS1 in tPCLS leads to a phenotypic switch of the TAMs, then influencing tumor cell functions. By use of the tPCLS we were able to strikingly demonstrate, that high expression of ADPGK-AS1 in macrophages contributes to lung tumor growth, while ADPGK-AS1 knockdown reduces lung tumor progression *ex vivo*.

5.5 Conclusion

Within the TME, macrophages and tumor cells communicate extensively through several secretory molecules. In the present study, we provide strong evidence that lncRNA ADPGK-AS1 is highly expressed in TAMs and M2-like macrophages and that it is associated with macrophage mitochondria (Figure 5-1). High expression of ADPGK-AS1 seems to be associated with an increased number of mitochondria and induction of mitochondrial fission process. Within the mitochondria, ADPGK-AS1 interacts with mitochondrial ribosomal proteins MRPL35 and MRPL15 and influences energy production by enhancing oxidative phosphorylation, ATP production and mitochondrial membrane potential. On the other hand, ROS are downregulated. With these changes in macrophage metabolism and mitochondrial dynamics, ADPGK-AS1 influences the macrophage activation process by inducing a tumor promoting M2-like phenotype *in vitro* by downregulation of TNFα and IL-8 and upregulation of CD206 and CSF-1R. Knockdown of ADPGK-AS1 reverses this effect *in vitro*, leads to reduced lung tumor growth in a humanized *in vivo* mouse tumor model, and reduces tumor progression in the *ex vivo* system of human tumor precision cut lung slices. Altogether, these data demonstrate that downregulation of ADPGK-AS1 in macrophages has the potential of

reversing a tumor promoting M2-like phenotype towards an anti-tumorigenic M1-like phenotype. Therefore, ADPGK-AS1 represents an interesting target for development of novel lung cancer treatments.

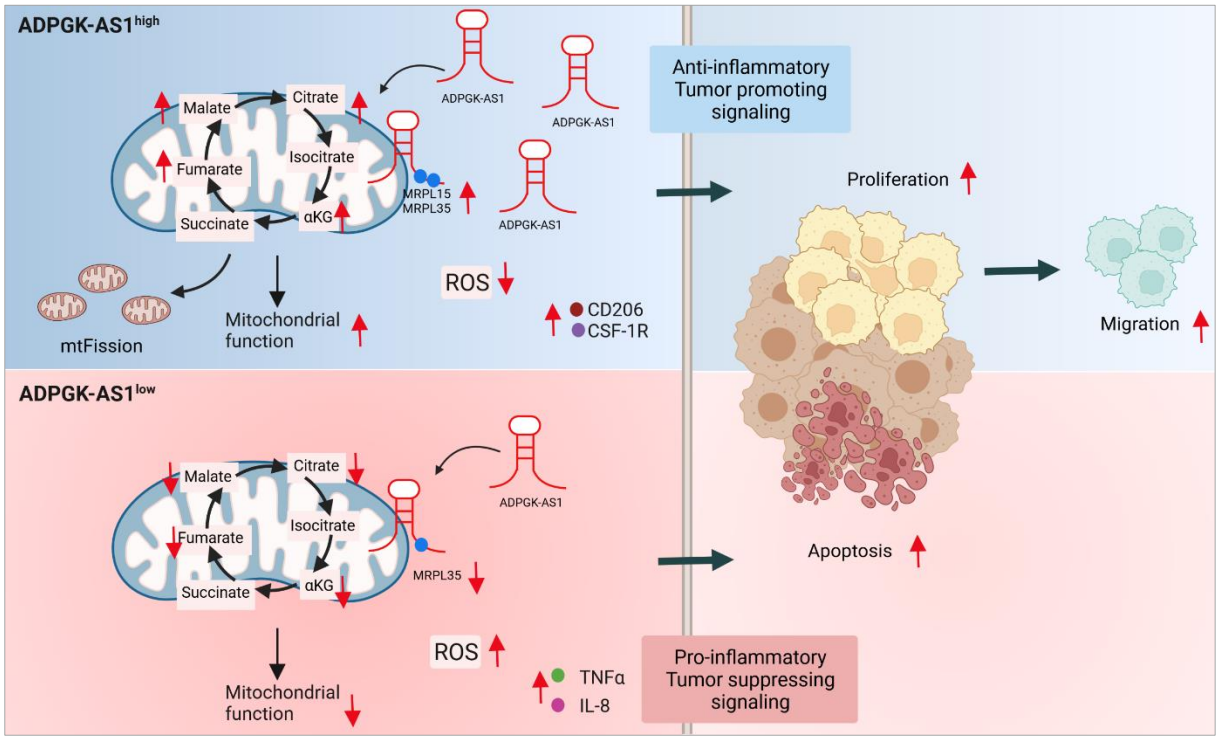

Figure 5-1 Suggested signaling pathway of ADPGK-AS1 in macrophages in context of the lung tumor microenvironment. LncRNA ADPGK-AS1 is located in the cytoplasm and mitochondria of macrophages. Within mitochondria, ADPGK-AS1 binds to MRPL35 and MRPL15, enhances TCA cycle metabolites, mitochondrial energy production and induces mitochondrial fission process. Macrophages with high expression of ADPGK-AS1 are activated towards an anti-inflammatory phenotype, upregulate M2-like marker gene expression, and increase tumor cell proliferation and migration. Macrophages with low ADPGK-AS1 expression have a high ROS production, are activated towards the pro-inflammatory M1-like phenotype, increase M1-like marker genes, and induce tumor cell apoptosis.

6 Future perspectives

Lung cancer is still one of the most diagnosed and most fatal cancer types of all. Existing therapies, including recently developed targeted and immunotherapy, are still faced with limited success. Thus, identification of novel and more specific factors and targets are required to gain a deeper insight into the molecular background of lung cancer itself, but also the immune cells in the tumor microenvironment. This study aimed to assess the role of lncRNAs in tumor associated macrophages and the macrophage activation process, to understand how these lncRNAs, particularly ADPGK-AS1, can be used to develop novel

therapeutic strategies in lung cancer. However, there are still open questions that need to be addressed in more detail.

For once, further investigation is needed regarding the interaction of ADPGK-AS1 and MRPL35 and MRPL15. Here, we still lack a detailed mechanism of how ADPGK-AS1 is regulating the mitochondrial metabolism via the MRPs. We hypothesize, that ADPGK-AS1 is influencing the protein stability of those MRPs, therefore leading to the observed increased amount of ADPGK-AS1 OE macrophages. To analyze this, actinomycin D treatment, which is used to block RNA transcription, could be carried out at several time points in control and ADPGK-AS1 OE macrophages. Subsequently, western blot analysis of the MRPs could show whether the proteins might be remaining stable for longer periods of time with higher amounts of ADPGK-AS1 in the cell. In particular, the interaction partner MRPL35 should be in focus since it seems to be consistently regulated in all experiments and was able to “rescue” the ADPGK-AS1 OE phenotype after knockdown.

In addition, the upstream signaling pathway should be clearly deciphered. αKG seems to be a good candidate for being part of the signaling pathway. However, it should be analyzed by ChIP whether αKG treatment in macrophages induces epigenetic changes on the ADPGK-AS1 promotor region, leading to enhanced expression of ADPGK-AS1.

Moreover, the tumor PCLS method is a very promising approach to understand key molecular and cellular pathways related to tumor malignancy. It could be used for a wide range of applications, e.g. identification of patient-specific cancer inhibitors following treatment. In addition, this method displays a great advantage over mouse experiments, since it is less time consuming, less tissue is needed to gain a great amount of experimental material, and it allows you to generate data with direct human relevance. For the future, this method should be further optimized and expanded for the use of even more applications.

Finally, ADPGK-AS1 should be considered as a therapeutic target to develop novel immunotherapeutics for lung cancer treatment. In addition, combination therapies with existing chemotherapies and targeted therapies could be an option that needs to be further investigated. For this, more extensive patient studies need to be performed.

7 Summary

Recent immunometabolism studies have shown that alterations in the metabolic profile of macrophages determine the macrophage phenotype and function. Long non-coding RNAs (lncRNAs) regulate macrophage activation and inflammatory gene network, but their role in mitochondrial bioenergetics and metabolism during inflammation and lung cancer progression has been largely unexplored. In this study, we identified lncRNA ADPGK-AS1 in M2-like activated macrophages and tumor associated macrophages (TAMs) to be highly expressed. We found that ADPGK-AS1 can translocate into the mitochondria of macrophages and bind to mitochondrial ribosomal proteins (MRPs), such as MRPL35 and MRPL15. Interaction with the MRPs leads to enhanced number of mitochondria, increased mitochondrial energy production, higher amounts of TCA metabolites fumarate, malate, citrate, and αKG, as well as reduced accumulation of ROS, as seen in ADPGK-AS1 overexpressing macrophages. In addition, in macrophage-tumor-cell crosstalk, ADPGK-AS1 expression was also induced and comparable changes were seen in TCA metabolites. Additionally, we found evidences that ADPGK-AS1 in our co-culture model might be induced by tumor-cell secreted αKG. Notably, ADPGK-AS1 expression modulation and the following alteration in mitochondrial-associated macrophage metabolism was linked to a change in macrophage phenotype. This was observed in (i) *in vitro* experiments leading to upregulation of inflammatory M1-like markers and downregulation of anti-inflammatory M2-like markers, as well as increased tumor cell apoptosis and decreased tumor cell migration after ADPGK-AS1 knockdown in M2-like macrophages; (ii) *in vivo* experiments, showing decrease of tumor growth under influence of M2-like macrophages with a ADPGK-AS1 knockdown in NSG mice and (iii) *ex vivo* experiments leading to a decrease of proliferation and enhanced apoptosis in human tumor precision cut lung slices. Interestingly, MRPL35 was upregulated in ADPGK-AS1 overexpressing macrophages, and the expression pattern of this protein was consistent in all of our models. This suggests that the mitochondrial metabolic regulation of ADPGK-AS1 in macrophages as seen in this study goes via interaction with MRPL35 in the mitochondria.

The significance of the present study lies in the exploration of alternative routes for target therapy i.e., knockdown of lncRNA ADPGK-AS1. This influences mitochondrial energy production, thereby causing changes in the macrophage phenotype and finally leading to elevated inflammatory signals and reduced lung tumor growth. The newly discovered pathway constitutes a target for tumor therapy. Thus, targeting ADPGK-AS1 could be a novel approach in treatment of several pathologies associated with macrophage deregulation, particularly lung cancer.

8 Zusammenfassung

Neueste Studien des Immunstoffwechsels zeigen, dass Veränderungen im Stoffwechsel von Makrophagen den Phänotyp und ihre Funktion entscheidend beeinflussen können. Lange nicht-kodierende RNAs (LncRNAs) regulieren die Aktivierung von Makrophagen, ihre Rolle im mitochondrialen Stoffwechsel sowie in Entzündungsreaktionen und in der Lungenkrebsentwicklung sind jedoch bisher nicht vollständig aufgeklärt. Die vorliegende Studie identifizierte ADPGK-AS1 als eine in M2-ähnlichen Makrophagen und Tumor-assoziierten Makrophagen (TAMs) stark exprimierte lncRNA. Es wurde gezeigt, dass ADPGK-AS1 in den Mitochondrien von Makrophagen vorliegt und an mitochondriale ribosomale Proteine (MRPs), unter anderen MRPL15 und MRPL35, binden kann. In Makrophagen mit einer Überexpression von ADPGK-AS1 führt die Interaktion mit den MRPs zu erhöhter Anzahl an Mitochondrien durch erhöhte Teilungsrate (*Fission*), verstärkte mitochondriale Energiegewinnung, vermehrte Mengen an Stoffwechselprodukten des Zitratzyklus, wie Fumarat, Malat, Zitrat und α-Ketoglutarat (αKG), sowie verminderte Akkumulation von reaktiven Sauerstoffspezies (ROS). Ko-Kultur von Makrophagen mit Tumorzellen konnte ebenfalls die Expression von ADPGK-AS1 in Makrophagen induzierten, wobei ähnliche Veränderungen des Stoffwechsels zu beobachten waren. Zudem konnte im Ko-Kultur Modell gezeigt werden, dass womöglich von Tumorzellen sekretiertes αKG für die Induktion der Expression von ADPGK-AS1 verantwortlich ist. Interessanterweise führte die Manipulation der Expression von ADPGK-AS1 in Makrophagen und die folgenden Veränderungen im mitochondrialen Stoffwechsel zu einer Veränderung des Makrophagen Phänotyps. Dies konnte nachgewiesen werden durch (i) *in vitro* Experimente, bei denen M1-ähnliche Marker-Gene hochreguliert und M2-ähnliche Marker-Gene herunterreguliert wurden, gemeinsam mit erhöhter Tumorzell-Apoptose und reduzierter Tumorzell-Migration und Proliferation nach *knockdown* von ADPGK-AS1 in M2-ähnlichen Makrophagen; (ii) *in vivo* Experimente, welche reduziertes Tumorwachstum unter Einfluss von M2-ähnlichen Makrophagen mit ADPGK-AS1 *knockdown* in NSG Mäusen zeigten; (iii) *ex vivo* Experimente, in denen ein *knockdown* von ADPGK-AS1 in humanen *precision cut lung slices* zu reduzierter Tumorzell-Proliferation und erhöhter Tumorzell-Apoptose führte. Zudem wurde erhöhte Expression von MRPL35 in ADPGK-AS1 Überexpressions-Makrophagen detektiert und das Expressionsmuster von MRPL35 war einheitlich in all den untersuchten Modellen. Diese Daten legen nah, dass die beschriebenen Veränderungen des mitochondrialen Stoffwechsels in Makrophagen über die Interaktion von ADPGK-AS1 mit MRPL35 in den Mitochondrien reguliert werden.

Die vorliegende Studie trägt maßgeblich dazu bei alternative Signalwege für gezielte Krebstherapie und Immunkrebstherapie zu identifizieren, so wie beispielsweise Herunterregulation der lncRNA ADPGK-AS1. Diese beeinflusst die mitochondriale

Energieproduktion, verändert dadurch den Makrophagen Phänotyp und führt letztendlich zu veränderter Entzündungsreaktion und reduziertem Lungentumorwachstum. Gezielte Maßnahmen gegen ADPGK-AS1 und den hier identifizierten Signalweg könnten daher einen neuartigen Ansatz bieten in der Entwicklung von Therapien für verschiedene Krankheiten, welche mit einer Deregulation von Makrophagen assoziiert sind, insbesondere Lungenkrebs.

9 Figures and Tables

9.1 Figures

9.2 Tables

10 Appendix

10.1 List of Primers

Table 10-1 Human Primer List purchased from Sigma-Aldrich (Missouri, USA)

Target gene	Forward Primer 5'→3'	Reverse Primer 3'→5'
47S-rRNA	GCTGACACGCTGTCCTCTG	ACGCGCGAGAGAACAGCAG
β-actin	CATGTACGTTGCTATCCAGGC	CTCCTTAATGTCACGCACGAT
α-Tubulin	AGATGCTGCCAATAACTATG	CTTGCCATAATCAACTGAGAG
AC007880.1-1	GTGTCTGCAGCCCACAGTAA	GCCACCTGTCTGATGGTCTT
AC007880.1-2	CCCCAGGGTCATGCAAATCA	CCAACAAGGACCCTGCCTAT
ADPGK	TCATCTTCTCTCACGACCTCTC	AGCTCCCTGTTAGTCATACTGG
ADPGK-AS1-1	CCAACTCCTTTCCTAGCCCG	TGTGACGTAGCGCTTGTGT
ADPGK-AS1-2	TGCTGACTGTCCAGCGATCATT	TCCACCCTTTAGCCTTGTGTGA
ALOX15	CTTCCAAGCTTATAATTCCCCAC	GATTCCTTCCACATACCGATAG
CCR7	GCTGGTGGTGGCTCTCCTT	GTAATCGTCCGTGACCTCATCTT
CD206	TTCGGACACCCATCGGAATTT	CACAAGCGCTGCGTGGAT
CD80	AGGGAACATCACCATCCAAG	TGCCAGTAGATGCGAGTTTG
CSF-1R	GAGAGCTATGAGGGCAACAG	TCCGAGGGTCTTACCAAACT
CTD-2545M3.8-1	CCAGGAAGGCGGAAACAAAG	GGGTTCCCTCGAAGTCTCTG
CTD-2545M3.8-2	GATACACAGCACAAATGAGA	CTTCAGGCAAGGTCGGGTTC
CXCL10	GTGGCATTCAAGGAGTACCTC	TGATGGCCTTCGATTCTGGATT
GLUT1	GGCCAAGAGTGTGCTAAAGAA	ACAGCGTTGATGCCAGACAG
HPRT1	TGACACTGGCAAAACAAT	GGTCCTTTTCACCAGCAA
IDH1	CGGAACCCAAAAGGTGACAT	TGGCAACACCACCACCTTCT
IL-8	ACAGCAGAGCACACAAGCTTC	CAGGAAGGCTGCCAAGAG
IL-10	GAGGCTACGGCGCTGTCA	TCCACGCCTTGCTCTTG
IL-1β	AGAAACTGCAGATTCCAAACC	TGGAAGGAGCACTTCATCTGT
IL-1Rα	CTATCAGGCCCTCCCCATGGC	CAACTAGTTGGTTGTTCCTCC
LDH	GAAGATAAGTGGTTTTCCCAAAAC	CTTTGAGTTTGATCACCTCATAAGC
MDH2	AAGAACAGCCCCTTGGTGAG	GGTCCGAGGTAGCCTTTCAC
Mt-ATP6	ACCACAAGGCACACCTACAC	TATTGCTAGGGTGGCGCTTC
Mt-ATP8	ACTACCACCTACCTCCCTCAC	GGATTGTGGGGGCAATGAATG
Mt-CO1	CTTTTCACCGTAGGTGGCCT	AGTGGAAGTGGGCTACAACG
Mt-CO2	CCGTCTGAACTATCCTGCCC	GAGGGATCGTTGACCTCGTC
Mt-CyB	ACCCCCTAGGAATCACCTCC	GCCTAGGAGGTCTGGTGAGA
Mt-ND1	GCTCTCACCATCGCTCTTCT	CCGATCAGGGCGTAGTTTGA
Mt-ND2	AGCACCACGACCCTACTACT	TGGTGGGGATGATGAGGCTA
Mt-ND4	ACAAGCTCCATCTGCCTACG	GCTTCAGGGGGTTTGGATGA
RP11-10J5.1-1	ACCTCCGCAGAGATAACCAG	CACTGACAGAAACGTCAGCC
RP11-10J5.1-2	TGGCTGACGTTTCTGTCAGT	AGCACTCTCTGGAGTTCACAA
RP11-184M15.1-1	CATCCAGGACATGCCAGCTA	GCGGGATTGTCTGGTTTCAA
RP11-184M15.1-2	GGCATGGACTGGATCTGACAA	GCAGTGTGTTATGGGGCGAT
RP11-333E1.1-1	CAATGACAAAGCAGTCGTACCA	GTCTACAGACGACACTTCTCT
RP11-333E1.1-2	CACAGACGAGTTTGCCGTGA	TGGATCTGTCTCTGCATGGG
RP4-644L1.2-1	GAAATGGCACTGAACAGCCG	TCACCTCTGCCCGTTAGAGA
RP4-644L1.2-2	AAGGTCCTTCGAGTGTTGGC	GTGCCCTTGGGGAGCTATTT
RP4-79H19.4-1-1	GCTTGGACACAATTGCAGGC	GACGAGTCCTTTTGGAGGCT
RP4-79H19.4-1-2	ACACAATTGCAGGCCCTTGA	GAGGAGGATGGAGGGGTATCA
SDH	TGGGAACAAGAGGGCATCTG	CCACCACTGCATCAAATTCATG
TAPSAR-1	GGAAAGACATCGGACCGTCA	TGGGAAACGTTGGTGTCCTT
TNFα	GAGGCCAAGCCCTGGTATG	CGGCCGATTGATCTCAGC
USP30-AS1-1	GAACGTAGACCGCAGGACAG	GACGTGGTCCGTCAGCTATT
USP30-AS1-2	ATGACATCACGAGGAGAGTGG	GCGCTTCCTCATAGCAGAGTTG

Table 10-2 Primer used for cloning purchased from Sigma-Aldrich (Missouri, USA)

Target gene	Forward Primer 5'→3'	Reverse Primer 3'→5'
ADPGK promotor - XhoI HindIII	ATATTACTCGAGTGGCT CAGTCCCCTCTGGGTGCCA	ATTTAAGCTTCTAGCCCGC GCCTCTTCCGGGCTC
ADPGK-AS1 - Acc65I NotI-1	ATATTAGGTACCAAAAGTACA AAGAAAGGAGGTAGTGTC	ATTTGCGGCCGCCTTTTACA CTTGTTCATTTTTTA

10.2 List of antibodies

Table 10-3 List of human antibodies used in this study

Target gene	Host	Source	Catalog No.	Application	Dilution
αb-crystallin	Rabbit	Abcam	ab13497	WB	1:1000
β-actin	Mouse	Abcam	ab8227	WB	1:5000
AMPKα	Rabbit	Cell signaling	2532	WB	1:1000
pAMPK (Thr172)	Rabbit	Cell signaling	2535	WB	1:500
ALOX15	Mouse	Life technologies	A2412	IF	1:200
CD68	Mouse	Abcam	ab955	IF	1:250
Cleaved caspase 3	Rabbit	Cell signaling	9664	WB, IF	1:500, 1:200
Cytochrome C	Mouse	Invitrogen	33-8200	WB	1:500
Cytokeratin 18	Rabbit	Abcam	ab181597	IF	1:250
Drp1	Rabbit	Cell signaling	8570	WB	1:1000
IL-8	Mouse	eBioscience™	14-7189-82	IF	1:200
Ki67	Rabbit	Abcam	ab16667	IF	1:250
Mfn1	Rabbit	Cell signaling	14739	WB	1:1000
MRPL15	Rabbit	GBiosciences	ITT2848	WB	1:1000
MRPL35	Rabbit	Invitrogen	PA5-38964	WB	1:1000
Opa1	Rabbit	Cell signaling	80471	WB	1:1000
PCG-1	Rabbit	Abcam	ab72230	WB	1:1000
SDHA	Rabbit	Cell signaling	5839	WB	1:1000
TOM20	Rabbit	Abcam	ab186734	WB, IF	1:1000, 1:300
Anti-mouse IgG HRP-linked	Goat	Promega	W4018	WB	1:5000
Anti-rabbit IgG HRP-linked	Goat	Promega	W4028	WB	1:5000
Anti-rabbit IgG Alexa-Fluor-488-linked	Goat	Life technologies	A-11008	IF	1:300
Anti-mouse IgG Alexa-Fluor-555-linked	Goat	Life technologies	A-21422	IF	1:300

10.3 Plasmids

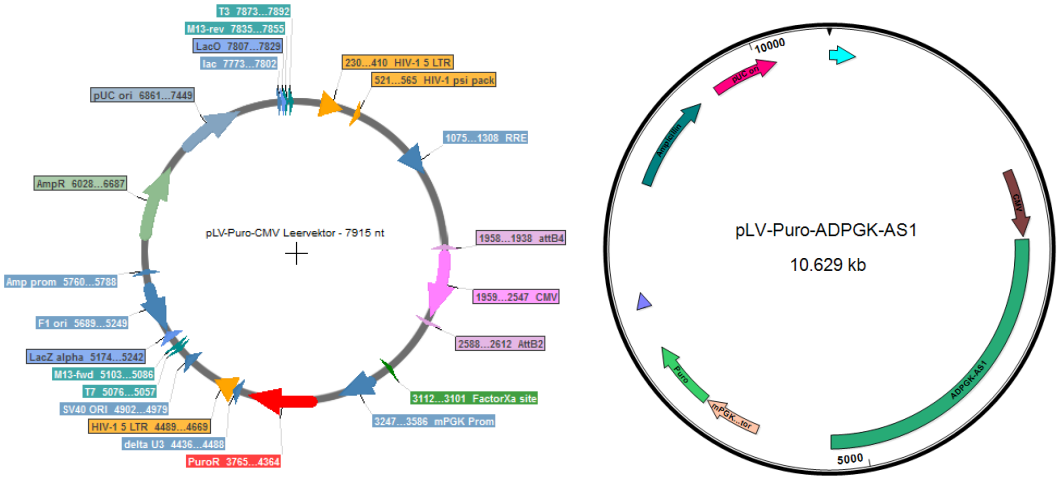

Appendix Figure 1 a: pLV-Puro-CMV empty vector **b:** pLV-Puro-CMV-ADPGK-AS1 overexpression vector.

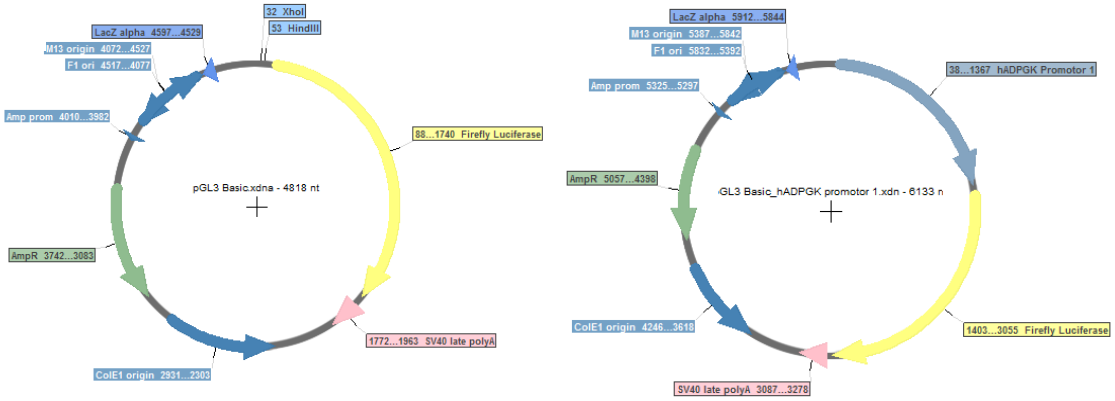

Appendix Figure 2 a: pGL3 basic **b:** pGL3_hADPGK-Promotor.

References

Abla, H., M. Sollazzo, G. Gasparre, L. Iommarini, and A. M. Porcelli. 2020. 'The multifaceted contribution of alpha-ketoglutarate to tumor progression: An opportunity to exploit?', *Semin Cell Dev Biol*, 98: 26-33.

Abplanalp, W. T., A. Fischer, D. John, A. M. Zeiher, W. Gosgnach, H. Darville, R. Montgomery, L. Pestano, G. Allee, I. Paty, F. Fougerousse, and S. Dimmeler. 2020. 'Efficiency and Target Derepression of Anti-miR-92a: Results of a First in Human Study', *Nucleic Acid Ther*, 30: 335-45.

ACS. 2019. 'Non-Small Cell Lung Cancer Stages', American Cancer Society, Accessed October 28.

Altieri, D. C. 2019. 'Mitochondrial dynamics and metastasis', *Cell Mol Life Sci*, 76: 827-35.

Ambade, A., A. Satishchandran, B. Saha, B. Gyongyosi, P. Lowe, K. Kodys, D. Catalano, and G. Szabo. 2016. 'Hepatocellular carcinoma is accelerated by NASH involving M2 macrophage polarization mediated by hif-1alphainduced IL-10', *Oncoimmunology*, 5: e1221557.

Ambrosi, C. M., G. Sadananda, J. L. Han, and E. Entcheva. 2019. 'Adeno-Associated Virus Mediated Gene Delivery: Implications for Scalable in vitro and in vivo Cardiac Optogenetic Models', *Front Physiol*, 10: 168.

Amodio, N., M. A. Stamato, G. Juli, E. Morelli, M. Fulciniti, M. Manzoni, E. Taiana, L. Agnelli, M. E. G. Cantafio, E. Romeo, L. Raimondi, D. Caracciolo, V. Zuccala, M. Rossi, A. Neri, N. C. Munshi, P. Tagliaferri, and P. Tassone. 2018. 'Drugging the lncRNA MALAT1 via LNA gapmeR ASO inhibits gene expression of proteasome subunits and triggers anti-multiple myeloma activity', *Leukemia*, 32: 1948-57.

Ancel, J., J. M. Perotin, M. Dewolf, C. Launois, P. Mulette, B. Nawrocki-Raby, V. Dalstein, C. Gilles, G. Deslee, M. Polette, and V. Dormoy. 2021. 'Hypoxia in Lung Cancer Management: A Translational Approach', *Cancers (Basel)*, 13.

Ardura, J. A., G. Rackov, E. Izquierdo, V. Alonso, A. R. Gortazar, and M. M. Escribese. 2019. 'Targeting Macrophages: Friends or Foes in Disease?', *Front Pharmacol*, 10: 1255.

Arun, G., S. Diermeier, M. Akerman, K. C. Chang, J. E. Wilkinson, S. Hearn, Y. Kim, A. R. MacLeod, A. R. Krainer, L. Norton, E. Brogi, M. Egeblad, and D. L. Spector. 2016. 'Differentiation of mammary tumors and reduction in metastasis upon Malat1 lncRNA loss', *Genes Dev*, 30: 34-51.

Asghar, W., R. El Assal, H. Shafiee, S. Pitteri, R. Paulmurugan, and U. Demirci. 2015. 'Engineering cancer microenvironments for in vitro 3-D tumor models', *Mater Today (Kidlington)*, 18: 539-53.

Aubert, M., M. F. O'Donohue, S. Lebaron, and P. E. Gleizes. 2018. 'Pre-Ribosomal RNA Processing in Human Cells: From Mechanisms to Congenital Diseases', *Biomolecules*, 8.

Auffray, C., M. H. Sieweke, and F. Geissmann. 2009. 'Blood monocytes: development, heterogeneity, and relationship with dendritic cells', *Annu Rev Immunol*, 27: 669-92.

Azad, A. K., M. V. Rajaram, and L. S. Schlesinger. 2014. 'Exploitation of the Macrophage Mannose Receptor (CD206) in Infectious Disease Diagnostics and Therapeutics', *J Cytol Mol Biol*, 1.

Baskar, R., K. A. Lee, R. Yeo, and K. W. Yeoh. 2012. 'Cancer and radiation therapy: current advances and future directions', *Int J Med Sci*, 9: 193-9.

Beckett, E. L. , R. L. Stevens, A. G. Jarnicki, R. Y. Kim, I. Hanish, Hansbron N. G., A. Deane, S. Keely, J. C. Horvat, M. Yang, B. G. Oliver, N. Van Rooijen, M. D. Inman, R. Adachi, R. J. Soberman, S. Hamadi, P. A. Wark, P. S. Foster, and P. M. Hansbro. 2013. 'A new short-term mouse model of chronic obstructive pulmonary disease identifies a role for mast cell tryptase in pathogenesis', *J Allergy Clin Immunol*, 131: 752-62.

Betts, J. A., M. Moradi Marjaneh, F. Al-Ejeh, Y. C. Lim, W. Shi, H. Sivakumaran, R. Tropee, A. M. Patch, M. B. Clark, N. Bartonicek, A. P. Wiegmans, K. M. Hillman, S.

Kaufmann, A. L. Bain, B. S. Gloss, J. Crawford, S. Kazakoff, S. Wani, S. W. Wen, B. Day, A. Moller, N. Cloonan, J. Pearson, M. A. Brown, T. R. Mercer, N. Waddell, K. K. Khanna, E. Dray, M. E. Dinger, S. L. Edwards, and J. D. French. 2017. 'Long Noncoding RNAs CUPID1 and CUPID2 Mediate Breast Cancer Risk at 11q13 by Modulating the Response to DNA Damage', *Am J Hum Genet*, 101: 255-66.

Box, J. M., J. Kaur, and R. A. Stuart. 2017. 'MrpL35, a mitospecific component of mitoribosomes, plays a key role in cytochrome c oxidase assembly', *Mol Biol Cell*, 28: 3489-99.

Brambilla, E., and A. Gazdar. 2009. 'Pathogenesis of lung cancer signalling pathways: roadmap for therapies', *Eur Respir J*, 33: 1485-97.

Broughton, J. P., M. T. Lovci, J. L. Huang, G. W. Yeo, and A. E. Pasquinelli. 2016. 'Pairing beyond the Seed Supports MicroRNA Targeting Specificity', *Mol Cell*, 64: 320-33.

Buchbinder, E. I., and A. Desai. 2016. 'CTLA-4 and PD-1 Pathways: Similarities, Differences, and Implications of Their Inhibition', *Am J Clin Oncol*, 39: 98-106.

Cannarile, M. A., M. Weisser, W. Jacob, A. M. Jegg, C. H. Ries, and D. Ruttinger. 2017. 'Colony-stimulating factor 1 receptor (CSF1R) inhibitors in cancer therapy', *J Immunother Cancer*, 5: 53.

Chavez-Galan, L., M. L. Olleros, D. Vesin, and I. Garcia. 2015. 'Much More than M1 and M2 Macrophages, There are also CD169(+) and TCR(+) Macrophages', *Front Immunol*, 6: 263.

Chen, C., W. He, J. Huang, B. Wang, H. Li, Q. Cai, F. Su, J. Bi, H. Liu, B. Zhang, N. Jiang, G. Zhong, Y. Zhao, W. Dong, and T. Lin. 2018. 'LNMAT1 promotes lymphatic metastasis of bladder cancer via CCL2 dependent macrophage recruitment', *Nat Commun*, 9: 3826.

Chen, J., L. Ao, and J. Yang. 2019. 'Long non-coding RNAs in diseases related to inflammation and immunity', *Ann Transl Med*, 7: 494.

Chen, J., Z. Shen, Y. Zheng, S. Wang, and W. Mao. 2015. 'Radiotherapy induced Lewis lung cancer cell apoptosis via inactivating beta-catenin mediated by upregulated HOTAIR', *Int J Clin Exp Pathol*, 8: 7878-86.

Chen, Z., J. L. Li, S. Lin, C. Cao, N. T. Gimbrone, R. Yang, D. A. Fu, M. B. Carper, E. B. Haura, M. B. Schabath, J. Lu, A. L. Amelio, W. D. Cress, F. J. Kaye, and L. Wu. 2016. 'cAMP/CREB-regulated LINC00473 marks LKB1-inactivated lung cancer and mediates tumor growth', *J Clin Invest*, 126: 2267-79.

Chen, Z. Z., L. Huang, Y. H. Wu, W. J. Zhai, P. P. Zhu, and Y. F. Gao. 2016. 'LncSox4 promotes the self-renewal of liver tumour-initiating cells through Stat3-mediated Sox4 expression', *Nat Commun*, 7: 12598.

Chow, M. T., A. Moller, and M. J. Smyth. 2012. 'Inflammation and immune surveillance in cancer', *Semin Cancer Biol*, 22: 23-32.

Cooper, D. R., G. Carter, P. Li, R. Patel, J. E. Watson, and N. A. Patel. 2014. 'Long Non-Coding RNA NEAT1 Associates with SRp40 to Temporally Regulate PPARgamma2 Splicing during Adipogenesis in 3T3-L1 Cells', *Genes (Basel)*, 5: 1050-63.

da Cunha Santos, G., F. A. Shepherd, and M. S. Tsao. 2011. 'EGFR mutations and lung cancer', *Annu Rev Pathol*, 6: 49-69.

Damaghi, M., J. W. Wojtkowiak, and R. J. Gillies. 2013. 'pH sensing and regulation in cancer', *Front Physiol*, 4: 370.

Das, S., M. Kohr, B. Dunkerly-Eyring, D. I. Lee, D. Bedja, O. A. Kent, A. K. Leung, J. Henao-Mejia, R. A. Flavell, and C. Steenbergen. 2017. 'Divergent Effects of miR-181 Family Members on Myocardial Function Through Protective Cytosolic and Detrimental Mitochondrial microRNA Targets', *J Am Heart Assoc*, 6.

de Goede, K. E., A. J. M. Driessen, and J. Van den Bossche. 2020. 'Metabolic Cancer-Macrophage Crosstalk in the Tumor Microenvironment', *Biology (Basel)*, 9.

Decker, W. K., and A. Safdar. 2009. 'Bioimmunoadjuvants for the treatment of neoplastic and infectious disease: Coley's legacy revisited', *Cytokine Growth Factor Rev*, 20: 271-81.

Deng, Z., F. Shi, Z. Zhou, F. Sun, M. H. Sun, Q. Sun, L. Chen, D. Li, C. Y. Jiang, R. Z. Zhao, D. Cui, X. J. Wang, Y. F. Jing, S. J. Xia, and B. M. Han. 2019. 'M1 macrophage

mediated increased reactive oxygen species (ROS) influence wound healing via the MAPK signaling in vitro and in vivo', *Toxicol Appl Pharmacol*, 366: 83-95.

Dey, B. K., K. Pfeifer, and A. Dutta. 2014. 'The H19 long noncoding RNA gives rise to microRNAs miR-675-3p and miR-675-5p to promote skeletal muscle differentiation and regeneration', *Genes Dev*, 28: 491-501.

Djebali, S., C. A. Davis, A. Merkel, A. Dobin, T. Lassmann, A. Mortazavi, A. Tanzer, J. Lagarde, W. Lin, F. Schlesinger, C. Xue, G. K. Marinov, J. Khatun, B. A. Williams, C. Zaleski, J. Rozowsky, M. Roder, F. Kokocinski, R. F. Abdelhamid, T. Alioto, I. Antoshechkin, M. T. Baer, N. S. Bar, P. Batut, K. Bell, I. Bell, S. Chakrabortty, X. Chen, J. Chrast, J. Curado, T. Derrien, J. Drenkow, E. Dumais, J. Dumais, R. Duttagupta, E. Falconnet, M. Fastuca, K. Fejes-Toth, P. Ferreira, S. Foissac, M. J. Fullwood, H. Gao, D. Gonzalez, A. Gordon, H. Gunawardena, C. Howald, S. Jha, R. Johnson, P. Kapranov, B. King, C. Kingswood, O. J. Luo, E. Park, K. Persaud, J. B. Preall, P. Ribeca, B. Risk, D. Robyr, M. Sammeth, L. Schaffer, L. H. See, A. Shahab, J. Skancke, A. M. Suzuki, H. Takahashi, H. Tilgner, D. Trout, N. Walters, H. Wang, J. Wrobel, Y. Yu, X. Ruan, Y. Hayashizaki, J. Harrow, M. Gerstein, T. Hubbard, A. Reymond, S. E. Antonarakis, G. Hannon, M. C. Giddings, Y. Ruan, B. Wold, P. Carninci, R. Guigo, and T. R. Gingeras. 2012. 'Landscape of transcription in human cells', *Nature*, 489: 101-8.

Drake, R., W. Vogl, and A. W. M. Mitchell. 2014. *Gray's anatomy for students* (Elsevier).

Duan, Z., and Y. Luo. 2021. 'Targeting macrophages in cancer immunotherapy', *Signal Transduct Target Ther*, 6: 127.

El-Hattab, A. W., J. Suleiman, M. Almannai, and F. Scaglia. 2018. 'Mitochondrial dynamics: Biological roles, molecular machinery, and related diseases', *Mol Genet Metab*, 125: 315-21.

El-Nikhely, N., A. Karger, P. Sarode, I. Singh, A. Weigert, A. Wietelmann, T. Stiewe, R. Dammann, L. Fink, F. Grimminger, G. Barreto, W. Seeger, S. S. Pullamsetti, U. R. Rapp, and R. Savai. 2020. 'Metastasis-Associated Protein 2 Represses NF-kappaB to Reduce Lung Tumor Growth and Inflammation', *Cancer Res*, 80: 4199-211.

El-Nikhely, N., L. Larzabal, W. Seeger, A. Calvo, and R. Savai. 2012. 'Tumor-stromal interactions in lung cancer: novel candidate targets for therapeutic intervention', *Expert Opin Investig Drugs*, 21: 1107-22.

Fang, Z., W. Chen, Z. Yuan, X. Liu, and H. Jiang. 2018. 'LncRNA-MALAT1 contributes to the cisplatin-resistance of lung cancer by upregulating MRP1 and MDR1 via STAT3 activation', *Biomed Pharmacother*, 101: 536-42.

Farber, S., L. K. Diamond, R. D. Mercer, R. F. Sylvester, and J. A. Wolff. 1948. 'Temporary remissions in acute leukemia in children produced by folic antagonist, 4-aminopteroylglutamic acid (aminopterin)', *N Engl J Med*, 238: 787–93.

Fei, L., X. Ren, H. Yu, and Y. Zhan. 2021. 'Targeting the CCL2/CCR2 Axis in Cancer Immunotherapy: One Stone, Three Birds?', *Front Immunol*, 12: 771210.

Foo, B. J., J. Q. Eu, J. L. Hirpara, and S. Pervaiz. 2021. 'Interplay between Mitochondrial Metabolism and Cellular Redox State Dictates Cancer Cell Survival', *Oxid Med Cell Longev*, 2021: 1341604.

Forkasiewicz, A., M. Dorociak, K. Stach, P. Szelachowski, R. Tabola, and K. Augoff. 2020. 'The usefulness of lactate dehydrogenase measurements in current oncological practice', *Cell Mol Biol Lett*, 25: 35.

Franks, T. J., T. V. Colby, W. D. Travis, R. M. Tuder, H. Y. Reynolds, A. R. Brody, W. V. Cardoso, R. G. Crystal, C. J. Drake, J. Engelhardt, M. Frid, E. Herzog, R. Mason, S. H. Phan, S. H. Randell, M. C. Rose, T. Stevens, J. Serge, M. E. Sunday, J. A. Voynow, B. M. Weinstein, J. Whitsett, and M. C. Williams. 2008. 'Resident cellular components of the human lung: current knowledge and goals for research on cell phenotyping and function', *Proc Am Thorac Soc*, 5: 763-6.

Fu, G., J. Brkic, H. Hayder, and C. Peng. 2013. 'MicroRNAs in Human Placental Development and Pregnancy Complications', *Int J Mol Sci*, 14: 5519-44.

Galvan-Pena, S., and L. A. O'Neill. 2014. 'Metabolic reprograming in macrophage polarization', *Front Immunol*, 5: 420.

Gao, Z., Y. Li, F. Wang, T. Huang, K. Fan, Y. Zhang, J. Zhong, Q. Cao, T. Chao, J. Jia, S. Yang, L. Zhang, Y. Xiao, J. Y. Zhou, X. H. Feng, and J. Jin. 2017. 'Mitochondrial dynamics controls anti-tumour innate immunity by regulating CHIP-IRF1 axis stability', *Nat Commun*, 8: 1805.

Gazzeri, S., E. Brambilla, C. Caron de Fromentel, V. Gouyer, D. Moro, P. Perron, F. Berger, and C. Brambilla. 1994. 'p53 genetic abnormalities and myc activation in human lung carcinoma', *Int J Cancer*, 58: 24-32.

Gazzeri, S., E. Brambilla, C. Chauvin, M. Jacrot, A. L. Benabid, and C. Brambilla. 1990. 'Analysis of the activation of the myc family oncogene and of its stability over time in xenografted human lung carcinomas', *Cancer Res*, 50: 1566-70.

Gilman, A. . 1963. 'The initial clinical trial of nitrogen mustard', *Am J Surg*, 105: 574-78.

Goodkey, K., T. Aslesh, R. Maruyama, and T. Yokota. 2018. 'Nusinersen in the Treatment of Spinal Muscular Atrophy', *Methods Mol Biol*, 1828: 69-76.

Gracia-Hernandez, M., E. M. Sotomayor, and A. Villagra. 2020. 'Targeting Macrophages as a Therapeutic Option in Coronavirus Disease 2019', *Front Pharmacol*, 11: 577571.

Grudnik, P., M. M. Kaminski, K. P. Rembacz, K. Kuska, M. Madej, J. Potempa, M. Dawidowski, and G. Dubin. 2018. 'Structural basis for ADP-dependent glucokinase inhibition by 8-bromo-substituted adenosine nucleotide', *J Biol Chem*, 293: 11088-99.

Gubin, M. M., E. Esaulova, J. P. Ward, O. N. Malkova, D. Runci, P. Wong, T. Noguchi, C. D. Arthur, W. Meng, E. Alspach, Medrano. R. F. V., C. Fronick, M. Fehlings, E. W. Newell, R. S. Fulton, C. F. Sheehan, S. T. Oh, R. D. Schreiber, and M. N. Artyomov. 2018. 'High-Dimensional Analysis Delineates Myeloid and Lymphoid Compartment Remodeling during Successful Immune-Checkpoint Cancer Therapy', *Cell*, 175: 1014-30.

Guo, D., Y. Wang, K. Ren, and X. Han. 2018. 'Knockdown of LncRNA PVT1 inhibits tumorigenesis in non-small-cell lung cancer by regulating miR-497 expression', *Exp Cell Res*, 362: 172-79.

Guo, F., L. Guo, Y. Li, Q. Zhou, and Z. Li. 2015. 'MALAT1 is an oncogenic long non-coding RNA associated with tumor invasion in non-small cell lung cancer regulated by DNA methylation', *Int J Clin Exp Pathol*, 8: 15903-10.

Gupta, R. A., N. Shah, K. C. Wang, J. Kim, H. M. Horlings, D. J. Wong, M. C. Tsai, T. Hung, P. Argani, J. L. Rinn, Y. Wang, P. Brzoska, B. Kong, R. Li, R. B. West, M. J. van de Vijver, S. Sukumar, and H. Y. Chang. 2010. 'Long non-coding RNA HOTAIR reprograms chromatin state to promote cancer metastasis', *Nature*, 464: 1071-6.

Gutschner, T., M. Hammerle, M. Eissmann, J. Hsu, Y. Kim, G. Hung, A. Revenko, G. Arun, M. Stentrup, M. Gross, M. Zornig, A. R. MacLeod, D. L. Spector, and S. Diederichs. 2013. 'The noncoding RNA MALAT1 is a critical regulator of the metastasis phenotype of lung cancer cells', *Cancer Res*, 73: 1180-9.

Ha, M., and V. N. Kim. 2014. 'Regulation of microRNA biogenesis', *Nat Rev Mol Cell Biol*, 15: 509-24.

Han, L., E. B. Zhang, D. D. Yin, R. Kong, T. P. Xu, W. M. Chen, R. Xia, Y. Q. Shu, and W. De. 2015. 'Low expression of long noncoding RNA PANDAR predicts a poor prognosis of non-small cell lung cancer and affects cell apoptosis by regulating Bcl-2', *Cell Death Dis*, 6: e1665.

Hanahan, D., and R. A. Weinberg. 2011. 'Hallmarks of cancer: the next generation', *Cell*, 144: 646-74.

Hansen, T. B., T. I. Jensen, B. H. Clausen, J. B. Bramsen, B. Finsen, C. K. Damgaard, and J. Kjems. 2013. 'Natural RNA circles function as efficient microRNA sponges', *Nature*, 495: 384-8.

Haubner, F., E. Ohmann, F. Pohl, J. Strutz, and H. G. Gassner. 2012. 'Wound healing after radiation therapy: review of the literature', *Radiat Oncol*, 7: 162.

Hecht, S. S. 1999. 'Tobacco smoke carcinogens and lung cancer', *J Natl Cancer Inst*, 91: 1194-210.

Herbst, R. S., P. Baas, D. W. Kim, E. Felip, J. L. Perez-Gracia, J. Y. Han, J. Molina, J. H. Kim, C. D. Arvis, M. J. Ahn, M. Majem, M. J. Fidler, G. de Castro, Jr., M. Garrido, G.

M. Lubiniecki, Y. Shentu, E. Im, M. Dolled-Filhart, and E. B. Garon. 2016. 'Pembrolizumab versus docetaxel for previously treated, PD-L1-positive, advanced non-small-cell lung cancer (KEYNOTE-010): a randomised controlled trial', *Lancet*, 387: 1540-50.

Herzig, S., and R. J. Shaw. 2018. 'AMPK: guardian of metabolism and mitochondrial homeostasis', *Nat Rev Mol Cell Biol*, 19: 121-35.

Hess, A., L. Wang-Lauenstein, A. Braun, S. N. Kolle, R. Landsiedel, M. Liebsch, L. Ma-Hock, R. Pirow, X. Schneider, M. Steinfath, S. Vogel, C. Martin, and K. Sewald. 2016. 'Prevalidation of the ex-vivo model PCLS for prediction of respiratory toxicity', *Toxicol In Vitro*, 32: 347-61.

Hettinger, J., D. M. Richards, J. Hansson, M. M. Barra, A. C. Joschko, J. Krijgsveld, and M. Feuerer. 2013. 'Origin of monocytes and macrophages in a committed progenitor', *Nat Immunol*, 14: 821-30.

Hirsch, F. R., M. Varella-Garcia, P. A. Bunn, Jr., M. V. Di Maria, R. Veve, R. M. Bremmes, A. E. Baron, C. Zeng, and W. A. Franklin. 2003. 'Epidermal growth factor receptor in non-small-cell lung carcinomas: correlation between gene copy number and protein expression and impact on prognosis', *J Clin Oncol*, 21: 3798-807.

Hoeffel, G., and F. Ginhoux. 2015. 'Ontogeny of Tissue-Resident Macrophages', *Front Immunol*, 6: 486.

Hong, D. S., M. G. Fakih, J. H. Strickler, J. Desai, G. A. Durm, G. I. Shapiro, G. S. Falchook, T. J. Price, A. Sacher, C. S. Denlinger, Y. J. Bang, G. K. Dy, J. C. Krauss, Y. Kuboki, J. C. Kuo, A. L. Coveler, K. Park, T. W. Kim, F. Barlesi, P. N. Munster, S. S. Ramalingam, T. F. Burns, F. Meric-Bernstam, H. Henary, J. Ngang, G. Ngarmchamnanrith, J. Kim, B. E. Houk, J. Canon, J. R. Lipford, G. Friberg, P. Lito, R. Govindan, and B. T. Li. 2020. 'KRAS(G12C) Inhibition with Sotorasib in Advanced Solid Tumors', *N Engl J Med*, 383: 1207-17.

Howlader, N., G. Forjaz, M. J. Mooradian, R. Meza, C. Y. Kong, K. A. Cronin, A. B. Mariotto, D. R. Lowy, and E. J. Feuer. 2020. 'The Effect of Advances in Lung-Cancer Treatment on Population Mortality', *N Engl J Med*, 383: 640-49.

Huang, G., H. Li, and H. Zhang. 2020. 'Abnormal Expression of Mitochondrial Ribosomal Proteins and Their Encoding Genes with Cell Apoptosis and Diseases', *Int J Mol Sci*, 21.

Huang, Z., W. Lei, H. B. Hu, H. Zhang, and Y. Zhu. 2018. 'H19 promotes non-small-cell lung cancer (NSCLC) development through STAT3 signaling via sponging miR-17', *J Cell Physiol*, 233: 6768-76.

Hume, D. A., and K. P. MacDonald. 2012. 'Therapeutic applications of macrophage colony-stimulating factor-1 (CSF-1) and antagonists of CSF-1 receptor (CSF-1R) signaling', *Blood*, 119: 1810-20.

Inamura, K., K. Takeuchi, Y. Togashi, K. Nomura, H. Ninomiya, M. Okui, Y. Satoh, S. Okumura, K. Nakagawa, M. Soda, Y. L. Choi, T. Niki, H. Mano, and Y. Ishikawa. 2008. 'EML4-ALK fusion is linked to histological characteristics in a subset of lung cancers', *J Thorac Oncol*, 3: 13-7.

inHealth, JohnsHopkins. 2021. 'Immunotherapy: Precision Medicine in Action', Accessed October 30.

Islami, F., A. Goding Sauer, K. D. Miller, R. L. Siegel, S. A. Fedewa, E. J. Jacobs, M. L. McCullough, A. V. Patel, J. Ma, I. Soerjomataram, W. D. Flanders, O. W. Brawley, S. M. Gapstur, and A. Jemal. 2018. 'Proportion and number of cancer cases and deaths attributable to potentially modifiable risk factors in the United States', *CA Cancer J Clin*, 68: 31-54.

Jagannathan, R., D. Thapa, C. E. Nichols, D. L. Shepherd, J. C. Stricker, T. L. Croston, W. A. Baseler, S. E. Lewis, I. Martinez, and J. M. Hollander. 2015. 'Translational Regulation of the Mitochondrial Genome Following Redistribution of Mitochondrial MicroRNA in the Diabetic Heart', *Circ Cardiovasc Genet*, 8: 785-802.

Jeandard, D., A. Smirnova, I. Tarassov, E. Barrey, A. Smirnov, and N. Entelis. 2019. 'Import of Non-Coding RNAs into Human Mitochondria: A Critical Review and Emerging Approaches', *Cells*, 8.

Ji, J., Y. Yin, H. Ju, X. Xu, W. Liu, Q. Fu, J. Hu, X. Zhang, and B. Sun. 2018. 'Long non-coding RNA Lnc-Tim3 exacerbates CD8 T cell exhaustion via binding to Tim-3 and inducing nuclear translocation of Bat3 in HCC', *Cell Death Dis*, 9: 478.

Ji, P., S. Diederichs, W. Wang, S. Boing, R. Metzger, P. M. Schneider, N. Tidow, B. Brandt, H. Buerger, E. Bulk, M. Thomas, W. E. Berdel, H. Serve, and C. Muller-Tidow. 2003. 'MALAT-1, a novel noncoding RNA, and thymosin beta4 predict metastasis and survival in early-stage non-small cell lung cancer', *Oncogene*, 22: 8031-41.

Jia, Y., and Y. Zhou. 2020. 'Involvement of lncRNAs and Macrophages: Potential Regulatory Link to Angiogenesis', *J Immunol Res*, 2020: 1704631.

Jiang, C., Y. Yang, Y. Yang, L. Guo, J. Huang, X. Liu, C. Wu, and J. Zou. 2018. 'Long Noncoding RNA (lncRNA) HOTAIR Affects Tumorigenesis and Metastasis of Non-Small Cell Lung Cancer by Upregulating miR-613', *Oncol Res*, 26: 725-34.

Jiang, H. Y., and Z. J. Wang. 2020. 'ADPGK-AS1 promotes the progression of colorectal cancer via sponging miR-525 to upregulate FUT1', *European Review for Medical and Pharmacological Sciences*, 24: 2380-86.

Jiang, M. C., J. J. Ni, W. Y. Cui, B. Y. Wang, and W. Zhuo. 2019. 'Emerging roles of lncRNA in cancer and therapeutic opportunities', *Am J Cancer Res*, 9: 1354-66.

Jiang, R., J. Tang, Y. Chen, L. Deng, J. Ji, Y. Xie, K. Wang, W. Jia, W. M. Chu, and B. Sun. 2017. 'The long noncoding RNA lnc-EGFR stimulates T-regulatory cells differentiation thus promoting hepatocellular carcinoma immune evasion', *Nat Commun*, 8: 15129.

Jiang, W., D. Zhang, B. Xu, Z. Wu, S. Liu, L. Zhang, Y. Tian, X. Han, and D. Tian. 2015. 'Long non-coding RNA BANCR promotes proliferation and migration of lung carcinoma via MAPK pathways', *Biomed Pharmacother*, 69: 90-5.

Jin, Y., S. J. Feng, S. Qiu, N. Shao, and J. H. Zheng. 2017. 'LncRNA MALAT1 promotes proliferation and metastasis in epithelial ovarian cancer via the PI3K-AKT pathway', *Eur Rev Med Pharmacol Sci*, 21: 3176-84.

Jo, M. H., S. Shin, S. R. Jung, E. Kim, J. J. Song, and S. Hohng. 2015. 'Human Argonaute 2 Has Diverse Reaction Pathways on Target RNAs', *Mol Cell*, 59: 117-24.

Johnsson, P., L. Lipovich, D. Grander, and K. V. Morris. 2014. 'Evolutionary conservation of long non-coding RNAs; sequence, structure, function', *Biochim Biophys Acta*, 1840: 1063-71.

Jung, K. Y., S. W. Cho, Y. A. Kim, D. Kim, B. C. Oh, D. J. Park, and Y. J. Park. 2015. 'Cancers with Higher Density of Tumor-Associated Macrophages Were Associated with Poor Survival Rates', *J Pathol Transl Med*, 49: 318-24.

Karger, A., R. Nandigama, A. Stenzinger, F. Grimminger, S. S. Pullamsetti, W. Seeger, and R. Savai. 2021. 'Hidden Treasures: Macrophage Long Non-Coding RNAs in Lung Cancer Progression', *Cancers (Basel)*, 13.

Kawamata, T., and Y. Tomari. 2010. 'Making RISC', *Trends Biochem Sci*, 35: 368-76.

Kelly, B., and L. A. O'Neill. 2015. 'Metabolic reprogramming in macrophages and dendritic cells in innate immunity', *Cell Res*, 25: 771-84.

Kelly, K., J. Crowley, P. A. Bunn, Jr., C. A. Presant, P. K. Grevstad, C. M. Moinpour, S. D. Ramsey, A. J. Wozniak, G. R. Weiss, D. F. Moore, V. K. Israel, R. B. Livingston, and D. R. Gandara. 2001. 'Randomized phase III trial of paclitaxel plus carboplatin versus vinorelbine plus cisplatin in the treatment of patients with advanced non--small-cell lung cancer: a Southwest Oncology Group trial', *J Clin Oncol*, 19: 3210-8.

Kim, K., I. Jutooru, G. Chadalapaka, G. Johnson, J. Frank, R. Burghardt, S. Kim, and S. Safe. 2013. 'HOTAIR is a negative prognostic factor and exhibits pro-oncogenic activity in pancreatic cancer', *Oncogene*, 32: 1616-25.

Kooistra, S. M., and K. Helin. 2012. 'Molecular mechanisms and potential functions of histone demethylases', *Nat Rev Mol Cell Biol*, 13: 297-311.

Kopp, F., and J. T. Mendell. 2018. 'Functional Classification and Experimental Dissection of Long Noncoding RNAs', *Cell*, 172: 393-407.

Krumdieck, C. L., J. E. dos Santos, and K. J. Ho. 1980. 'A new instrument for the rapid preparation of tissue slices', *Anal Biochem*, 104: 118-23.

Labani-Motlagh, A., M. Ashja-Mahdavi, and A. Loskog. 2020. 'The Tumor Microenvironment: A Milieu Hindering and Obstructing Antitumor Immune Responses', *Front Immunol*, 11: 940.

Lambrou, G. I., K. Hatziagapiou, and A. Zaravinos. 2020. 'The Non-Coding RNA GAS5 and Its Role in Tumor Therapy-Induced Resistance', *Int J Mol Sci*, 21.

Laoui, D., K. Movahedi, E. Van Overmeire, J. Van den Bossche, E. Schouppe, C. Mommer, A. Nikolaou, Y. Morias, P. De Baetselier, and J. A. Van Ginderachter. 2011. 'Tumor-associated macrophages in breast cancer: distinct subsets, distinct functions', *Int J Dev Biol*, 55: 861-7.

Leucci, E., R. Vendramin, M. Spinazzi, P. Laurette, M. Fiers, J. Wouters, E. Radaelli, S. Eyckerman, C. Leonelli, K. Vanderheyden, A. Rogiers, E. Hermans, P. Baatsen, S. Aerts, F. Amant, S. Van Aelst, J. van den Oord, B. de Strooper, I. Davidson, D. L. Lafontaine, K. Gevaert, J. Vandesompele, P. Mestdagh, and J. C. Marine. 2016. 'Melanoma addiction to the long non-coding RNA SAMMSON', *Nature*, 531: 518-22.

Ley, K. 2017. 'M1 Means Kill; M2 Means Heal', *J Immunol*, 199: 2191-93.

Li, M., X. Ding, Y. Zhang, X. Li, H. Zhou, L. Yang, Y. Li, P. Yang, X. Zhang, J. Hu, E. Nice, H. Wu, and H. Xu. 2020. 'Antisense oligonucleotides targeting lncRNA AC104041.1 induces antitumor activity through Wnt2B/beta-catenin pathway in head and neck squamous cell carcinomas', *Cell Death Dis*, 11: 672.

Li, Y., Y. He, K. Miao, Y. Zheng, C. Deng, and T. M. Liu. 2020. 'Imaging of macrophage mitochondria dynamics in vivo reveals cellular activation phenotype for diagnosis', *Theranostics*, 10: 2897-917.

Li, Y., Y. Zheng, T. Li, Q. Wang, J. Qian, Y. Lu, M. Zhang, E. Bi, M. Yang, F. Reu, Q. Yi, and Z. Cai. 2015. 'Chemokines CCL2, 3, 14 stimulate macrophage bone marrow homing, proliferation, and polarization in multiple myeloma', *Oncotarget*, 6: 24218-29.

Liu, B., L. Sun, Q. Liu, C. Gong, Y. Yao, X. Lv, L. Lin, H. Yao, F. Su, D. Li, M. Zeng, and E. Song. 2015. 'A cytoplasmic NF-kappaB interacting long noncoding RNA blocks IkappaB phosphorylation and suppresses breast cancer metastasis', *Cancer Cell*, 27: 370-81.

Liu, B., W. Xiang, J. Liu, J. Tang, J. Wang, B. Liu, Z. Long, L. Wang, G. Yin, and J. Liu. 2021. 'The regulatory role of antisense lncRNAs in cancer', *Cancer Cell Int*, 21: 459.

Liu, G., C. Betts, D. M. Cunoosamy, P. M. Aberg, J. J. Hornberg, K. B. Sivars, and T. S. Cohen. 2019. 'Use of precision cut lung slices as a translational model for the study of lung biology', *Respir Res*, 20: 162.

Liu, J., L. Wan, K. Lu, M. Sun, X. Pan, P. Zhang, B. Lu, G. Liu, and Z. Wang. 2015. 'The Long Noncoding RNA MEG3 Contributes to Cisplatin Resistance of Human Lung Adenocarcinoma', *PLoS One*, 10: e0114586.

Liu, P. S., H. Wang, X. Li, T. Chao, T. Teav, S. Christen, G. Di Conza, W. C. Cheng, C. H. Chou, M. Vavakova, C. Muret, K. Debackere, M. Mazzone, H. D. Huang, S. M. Fendt, J. Ivanisevic, and P. C. Ho. 2017. 'alpha-ketoglutarate orchestrates macrophage activation through metabolic and epigenetic reprogramming', *Nat Immunol*, 18: 985-94.

Liu, X., Z. D. Xiao, L. Han, J. Zhang, S. W. Lee, W. Wang, H. Lee, L. Zhuang, J. Chen, H. K. Lin, J. Wang, H. Liang, and B. Gan. 2016. 'LncRNA NBR2 engages a metabolic checkpoint by regulating AMPK under energy stress', *Nat Cell Biol*, 18: 431-42.

Liu, Z., M. Sun, K. Lu, J. Liu, M. Zhang, W. Wu, W. De, Z. Wang, and R. Wang. 2013. 'The long noncoding RNA HOTAIR contributes to cisplatin resistance of human lung adenocarcinoma cells via downregualtion of p21(WAF1/CIP1) expression', *PLoS One*, 8: e77293.

Luo, W., and Y. Wang. 2019. 'Hypoxia Mediates Tumor Malignancy and Therapy Resistance', *Adv Exp Med Biol*, 1136: 1-18.

Luo, X. F., X. J. Wu, X. Wei, A. G. Wang, S. H. Wang, and J. L. Wang. 2019. 'LncRNA ADPGK-AS1 regulated cell proliferation, invasion, migration and apoptosis via targeting miR-542-3p in osteosarcoma', *Eur Rev Med Pharmacol Sci*, 23: 8751-60.

Ma, L., V. B. Bajic, and Z. Zhang. 2013. 'On the classification of long non-coding RNAs', *RNA Biol*, 10: 925-33.
Ma, Y., L. Wang, and R. Jia. 2020. 'The role of mitochondrial dynamics in human cancers', *Am J Cancer Res*, 10: 1278-93.
Maeda, Y., V. Dave, and J. A. Whitsett. 2007. 'Transcriptional control of lung morphogenesis', *Physiol Rev*, 87: 219-44.
Malhotra, V., and M. C. Perry. 2003. 'Classical chemotherapy: mechanisms, toxicities and the therapeutic window', *Cancer Biol Ther*, 2: S2-4.
Mantovani, A., S. Sozzani, M. Locati, P. Allavena, and A. Sica. 2002. 'Macrophage polarization: tumor-associated macrophages as a paradigm for polarized M2 mononuclear phagocytes', *Trends Immunol*, 23: 549-55.
Mardis, E. R., L. Ding, D. J. Dooling, D. E. Larson, M. D. McLellan, K. Chen, D. C. Koboldt, R. S. Fulton, K. D. Delehaunty, S. D. McGrath, L. A. Fulton, D. P. Locke, V. J. Magrini, R. M. Abbott, T. L. Vickery, J. S. Reed, J. S. Robinson, T. Wylie, S. M. Smith, L. Carmichael, J. M. Eldred, C. C. Harris, J. Walker, J. B. Peck, F. Du, A. F. Dukes, G. E. Sanderson, A. M. Brummett, E. Clark, J. F. McMichael, R. J. Meyer, J. K. Schindler, C. S. Pohl, J. W. Wallis, X. Shi, L. Lin, H. Schmidt, Y. Tang, C. Haipek, M. E. Wiechert, J. V. Ivy, J. Kalicki, G. Elliott, R. E. Ries, J. E. Payton, P. Westervelt, M. H. Tomasson, M. A. Watson, J. Baty, S. Heath, W. D. Shannon, R. Nagarajan, D. C. Link, M. J. Walter, T. A. Graubert, J. F. DiPersio, R. K. Wilson, and T. J. Ley. 2009. 'Recurring mutations found by sequencing an acute myeloid leukemia genome', *N Engl J Med*, 361: 1058-66.
Memczak, S., M. Jens, A. Elefsinioti, F. Torti, J. Krueger, A. Rybak, L. Maier, S. D. Mackowiak, L. H. Gregersen, M. Munschauer, A. Loewer, U. Ziebold, M. Landthaler, C. Kocks, F. le Noble, and N. Rajewsky. 2013. 'Circular RNAs are a large class of animal RNAs with regulatory potency', *Nature*, 495: 333-8.
Miller, A., C. Nagy, B. Knapp, J. Laengle, E. Ponweiser, M. Groeger, P. Starkl, M. Bergmann, O. Wagner, and A. Haschemi. 2017. 'Exploring Metabolic Configurations of Single Cells within Complex Tissue Microenvironments', *Cell Metab*, 26: 788-800 e6.
Mills, E. L., B. Kelly, A. Logan, A. S. H. Costa, M. Varma, C. E. Bryant, P. Tourlomousis, J. H. M. Dabritz, E. Gottlieb, I. Latorre, S. C. Corr, G. McManus, D. Ryan, H. T. Jacobs, M. Szibor, R. J. Xavier, T. Braun, C. Frezza, M. P. Murphy, and L. A. O'Neill. 2016. 'Succinate Dehydrogenase Supports Metabolic Repurposing of Mitochondria to Drive Inflammatory Macrophages', *Cell*, 167: 457-70 e13.
Mohapatra, S., C. Pioppini, B. Ozpolat, and G. A. Calin. 2021. 'Non-coding RNAs regulation of macrophage polarization in cancer', *Mol Cancer*, 20: 24.
Monne, M., D. V. Miniero, V. Iacobazzi, F. Bisaccia, and G. Fiermonte. 2013. 'The mitochondrial oxoglutarate carrier: from identification to mechanism', *J Bioenerg Biomembr*, 45: 1-13.
Mowel, W. K., J. J. Kotzin, S. J. McCright, V. D. Neal, and J. Henao-Mejia. 2018. 'Control of Immune Cell Homeostasis and Function by lncRNAs', *Trends Immunol*, 39: 55-69.
Naemura, M., C. Murasaki, Y. Inoue, H. Okamoto, and Y. Kotake. 2015. 'Long Noncoding RNA ANRIL Regulates Proliferation of Non-small Cell Lung Cancer and Cervical Cancer Cells', *Anticancer Res*, 35: 5377-82.
Nakayama, Y., K. Fujiu, R. Yuki, Y. Oishi, M. S. Morioka, T. Isagawa, J. Matsuda, T. Oshima, T. Matsubara, J. Sugita, F. Kudo, A. Kaneda, Y. Endo, T. Nakayama, R. Nagai, I. Komuro, and I. Manabe. 2020. 'A long noncoding RNA regulates inflammation resolution by mouse macrophages through fatty acid oxidation activation', *Proc Natl Acad Sci U S A*, 117: 14365-75.
NCI. 2019a. 'Non-Small Cell Lung Cancer Treatment', National Cancer Institute, Accessed October 10th.
———. 2019b. 'Radiation Therapy to Treat Cancer', National Cancer Institute.

Netea-Maier, R. T., J. W. A. Smit, and M. G. Netea. 2018. 'Metabolic changes in tumor cells and tumor-associated macrophages: A mutual relationship', *Cancer Lett*, 413: 102-09.

Neuhaus, V., D. Schaudien, T. Golovina, U. A. Temann, C. Thompson, T. Lippmann, C. Bersch, O. Pfennig, D. Jonigk, P. Braubach, H. G. Fieguth, G. Warnecke, V. Yusibov, K. Sewald, and A. Braun. 2017. 'Assessment of long-term cultivated human precision-cut lung slices as an ex vivo system for evaluation of chronic cytotoxicity and functionality', *J Occup Med Toxicol*, 12: 13.

Nicholson, R. I., J. M. Gee, and M. E. Harper. 2001. 'EGFR and cancer prognosis', *Eur J Cancer*, 37 Suppl 4: S9-15.

Oiseth, S. J., and M. S. Aziz. 2017. 'Cancer immunotherapy: a brief review of the history, possibilities, and challenges ahead', *J Cancer Metastasis Treat*, 3: 250-61.

Olivier, M., A. Petitjean, V. Marcel, A. Petre, M. Mounawar, A. Plymoth, C. C. de Fromentel, and P. Hainaut. 2009. 'Recent advances in p53 research: an interdisciplinary perspective', *Cancer Gene Ther*, 16: 1-12.

Ortega, R. A. , W. Barham, K. Sharman, O. Tikhomirov, T. D. Giorgio, and F. E. Yull. 2016. 'Manipulating the NF-κB pathway in macrophages using mannosylated, siRNA-delivering nanoparticles can induce immunostimulatory and tumor cytotoxic functions', *Int J Nanomedicine*, 11: 2163-77.

Ozes, A. R., Y. Wang, X. Zong, F. Fang, J. Pilrose, and K. P. Nephew. 2017. 'Therapeutic targeting using tumor specific peptides inhibits long non-coding RNA HOTAIR activity in ovarian and breast cancer', *Sci Rep*, 7: 894.

Padua Alves, C., A. S. Fonseca, B. R. Muys, E. Lima Bueno R. de Barros, M. C. Burger, J. E. de Souza, V. Valente, M. A. Zago, and W. A. Silva, Jr. 2013. 'Brief report: The lincRNA Hotair is required for epithelial-to-mesenchymal transition and stemness maintenance of cancer cell lines', *Stem Cells*, 31: 2827-32.

Pan, Y., Y. Yu, X. Wang, and T. Zhang. 2020. 'Tumor-Associated Macrophages in Tumor Immunity', *Front Immunol*, 11: 583084.

Pang, K. C., M. E. Dinger, T. R. Mercer, L. Malquori, S. M. Grimmond, W. Chen, and J. S. Mattick. 2009. 'Genome-wide identification of long noncoding RNAs in CD8+ T cells', *J Immunol*, 182: 7738-48.

Papa, S., P. L. Martino, G. Capitanio, A. Gaballo, D. De Rasmo, A. Signorile, and V. Petruzzella. 2012. 'The oxidative phosphorylation system in mammalian mitochondria', *Adv Exp Med Biol*, 942: 3-37.

Paul, P., A. Chakraborty, D. Sarkar, M. Langthasa, M. Rahman, M. Bari, R. S. Singha, A. K. Malakar, and S. Chakraborty. 2018. 'Interplay between miRNAs and human diseases', *J Cell Physiol*, 233: 2007-18.

Pei, B. X., B. S. Sun, Z. F. Zhang, A. L. Wang, and P. Ren. 2014. 'Interstitial tumor-associated macrophages combined with tumor-derived colony-stimulating factor-1 and interleukin-6, a novel prognostic biomarker in non-small cell lung cancer', *J Thorac Cardiovasc Surg*, 148: 1208-16 e2.

Pelechano, V., and L. M. Steinmetz. 2013. 'Gene regulation by antisense transcription', *Nat Rev Genet*, 14: 880-93.

Peranzoni, E., J. Lemoine, L. Vimeux, V. Feuillet, S. Barrin, C. Kantari-Mimoun, N. Bercovici, M. Guérin, J. Biton, H. Ouakrim, F. Régnier, A. Lupo, M. Alifano, D. Damotte, and E. Donnadieu. 2018. 'Macrophages impede CD8 T cells from reaching tumor cells and limit the efficacy of anti-PD-1 treatment', *Proc Natl Acad Sci U S A*, 115: E4041-e50.

Poller, W., S. Dimmeler, S. Heymans, T. Zeller, J. Haas, M. Karakas, D. M. Leistner, P. Jakob, S. Nakagawa, S. Blankenberg, S. Engelhardt, T. Thum, C. Weber, B. Meder, R. Hajjar, and U. Landmesser. 2018. 'Non-coding RNAs in cardiovascular diseases: diagnostic and therapeutic perspectives', *Eur Heart J*, 39: 2704-16.

Pound, P., and M. Ritskes-Hoitinga. 2018. 'Is it possible to overcome issues of external validity in preclinical animal research? Why most animal models are bound to fail', *J Transl Med*, 16: 304.

Preuss, E. B., S. Schubert, C. Werlein, H. Stark, P. Braubach, A. Hofer, E. K. J. Plucinski, H. R. Shah, R. Geffers, K. Sewald, A. Braun, D. D. Jonigk, and M. P. Kuhnel. 2021. 'The Challenge of Long-Term Cultivation of Human Precision-Cut Lung Slices', *Am J Pathol*.

Puchalapalli, M., X. Zeng, L. Mu, A. Anderson, L. Hix Glickman, M. Zhang, M. R. Sayyad, S. Mosticone Wangensteen, C. V. Clevenger, and J. E. Koblinski. 2016. 'NSG Mice Provide a Better Spontaneous Model of Breast Cancer Metastasis than Athymic (Nude) Mice', *PLoS One*, 11: e0163521.

Qian, C. S., L. J. Li, H. W. Huang, H. F. Yang, and D. P. Wu. 2020. 'MYC-regulated lncRNA NEAT1 promotes B cell proliferation and lymphomagenesis via the miR-34b-5p-GLI1 pathway in diffuse large B-cell lymphoma', *Cancer Cell Int*, 20: 87.

Quemener, A. M., L. Bachelot, A. Forestier, E. Donnou-Fournet, D. Gilot, and M. D. Galibert. 2020. 'The powerful world of antisense oligonucleotides: From bench to bedside', *Wiley Interdiscip Rev RNA*, 11: e1594.

Rapicavoli, N. A., K. Qu, J. Zhang, M. Mikhail, R. M. Laberge, and H. Y. Chang. 2013. 'A mammalian pseudogene lncRNA at the interface of inflammation and anti-inflammatory therapeutics', *Elife*, 2: e00762.

Rashid, F., A. Shah, and G. Shan. 2016. 'Long Non-coding RNAs in the Cytoplasm', *Genomics Proteomics Bioinformatics*, 14: 73-80.

Reck, M., D. Rodriguez-Abreu, A. G. Robinson, R. Hui, T. Csoszi, A. Fulop, M. Gottfried, N. Peled, A. Tafreshi, S. Cuffe, M. O'Brien, S. Rao, K. Hotta, M. A. Leiby, G. M. Lubiniecki, Y. Shentu, R. Rangwala, J. R. Brahmer, and Keynote- Investigators. 2016. 'Pembrolizumab versus Chemotherapy for PD-L1-Positive Non-Small-Cell Lung Cancer', *N Engl J Med*, 375: 1823-33.

Ren, Y., H. H. Jia, Y. Q. Xu, X. Zhou, X. H. Zhao, Y. F. Wang, X. Song, Z. Y. Zhu, T. Sun, Y. Dou, W. P. Tian, X. L. Zhao, C. S. Kang, and M. Mei. 2018. 'Paracrine and epigenetic control of CAF-induced metastasis: the role of HOTAIR stimulated by TGF-ss1 secretion', *Mol Cancer*, 17: 5.

Rinaldi, C., and M. J. A. Wood. 2018. 'Antisense oligonucleotides: the next frontier for treatment of neurological disorders', *Nat Rev Neurol*, 14: 9-21.

Rodriguez, E. F., F. De Marchi, P. M. Lokhandwala, D. Belchis, R. Xian, C. D. Gocke, J. R. Eshleman, P. Illei, and M. T. Li. 2020. 'IDH1 and IDH2 mutations in lung adenocarcinomas: Evidences of subclonal evolution', *Cancer Med*, 9: 4386-94.

Ruffell, B., and L. M. Coussens. 2015. 'Macrophages and therapeutic resistance in cancer', *Cancer Cell*, 27: 462-72.

Rust, J. H. 1982. 'Animal models for human diseases', *Perspect Biol Med*, 25: 662-72.

Sang, L., H. Q. Ju, Z. Yang, Q. Ge, Z. Zhang, F. Liu, L. Yang, H. Gong, C. Shi, L. Qu, H. Chen, M. Wu, H. Chen, R. Li, Q. Zhuang, H. Piao, Q. Yan, W. Yu, L. Wang, J. Shao, J. Liu, W. Wang, T. Zhou, and A. Lin. 2021. 'Mitochondrial long non-coding RNA GAS5 tunes TCA metabolism in response to nutrient stress', *Nat Metab*, 3: 90-106.

Santosh, B., A. Varshney, and P. K. Yadava. 2015. 'Non-coding RNAs: biological functions and applications', *Cell Biochem Funct*, 33: 14-22.

Sarode, P., S. Mansouri, A. Karger, M. B. Schaefer, F. Grimminger, W. Seeger, and R. Savai. 2020. 'Epithelial cell plasticity defines heterogeneity in lung cancer', *Cell Signal*, 65: 109463.

Sarode, P., M. B. Schaefer, F. Grimminger, W. Seeger, and R. Savai. 2020. 'Macrophage and Tumor Cell Cross-Talk Is Fundamental for Lung Tumor Progression: We Need to Talk', *Front Oncol*, 10: 324.

Sarode, P., X. Zheng, G. A. Giotopoulou, A. Weigert, C. Kuenne, S. Gunther, A. Friedrich, S. Gattenlohner, T. Stiewe, B. Brune, F. Grimminger, G. T. Stathopoulos, S. S. Pullamsetti, W. Seeger, and R. Savai. 2020. 'Reprogramming of tumor-associated macrophages by targeting beta-catenin/FOSL2/ARID5A signaling: A potential treatment of lung cancer', *Sci Adv*, 6: eaaz6105.

Scagliotti, G. V., F. De Marinis, M. Rinaldi, L. Crino, C. Gridelli, S. Ricci, E. Matano, C. Boni, M. Marangolo, G. Failla, G. Altavilla, V. Adamo, A. Ceribelli, M. Clerici, F. Di Costanzo, L. Frontini, M. Tonato, and Project Italian Lung Cancer. 2002. 'Phase III

randomized trial comparing three platinum-based doublets in advanced non-small-cell lung cancer', *J Clin Oncol*, 20: 4285-91.
Schiller, J. H., D. Harrington, C. P. Belani, C. Langer, A. Sandler, J. Krook, J. Zhu, D. H. Johnson, and Group Eastern Cooperative Oncology. 2002. 'Comparison of four chemotherapy regimens for advanced non-small-cell lung cancer', *N Engl J Med*, 346: 92-8.
Schmall, A., H. M. Al-Tamari, S. Herold, M. Kampschulte, A. Weigert, A. Wietelmann, N. Vipotnik, F. Grimminger, W. Seeger, S. S. Pullamsetti, and R. Savai. 2015. 'Macrophage and cancer cell cross-talk via CCR2 and CX3CR1 is a fundamental mechanism driving lung cancer', *Am J Respir Crit Care Med*, 191: 437-47.
Schultze, J. L., A. Schmieder, and S. Goerdt. 2015. 'Macrophage activation in human diseases', *Semin Immunol*, 27: 249-56.
Schulz, C., E. Gomez Perdiguero, L. Chorro, H. Szabo-Rogers, N. Cagnard, K. Kierdorf, M. Prinz, B. Wu, S. E. Jacobsen, J. W. Pollard, J. Frampton, K. J. Liu, and F. Geissmann. 2012. 'A lineage of myeloid cells independent of Myb and hematopoietic stem cells', *Science*, 336: 86-90.
Seebacher, N. A., A. E. Stacy, G. M. Porter, and A. M. Merlot. 2019. 'Clinical development of targeted and immune based anti-cancer therapies', *J Exp Clin Cancer Res*, 38: 156.
Shapouri-Moghaddam, A., S. Mohammadian, H. Vazini, M. Taghadosi, S. A. Esmaeili, F. Mardani, B. Seifi, A. Mohammadi, J. T. Afshari, and A. Sahebkar. 2018. 'Macrophage plasticity, polarization, and function in health and disease', *J Cell Physiol*, 233: 6425-40.
Sharma, S. V., D. W. Bell, J. Settleman, and D. A. Haber. 2007. 'Epidermal growth factor receptor mutations in lung cancer', *Nat Rev Cancer*, 7: 169-81.
Siegel, R. L., K. D. Miller, H. E. Fuchs, and A. Jemal. 2021. 'Cancer Statistics, 2021', *CA Cancer J Clin*, 71: 7-33.
Siegel, R. L., K. D. Miller, and A. Jemal. 2020. 'Cancer statistics, 2020', *CA Cancer J Clin*, 70: 7-30.
Sivandzade, F., A. Bhalerao, and L. Cucullo. 2019. 'Analysis of the Mitochondrial Membrane Potential Using the Cationic JC-1 Dye as a Sensitive Fluorescent Probe', *Bio Protoc*, 9.
Soda, M., Y. L. Choi, M. Enomoto, S. Takada, Y. Yamashita, S. Ishikawa, S. Fujiwara, H. Watanabe, K. Kurashina, H. Hatanaka, M. Bando, S. Ohno, Y. Ishikawa, H. Aburatani, T. Niki, Y. Sohara, Y. Sugiyama, and H. Mano. 2007. 'Identification of the transforming EML4-ALK fusion gene in non-small-cell lung cancer', *Nature*, 448: 561-6.
Song, M., T. Liu, C. Shi, X. Zhang, and X. Chen. 2016. 'Bioconjugated Manganese Dioxide Nanoparticles Enhance Chemotherapy Response by Priming Tumor-Associated Macrophages toward M1-like Phenotype and Attenuating Tumor Hypoxia', *ACS Nano*, 10: 633-47.
Song, S., W. Yu, S. Lin, M. Zhang, T. Wang, S. Guo, and H. Wang. 2018. 'LncRNA ADPGK-AS1 promotes pancreatic cancer progression through activating ZEB1-mediated epithelial-mesenchymal transition', *Cancer Biol Ther*, 19: 573-83.
Sotgia, F., M. Fiorillo, and M. P. Lisanti. 2017. 'Mitochondrial markers predict recurrence, metastasis and tamoxifen-resistance in breast cancer patients: Early detection of treatment failure with companion diagnostics', *Oncotarget*, 8: 68730-45.
Spremulli, L. L. 2016. "The Protein Biosynthetic Machinery of Mitochondria." In *Encyclopedia of Cell Biology*, 545-54. Elsevier.
Stadie, W. C. 1944. 'The Relation of Insulin to Phosphate Metabolism', *Yale J Biol Med*, 16: 539-59.
Standiford, T. J., R. Kuick, U. Bhan, J. Chen, M. Newstead, and V. G. Keshamouni. 2011. 'TGF-beta-induced IRAK-M expression in tumor-associated macrophages regulates lung tumor growth', *Oncogene*, 30: 2475-84.
Statello, L., C. J. Guo, L. L. Chen, and M. Huarte. 2021. 'Gene regulation by long non-coding RNAs and its biological functions', *Nat Rev Mol Cell Biol*, 22: 96-118.

Sun, N., Y. Chen, W. Wu, H. Lin, Y. Chiang, C. F. Chang, H. C. Hsu, Chen C., W. Sun, and Cheng W. 2019. 'Blockade of PD-L1 Enhances Cancer Immunotherapy by Regulating Dendritic Cell Maturation and Macrophage Polarization', *Cancers (Basel)*, 11: 1400.

Sylvester, J. E., N. Fischel-Ghodsian, E. B. Mougey, and T. W. O'Brien. 2004. 'Mitochondrial ribosomal proteins: candidate genes for mitochondrial disease', *Genet Med*, 6: 73-80.

Taanman, J. W. 1999. 'The mitochondrial genome: structure, transcription, translation and replication', *Biochim Biophys Acta*, 1410: 103-23.

Tan, H. Y., N. Wang, S. Li, M. Hong, X. Wang, and Y. Feng. 2016. 'The Reactive Oxygen Species in Macrophage Polarization: Reflecting Its Dual Role in Progression and Treatment of Human Diseases', *Oxid Med Cell Longev*, 2016: 2795090.

Tang, Q., and S. S. Hann. 2018. 'HOTAIR: An Oncogenic Long Non-Coding RNA in Human Cancer', *Cell Physiol Biochem*, 47: 893-913.

Tang, Y., Y. He, L. Shi, L. Yang, J. Wang, Y. Lian, C. Fan, P. Zhang, C. Guo, S. Zhang, Z. Gong, X. Li, F. Xiong, X. Li, Y. Li, G. Li, W. Xiong, and Z. Zeng. 2017. 'Co-expression of AFAP1-AS1 and PD-1 predicts poor prognosis in nasopharyngeal carcinoma', *Oncotarget*, 8: 39001-11.

Tannahill, G. M., A. M. Curtis, J. Adamik, E. M. Palsson-McDermott, A. F. McGettrick, G. Goel, C. Frezza, N. J. Bernard, B. Kelly, N. H. Foley, L. Zheng, A. Gardet, Z. Tong, S. S. Jany, S. C. Corr, M. Haneklaus, B. E. Caffrey, K. Pierce, S. Walmsley, F. C. Beasley, E. Cummins, V. Nizet, M. Whyte, C. T. Taylor, H. Lin, S. L. Masters, E. Gottlieb, V. P. Kelly, C. Clish, P. E. Auron, R. J. Xavier, and L. A. O'Neill. 2013. 'Succinate is an inflammatory signal that induces IL-1beta through HIF-1alpha', *Nature*, 496: 238-42.

Torre, L. A., R. L. Siegel, and A. Jemal. 2016. 'Lung Cancer Statistics', *Adv Exp Med Biol*, 893: 1-19.

Travis, W. D., E. Brambilla, A. G. Nicholson, Y. Yatabe, J. H. M. Austin, M. B. Beasley, L. R. Chirieac, S. Dacic, E. Duhig, D. B. Flieder, K. Geisinger, F. R. Hirsch, Y. Ishikawa, K. M. Kerr, M. Noguchi, G. Pelosi, C. A. Powell, M. S. Tsao, I. Wistuba, and W. H. O. Panel. 2015. 'The 2015 World Health Organization Classification of Lung Tumors: Impact of Genetic, Clinical and Radiologic Advances Since the 2004 Classification', *J Thorac Oncol*, 10: 1243-60.

Travis, W. D., E. Brambilla, and G. J. Riely. 2013. 'New pathologic classification of lung cancer: relevance for clinical practice and clinical trials', *J Clin Oncol*, 31: 992-1001.

Tsai, M. C., O. Manor, Y. Wan, N. Mosammaparast, J. K. Wang, F. Lan, Y. Shi, E. Segal, and H. Y. Chang. 2010. 'Long noncoding RNA as modular scaffold of histone modification complexes', *Science*, 329: 689-93.

Tufekci, K. U., M. G. Oner, R. L. Meuwissen, and S. Genc. 2014. 'The role of microRNAs in human diseases', *Methods Mol Biol*, 1107: 33-50.

Vaidya, A. M., Z. Sun, N. Ayat, A. Schilb, X. Liu, H. Jiang, D. Sun, J. Scheidt, V. Qian, S. He, H. Gilmore, W. P. Schiemann, and Z. R. Lu. 2019. 'Systemic Delivery of Tumor-Targeting siRNA Nanoparticles against an Oncogenic LncRNA Facilitates Effective Triple-Negative Breast Cancer Therapy', *Bioconjug Chem*, 30: 907-19.

Van Dyken, S. J., and R. M. Locksley. 2013. 'Interleukin-4- and interleukin-13-mediated alternatively activated macrophages: roles in homeostasis and disease', *Annu Rev Immunol*, 31: 317-43.

van Furth, R., and Z. A. Cohn. 1968. 'The origin and kinetics of mononuclear phagocytes', *J Exp Med*, 128: 415-35.

van Lent, P. L. , L. van den Bersselaar, A. E. van den Hoek, M. van de Ende, C. D. Dijkstra, N. van Rooijen, L. B. van de Putte, and W. B. van den Berg. 1993. 'Reversible depletion of synovial lining cells after intra-articular treatment with liposome-encapsulated dichloromethylene diphosphonate', *Rheumatol Int.*, 13: 21-30.

Van Lent, P. L., A. E. Holthuysen, N. Van Rooijen, L. B. Van de Putte, and W. B. Van den Berg. 1998. 'Local removal of phagocytic synovial lining cells by clodronate-

liposomes decreases cartilage destruction during collagen type II arthritis', *Ann Rheum Dis*, 57: 408-13.
Vendramin, R., Y. Verheyden, H. Ishikawa, L. Goedert, E. Nicolas, K. Saraf, A. Armaos, R. Delli Ponti, K. Izumikawa, P. Mestdagh, D. L. J. Lafontaine, G. G. Tartaglia, N. Takahashi, J. C. Marine, and E. Leucci. 2018. 'SAMMSON fosters cancer cell fitness by concertedly enhancing mitochondrial and cytosolic translation', *Nat Struct Mol Biol*, 25: 1035-46.
Wai, T., and T. Langer. 2016. 'Mitochondrial Dynamics and Metabolic Regulation', *Trends Endocrinol Metab*, 27: 105-17.
Waldman, A. D., J. M. Fritz, and M. J. Lenardo. 2020. 'A guide to cancer immunotherapy: from T cell basic science to clinical practice', *Nat Rev Immunol*, 20: 651-68.
Wang, H., Q. Shao, J. Sun, C. Ma, W. Gao, Q. Wang, L. Zhao, and X. Qu. 2016. 'Interactions between colon cancer cells and tumor-infiltrated macrophages depending on cancer cell-derived colony stimulating factor 1', *Oncoimmunology*, 5: e1122157.
Wang, K. C., and H. Y. Chang. 2011. 'Molecular mechanisms of long noncoding RNAs', *Mol Cell*, 43: 904-14.
Wang, P., Y. Xue, Y. Han, L. Lin, C. Wu, S. Xu, Z. Jiang, J. Xu, Q. Liu, and X. Cao. 2014. 'The STAT3-binding long noncoding RNA lnc-DC controls human dendritic cell differentiation', *Science*, 344: 310-3.
Wang, Y., N. Li, X. Zhang, and T. Horng. 2021. 'Mitochondrial metabolism regulates macrophage biology', *J Biol Chem*, 297: 100904.
Warburg, O. 1923. 'Versuche an überlebendem Karzinomgewebe', *Biochem Z*: 317-33.
Wei, C., C. Yang, S. Wang, D. Shi, C. Zhang, X. Lin, Q. Liu, R. Dou, and B. Xiong. 2019. 'Crosstalk between cancer cells and tumor associated macrophages is required for mesenchymal circulating tumor cell-mediated colorectal cancer metastasis', *Mol Cancer*, 18: 64.
Winkle, M., S. M. El-Daly, M. Fabbri, and G. A. Calin. 2021. 'Noncoding RNA therapeutics - challenges and potential solutions', *Nat Rev Drug Discov*, 20: 629-51.
Wu, D., J. Zhu, Y. Fu, C. Li, and B. Wu. 2021. 'LncRNA HOTAIR promotes breast cancer progression through regulating the miR-129-5p/FZD7 axis', *Cancer Biomark*, 30: 203-12.
Wu, Q., W. Y. Meng, Y. Jie, and H. Zhao. 2018. 'LncRNA MALAT1 induces colon cancer development by regulating miR-129-5p/HMGB1 axis', *J Cell Physiol*, 233: 6750-57.
Xia, F., F. Dong, Y. Yang, A. Huang, S. Chen, D. Sun, S. Xiong, and J. Zhang. 2014. 'Dynamic transcription of long non-coding RNA genes during CD4+ T cell development and activation', *PLoS One*, 9: e101588.
Xiao, D., L. Zeng, K. Yao, X. Kong, G. Wu, and Y. Yin. 2016. 'The glutamine-alpha-ketoglutarate (AKG) metabolism and its nutritional implications', *Amino Acids*, 48: 2067-80.
Xie, J. H., Y. Y. Li, and J. Jin. 2020. 'The essential functions of mitochondrial dynamics in immune cells', *Cell Mol Immunol*, 17: 712-21.
Xu, L., B. Wei, H. Hui, Y. Sun, Y. Liu, X. Yu, and J. Dai. 2019. 'Positive feedback loop of lncRNA LINC01296/miR-598/Twist1 promotes non-small cell lung cancer tumorigenesis', *J Cell Physiol*, 234: 4563-71.
Yan, H., D. W. Parsons, G. Jin, R. McLendon, B. A. Rasheed, W. Yuan, I. Kos, I. Batinic-Haberle, S. Jones, G. J. Riggins, H. Friedman, A. Friedman, D. Reardon, J. Herndon, K. W. Kinzler, V. E. Velculescu, B. Vogelstein, and D. D. Bigner. 2009. 'IDH1 and IDH2 mutations in gliomas', *N Engl J Med*, 360: 765-73.
Yang, J., W. Wu, M. Wu, and J. Ding. 2019. 'Long noncoding RNA ADPGK-AS1 promotes cell proliferation, migration, and EMT process through regulating miR-3196/OTX1 axis in breast cancer', *In Vitro Cell Dev Biol Anim*, 55: 522-32.
Yang, Y., C. Jiang, Y. Yang, L. Guo, J. Huang, X. Liu, C. Wu, and J. Zou. 2018. 'Silencing of LncRNA-HOTAIR decreases drug resistance of Non-Small Cell Lung Cancer cells by inactivating autophagy via suppressing the phosphorylation of ULK1', *Biochem Biophys Res Commun*, 497: 1003-10.

Yona, S., K. W. Kim, Y. Wolf, A. Mildner, D. Varol, M. Breker, D. Strauss-Ayali, S. Viukov, M. Guilliams, A. Misharin, D. A. Hume, H. Perlman, B. Malissen, E. Zelzer, and S. Jung. 2013. 'Fate mapping reveals origins and dynamics of monocytes and tissue macrophages under homeostasis', *Immunity*, 38: 79-91.

Yu, T., Y. Zhao, Z. Hu, J. Li, D. Chu, J. Zhang, Z. Li, B. Chen, X. Zhang, H. Pan, S. Li, H. Lin, L. Liu, M. Yan, X. He, and M. Yao. 2017. 'MetaLnc9 Facilitates Lung Cancer Metastasis via a PGK1-Activated AKT/mTOR Pathway', *Cancer Res*, 77: 5782-94.

Zhai, N., Y. Xia, R. Yin, J. Liu, and F. Gao. 2016. 'A negative regulation loop of long noncoding RNA HOTAIR and p53 in non-small-cell lung cancer', *Onco Targets Ther*, 9: 5713-20.

Zhang, C., M. Yang, and A. C. Ericsson. 2021. 'Function of Macrophages in Disease: Current Understanding on Molecular Mechanisms', *Front Immunol*, 12: 620510.

Zhang, L., P. Lu, L. Yan, L. Yang, Y. Wang, J. Chen, J. Dai, Y. Li, Z. Kang, T. Bai, Y. Xi, J. Xu, G. Sun, and T. Yang. 2019. 'MRPL35 Is Up-Regulated in Colorectal Cancer and Regulates Colorectal Cancer Cell Growth and Apoptosis', *Am J Pathol*, 189: 1105-20.

Zhang, M., Y. He, X. Sun, Q. Li, W. Wang, A. Zhao, and W. Di. 2014. 'A high M1/M2 ratio of tumor-associated macrophages is associated with extended survival in ovarian cancer patients', *J Ovarian Res*, 7: 19.

Zhang, S., F. Ma, X. Xie, and Y. Shen. 2020. 'Prognostic value of long non-coding RNAs in triple negative breast cancer: A PRISMA-compliant meta-analysis', *Medicine (Baltimore)*, 99: e21861.

Zhang, X., X. Zuo, B. Yang, Z. Li, Y. Xue, Y. Zhou, J. Huang, X. Zhao, J. Zhou, Y. Yan, H. Zhang, P. Guo, H. Sun, L. Guo, Y. Zhang, and X. D. Fu. 2014. 'MicroRNA directly enhances mitochondrial translation during muscle differentiation', *Cell*, 158: 607-19.

Zhang, Y., J. Feng, H. Fu, C. Liu, Z. Yu, Y. Sun, X. She, P. Li, C. Zhao, Y. Liu, T. Liu, Q. Liu, Q. Liu, G. Li, and M. Wu. 2018. 'Coagulation Factor X Regulated by CASC2c Recruited Macrophages and Induced M2 Polarization in Glioblastoma Multiforme', *Front Immunol*, 9: 1557.

Zhao, J. M., W. Cheng, X. G. He, Y. L. Liu, F. F. Wang, and Y. F. Gao. 2018. 'Long non-coding RNA PICART1 suppresses proliferation and promotes apoptosis in lung cancer cells by inhibiting JAK2/STAT3 signaling', *Neoplasma*, 65: 779-89.

Zhao, Y., L. Sun, R. R. Wang, J. F. Hu, and J. Cui. 2018. 'The effects of mitochondria-associated long noncoding RNAs in cancer mitochondria: New players in an old arena', *Crit Rev Oncol Hematol*, 131: 76-82.

Zheng, X., S. Mansouri, A. Krager, F. Grimminger, W. Seeger, S. S. Pullamsetti, C. E. Wheelock, and R. Savai. 2020. 'Metabolism in tumour-associated macrophages: a quid pro quo with the tumour microenvironment', *Eur Respir Rev*, 29.

Zheng, X., K. Turkowski, J. Mora, B. Brune, W. Seeger, A. Weigert, and R. Savai. 2017. 'Redirecting tumor-associated macrophages to become tumoricidal effectors as a novel strategy for cancer therapy', *Oncotarget*, 8: 48436-52.

Zheng, X., A. Weigert, S. Reu, S. Guenther, S. Mansouri, B. Bassaly, S. Gattenlohner, F. Grimminger, S. Pullamsetti, W. Seeger, H. Winter, and R. Savai. 2020. 'Spatial Density and Distribution of Tumor-Associated Macrophages Predict Survival in Non-Small Cell Lung Carcinoma', *Cancer Res*, 80: 4414-25.

Zhou, M., X. Guo, M. Wang, and R. Qin. 2021. 'The patterns of antisense long non-coding RNAs regulating corresponding sense genes in human cancers', *J Cancer*, 12: 1499-506.

Zhou, X., S. Liu, G. Cai, L. Kong, T. Zhang, Y. Ren, Y. Wu, M. Mei, L. Zhang, and X. Wang. 2015. 'Long Non Coding RNA MALAT1 Promotes Tumor Growth and Metastasis by inducing Epithelial-Mesenchymal Transition in Oral Squamous Cell Carcinoma', *Sci Rep*, 5: 15972.

Zhou, Y., Y. Zhong, Y. Wang, X. Zhang, D. L. Batista, R. Gejman, P. J. Ansell, J. Zhao, C. Weng, and A. Klibanski. 2007. 'Activation of p53 by MEG3 non-coding RNA', *J Biol Chem*, 282: 24731-42.

Zhu, C., J. M. Kros, C. Cheng, and D. Mustafa. 2017. 'The contribution of tumor-associated macrophages in glioma neo-angiogenesis and implications for anti-angiogenic strategies', *Neuro Oncol*, 19: 1435-46.
Zhu, P., Y. Wang, J. Wu, G. Huang, B. Liu, B. Ye, Y. Du, G. Gao, Y. Tian, L. He, and Z. Fan. 2016. 'LncBRM initiates YAP1 signalling activation to drive self-renewal of liver cancer stem cells', *Nat Commun*, 7: 13608.

Statement of authenticity

I declare that I have completed this dissertation single-handedly without the unauthorized help of a second party and only with the assistance acknowledged therein. I have appropriately acknowledged and cited all text passages that are derived verbatim from or are based on the content of published work of others, and all information relating to verbal communications. I consent to the use of an anti-plagiarism software to check my thesis. I have abided by the principles of good scientific conduct laid down in the charter of the Justus Liebig University Giessen „Satzung der Justus-Liebig-Universität Gießen zur Sicherung guter wissenschaftlicher Praxis“ in carrying out the investigations described in the dissertation.

Ich erkläre: Ich habe die vorgelegte Dissertation selbstständig und ohne unerlaubte fremde Hilfe und nur mit den Hilfen angefertigt, die ich in der Dissertation angegeben habe. Alle Textstellen, die wörtlich oder sinngemäß aus veröffentlichten Schriften entnommen sind, und alle Angaben, die auf mündlichen Auskünften beruhen, sind als solche kenntlich gemacht. Ich stimme einer evtl. Überprüfung meiner Dissertation durch eine Antiplagiat-Software zu. Bei den von mir durchgeführten und in der Dissertation erwähnten Untersuchungen habe ich die Grundsätze guter wissenschaftlicher Praxis, wie sie in der „Satzung der Justus-Liebig-Universität Gießen zur Sicherung guter wissenschaftlicher Praxis“ niedergelegt sind, eingehalten.

_____ _____

Date Signature

Acknowledgments

It is a pleasure to express my sincere gratitude to everybody contributing to this thesis by giving me constant support, patience and guidance.

First of all, I would like to thank Prof. Dr. Werner Seeger for providing me the opportunity to perform by studies in his department and giving valuable advices regarding my project over the last years.

I am deeply grateful for the supervision, guidance and support of Prof. Dr. Rajkumar Savai. I appreciate your commitment, scientific enthusiasm and time for constant discussions about my project.

I would like to express my thankfulness to Prof. Dr. Reinhard Dammann from the Justus-Liebig-University Giessen for the continuous support throughout my studies and finally, accepting the co-supervision of this project.

I would like to thank Dr. Biruta Witte, Dr. Ibrahim Alkoudmani, Dr. Stefan Gattenlöhner, Dr. Clemens Ruppert, Dr. Dr. Peter Dorfmüller, and Prof. Dr. Andreas Günther from the University Hospital of Giessen and Marburg (UKGM) for inviting us into the surgical theater, giving us the opportunity to work with human lung tumor tissue, and for the support and patience during the establishment of a new method. I would also like to thank my MPI colleagues, especially Dr. Sascha Seidel, Dr. Rajender Nandigama and Dr. Siavash Mansouri for all the support concerning logistics and processing of the tissue.

I am sincerely grateful to our collaborators, Dr. Matthias Leisegang for his guidance and sharing his expertise in non-coding RNAs, Dr. Stefan Günther and Dr. Carsten Künne for RNA sequencing and the bioinformatics analysis, Dr. Sven Zukunft und Dr. Stephan Klatt for the efforts in metabolome measurements, and Dr. Ilka Wittig for the mass spectrometry analysis.

I would like to thank all my MPI colleagues for the continuous support, useful feedback, and for creating an encouraging work environment.

I owe the deepest gratitude to my family, especially my husband, for the unconditional support, love and endless patience with me and my work. Without you, this study would not have been completed.

Finally, a special thanks to my son Lukas for all the little distractions along the way. You made the time of this study longer, but worthwhile.